8-31-1990

Improving the throughput of plasticating extruders : measurement of the interparticulate friction coefficient for polymeric particulates with circular and profiled cross sections

Aiping Chen
New Jersey Institute of Technology

Copyright Warning & Restrictions

The copyright law of the United States (Title 17, United States Code) governs the making of photocopies or other reproductions of copyrighted material.

Under certain conditions specified in the law, libraries and archives are authorized to furnish a photocopy or other reproduction. One of these specified conditions is that the photocopy or reproduction is not to be "used for any purpose other than private study, scholarship, or research." If a, user makes a request for, or later uses, a photocopy or reproduction for purposes in excess of "fair use" that user may be liable for copyright infringement,

This institution reserves the right to refuse to accept a copying order if, in its judgment, fulfillment of the order would involve violation of copyright law.

Please Note: The author retains the copyright while the New Jersey Institute of Technology reserves the right to distribute this thesis or dissertation

Printing note: If you do not wish to print this page, then select "Pages from: first page # to: last page #" on the print dialog screen

ABSTRACT

Title of thesis: **Improving the Throughput of Plasticating Extruders: Measurement of the Interparticulate Friction Coefficient for Polymeric Particulates with Circular and Profiled Cross Sections**

Aiping Chen, Master of Science in Manufacturing Engineering, Aug. 1990

Thesis directed by: **Dr. Keith O'Brien**
Professor
Department of Mechanical and Industrial Engineering

This thesis deals with the coefficient of friction between individual polymeric pellets, the interparticulate friction coefficient (IPFC). It has been measured using a shear cell for a wide variety of circular and profiled cross–section pellets for a variery of polymeric materials. First, the thesis explains the reasons why it is desirable to enhance the IPFC based on the melting mechanisms in a single screw plasticating extruder. By making pellets with profiled cross–section pellets, the IPFC is greater than for pellets of circular cross–section. Second, it describes the test apparatus for measuring the IPFC and the method for calculating the IPFC. Third, it presents a comparison of the IPFC for different cross–sections and different materials.

IMPROVING THE THROUGHPUT OF PLASTICATING EXTRUDERS: MEASUREMENT OF THE INTERPARTICULATE FRICTION COEFFICIENT FOR POLYMERIC PARTICULATES WITH CIRCULAR AND PROFILED CROSS SECTIONS

by
AIPING CHEN

Thesis submitted to the Faculty of the Graduate School of the New Jersey Institute of Technology in partial fulfillment of the requirements for the degree of Master of Science in Manufacturing Engineering
1990

APPROVAL

Name of Candidate: Aiping Chen
Master of Science in Manufacturing Engineering, 1990

Thesis and Abstract Approved: _____ 8/29/90
Dr. Keith O'Brien, Advisor — Date
Professor
Department of Mechanical and Industrial Engineering

Signatures of other members: _____ 8/29/90
of the thesis committee. Dr. Raj Sodhi — Date
Associate Professor
Department of Mechanical and Industrial Engineering

_____ 08/31/90
Dr. Nouri Levy — Date
Associate Professor
Department of Mechanical and Industrial Engineering

VITA

Name: Aiping Chen

Permanent address:

Degree and date to be conferred: M.S.Mn.E., Aug. 1990

Date of birth:

Place of birth:

Collegiate institutions attended	Dates	Degree	Date of Degree
Shanghai University of Technology Shanghai, China	9/78-7/82	B.S.M.E	July, 1982
New Jersey Institute of Technology Newark, New Jersey	1/89-8/90	M.S.Mn.E	Aug. 1990

Major: Manufacturing Engineering

Position held: Research Assistant

Dept. of Mechanical and Industrial Engineering
New Jersey Institute of Technology
Newark, NJ 07102

ACKNOWLEDGEMENT

This thesis is on the subject of measurement of interparticulate friction coefficient for polymeric particulates with circular and profiled cross–sections in order to improve the output of single plasticating screw extruders. It has been by the efforts and support of many people. First, I would like to express my sincere appreciation to my advisor, Dr. Keith O'Brien, Director of the Plastic Processing Laboratory and Director of Manufacturing EngineeringPrograms, New Jersey Institute of Technology, for his guidance and advice. Without his valuable source and equipment, this work can not be done so quickly, and successfully. Also, I would like to thank Mr. Jia–ying Liu for his suggestion in designing the test apparatus and measuring the interparticulate friction coefficient. It is also a pleasure to express my thanks to the people who have been of assistance to me in the preparation of this thesis. Finally, thanks to my husband, parents, in–laws, sister and brothers that I would like to dedicate this thesis to them for their support.

Contents

List of Tables

List of Figures

Chapter 1

INTRODUCTION

The word *extrusion* is derived from the latin words *ex* and *trudere* meaning, respectively, *out* and *to thrust*, or *to push*. These words describe literally the process of extrusion, where a polymer melt is pushed across a metal die that continuously *shapes* the melt into the desired form. Polymer products that are *infinite* in one direction, which means that the cross section is constant, are manufactured by the extrusion process.

The heart of the screw extrusion process is an Archimedean screw rotating in a heated barrel (Figure 1.1). The raw polymer in the form of particulate solids is gravitationally fed onto the screw through a hopper. The solids are conveyed forward, plasticated, homogenized, and pressurized along the screw. Thus a uniformly molten polymer is pumped, or pushed, across the die attached to the extruder *head*. The screw is rotated by electric motors through a gear reducer. The barrel is heated electrically, or by a fluid heat exchanger system. Thermocouples placed in the metal barrel wall record, and help to control barrel temperature settings. Sections of barrel, however, are often cooled to remove the excessive heat generated by viscous dissipation. A well designed screw will require a minimum of energy interchanges.

The main operating variables are the frequency of screw rotation and barrel temperature profile. The main design variables are screw diameter and length — -usually expressed as length–to–diameter ratio L/D. These determine to a large

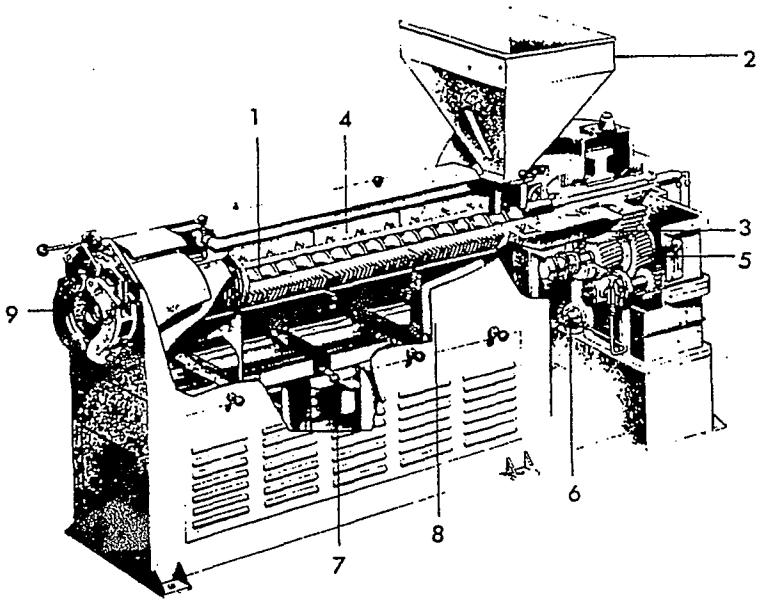

Figure 1.1: Sectional view of a single screw plastics extruder. 1. screw; 2. hopper; 3. feed section; 4. barrel heaters; 5. gear box; 6. lubrication system; 7. air blowers to control barrel heating and cooling temperatures; 8. double walled hood for balanced air flow; 9. die clamp assembly. (From Francis Shaw Co., Ltd., Manchester, England.)

extent extruder throughput, polymer residence time in the extruder, and available barrel surface for heat transfer.

Inherent in the extrusion process is the softening by heat, or solvents, of the materials being formed so that it can be readily conveyed and formed without destroying the desirable final properties of the materials. The machine in which this process takes place is called an *extruder* in the plastics industry.

About 70,000 extruders are in operation in the United States. The plastic–capacity is expanding[1]. The Federal Reserve Board reports that plastics processing capacity–utilization rate averaged 85% in 1989, a sign that more capacity is needed. Cahners Economics, which develops forecasts for *Plastics World* predicts that plastic–parts production will advance 6% this year and resin output will increase by 7%. Freedonia Group of Cleveland says that North American processors bought nearly 600 million lb. of nylon in 1988. High performance application in electrical/electronics markets will help drive nylon consumption up to 780 million lbs. by 1993. In additon, more entries in the medical–equipment category than in the usually dominant computer and business–machine group causes the surging action in the health care market.

Roughly speaking, American consumption of plastics is 70 billion lbs/year. The extrusion products include wires, cables, rods, tubes, pipes, films, sheets, and filaments. With ingenious engineering, even nets and corrugated tubes can be continuously extruded. And with only a few exceptions, all polymers can be extruded, and many may pass a screw extruder not once but twice during their journey from the reactor to the finished product—first a pelletizing extruder after the reactor, then a shaping extruder.

However, the importance is that the extruder must be capable of providing a uniform pressure, or a uniform flow rate, to a sufficiently large, continuous, supply of polymer so that a more or less continuously formed product, or extrudate, will

emerge. That is why this research is being undertaken on how to enhance the polymer particulates with circular and profiled cross–sections because it can make the extrusion of melt process very steady and it can increase both the outputs and quality from extruders.

Chapter 2

INDUSTRIAL BASIS FOR ENHANCING THE INTERPARTICULATE FRICTION COEFFICIENT (IPFC)

2.1 The Single Screw Extrusion Process

Most of the single screw extruders used in the plastics industry are *plasticating extruders*; that is, they are fed by polymer in a particulate solids form. The solids flow gravitationally through the hopper and into the screw channel, where they are conveyed and compressed by a drag induced mechanism. The plasticating extrusion process shown in figure 2.1 consists of four elementary steps: handling of particulate solids in regions 1, 2, and 3; melting pumping, and mixing in region 3, and pumping and mixing in region 4. Devolatilization may also occur in region 3 and 4 by appropriate screw design and operating conditions.

Extruders are manufactured in a very broad range of sizes, starting from diameters of 2 cm, used for laboratory purposes, up to diameters of 50 cm and above, delivering polymers at a rate of 10 tons/hr. Typical length–to–diameter ratios are 18:1–40:1, which gradually evolved from the short (8–10) L/D) rubber extruder. The trend is still toward large L/D ratios, in particular for two stage, and

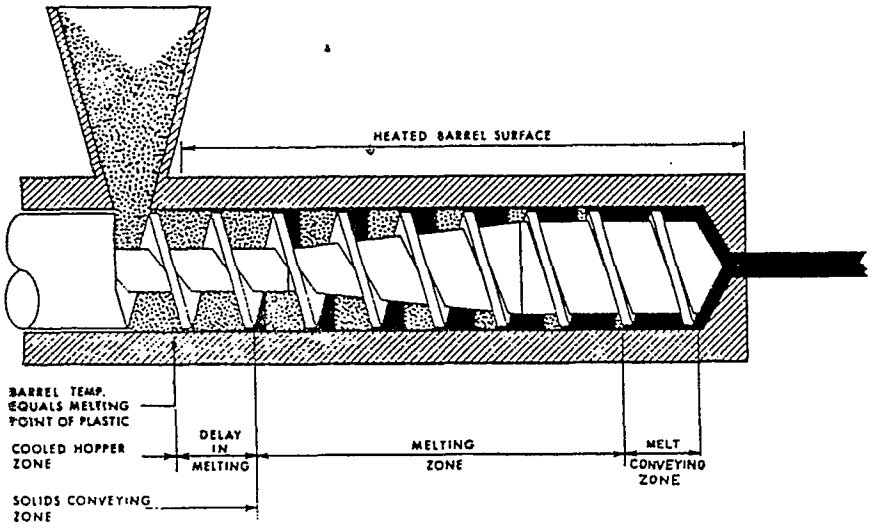

Figure 2.1: Schematic representation of a plasticating extruder. The barrel is cooled in the hopper region and heated downstream

three stage vented extruders and for special purpose extruders, which may reach an L/D ratio of 36–40. Figure 2.2 shows a typical extruder.

The finished product of the extrusion process is determined by the die, which shapes the product, and by the *sizing* equipment, the cooling system, and the cutting equipment, which in turn set the final size and surface quality of the product.

The principle upon which such extruders are based is melt viscosity. The shear stress is the same in all parts of a viscous fluid sheared between parallel plates and the shear rate is directly proportional to the stress and inversely proportional to the viscosity (internal friction) of the fluid.

$$\sigma = \frac{F}{A} \tag{2.1}$$

where σ represents shear stress, F represents shear force, and A represents shear area.

When a plastics granulate is fed to the rotating screw, the material moves forward and, due to shearing of the plastics, frictional heat is generated to melt the materials. To aid in this transition, the outer surface of the barrel is fitted with electrical heaters whose temperature is controlled by thermocouples. The screw acts as a pump and also generates pressure on the melt.

2.2 Extrusion Quality

Due to the growing demands for high output and the development of improved instrumentation for measuring product quality and uniformity, *extrusion quality* has received increasing attention[2]. Extrudate quality is usually measured by appearance, dimensional uniformity or by mechanical weakness.

The quality of the extrudate depends primarily on the melting performance of the extruder and the melting mechanism. Poor extrudate quality is frequently related to cyclic, or random, fluctuations of extrudate temperature, pressure at the die and flow rate due to solid bed breaking–up[3].

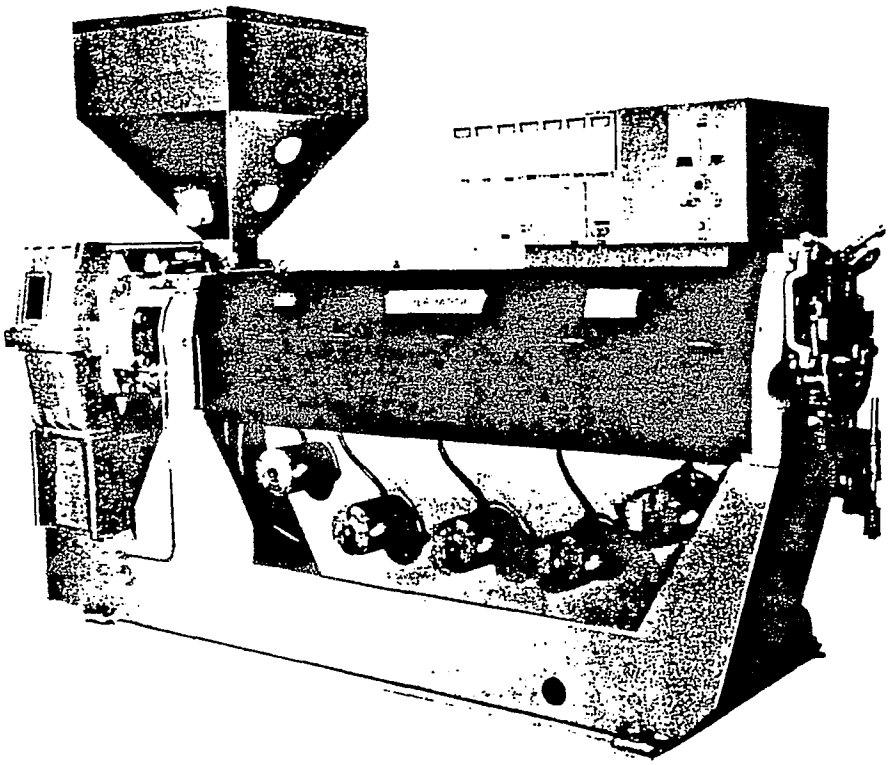

Figure 2.2: A Davis Standard, Thermatic III single screw extruder.(From Davis Standard Co., Pawcatuck, Conn.)

2.3 Melting Mechanisms

Extrusion of melts is one of the critical steps in the processing of plastics. A simple and ingenious experimental technique that permitted a visual analysis of the plasticating extrusion melting process was developed by Maddock[4] and Street.[6] This experimental technique consists of abruptly stopping an extruder operating at steady state, chilling both barrel and screw, pushing out the screw from the barrel, unwinding the polymer from the screw and slicing thin representative sections perpendicular to the flights.

The experimental results showed that the solid and melt phases coexist in screw type extruders. They are clearly segregated from each other, with the melt phase accumulating at the pushing flight in a melting pool and solids segregated at the trailing flight as a solid bed as shown in Figure 2.3. The width of the melt pool gradually increases in the downstream channel direction, whereas that of the solid bed generally decreases. The solid bed, shaped as a continuous long, helical ribbon of varying width and height, slowly turns in the channel sliding toward the exit, while gradually melting. Upstream from the point where melting starts, the whole channel cross–section is occupied by the solid–bed. The continuity of the solid bed provides an explanation for the capability of the screw extruder to generate melt that is free of air bubbles: The porous continuous solid bed provides uninterrupted air–filled passages from deep in the extruder all the way back to the hopper. This phenomenon explains why air entrapped between the solid particles is eliminated.

As the solid bed gradually melts at the interface, there is ample time for the air between the particles to escape through the solid bed and out towards the hopper. Another way to look upon the removal of air, as Street [6] points out, is to consider it stationary and the pellets moving forward.

Further visual analysis of the experimental results by Tadmor et al[20] reveals a tendency of the melt pool to penetrate *under* the solid bed, and occasionally to

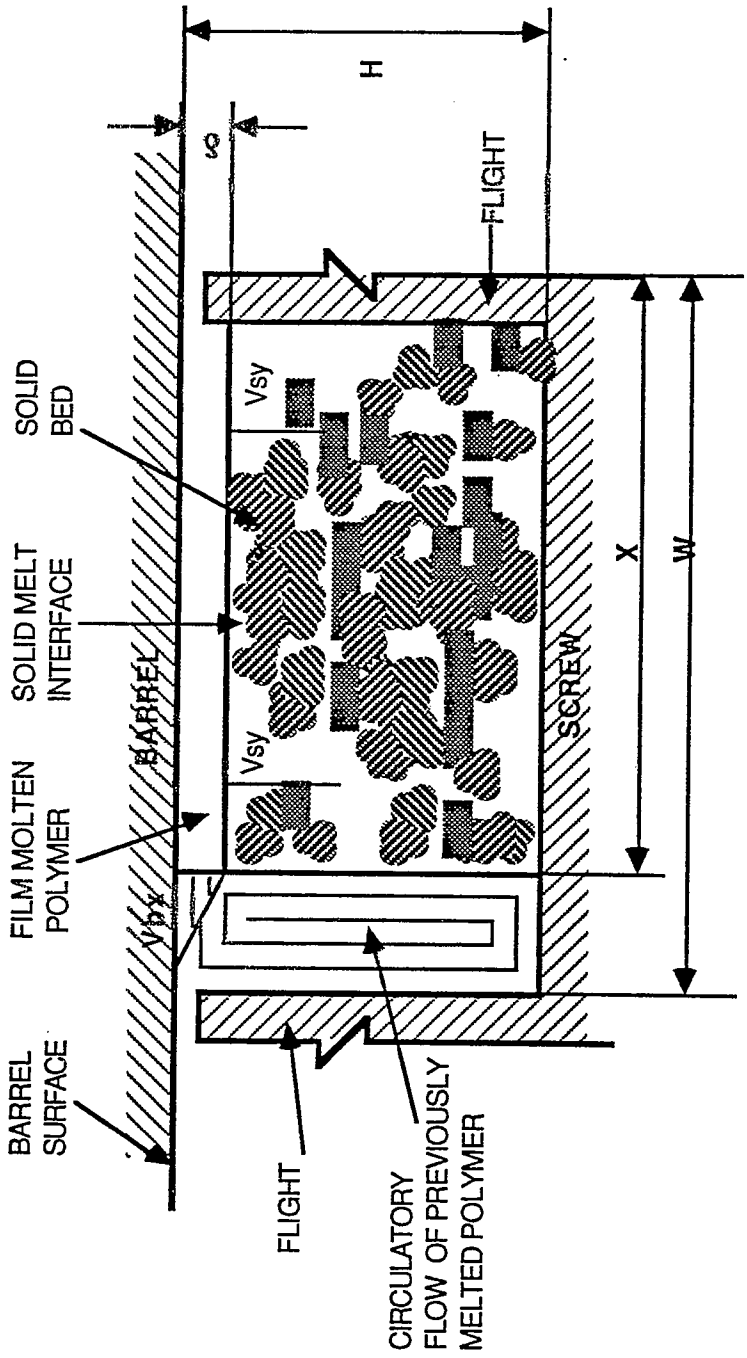

Figure 2.3: Solid bed in the plasticating extruder

completely surround it. Frequently the continuity of the solid bed is broken, and a melt filled gap appears. This tendency of solid bed breakup seems to occur in the tapered sections of the extruder, and it appears to be a source of *surging* (that is fluctuation in time of temperature, pressure, and flow rate) of the extrudate at the die as well as a source of entrapping some air bubbles into the melt stream[18].

This breaking up process is not accidental or random. The solid bed is dragged forward by the barrel. Large pressure gradients exist in the channel, and the solid bed has a different velocity from that of neighboring melt. If the solid bed is relatively weak, it is conceivable that a situation may arise, where the external forces overcome the strength of the bed and cause it to break up. Meanwhile, the rest of the solid bed will move forward until once more external forces overcome it and break it up again. This second, and subsequent, breaking of the solid bed usually occurs at approximately the same point in the extruder as the previous one,. In other words, if the IPFC is relatively strong, the solid bed becomes sturdier, and less easy to break up. Then the sturdier solid bed reduces surging in the entire melting process. So the melting process in an extruder may become very smooth. Therefore the quality of extrusion products is greatly improved, along with enhanced outputs.

As Tadmor[9] pointed out, the breaking up process seems to depend more on the polymer pellet size and screw geometry than on operating conditions. Thus, in the experiment with a smaller pellet size of polypropylene illustrated in Figure 2.4, the solid bed broke only at the very end of the melting process, while in the experiment with large size pellets of low density polyethylene, the solid bed broke much earlier as illustrated in Figure 2.5. Furthermore, in an experiment with powdered rigid polyvinyl chloride the solid bed did not break up at all as shown in Figure 2.6.

It was concluded that the smaller the pellets, the sturdier the solid bed, the

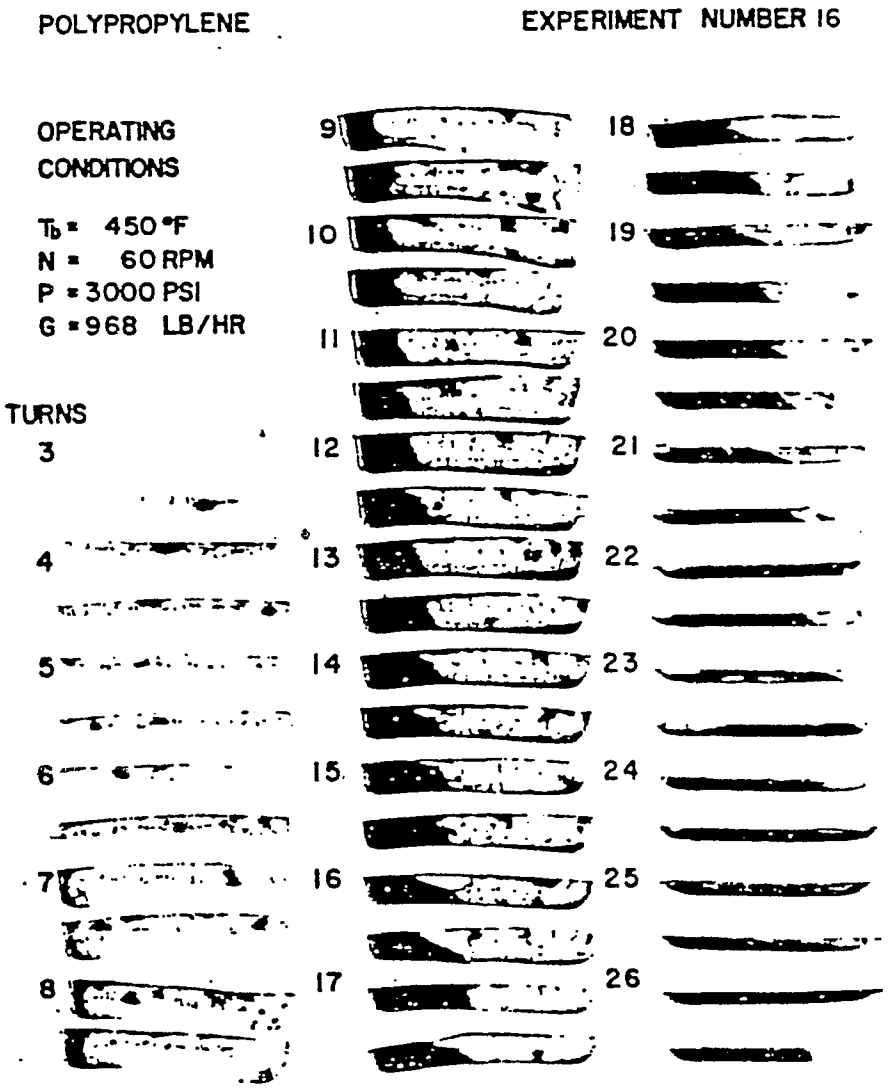

Figure 2.4: Cross–sections obtained from cooling experiment. Polypropylene was extruded at the conditions listed on the figure

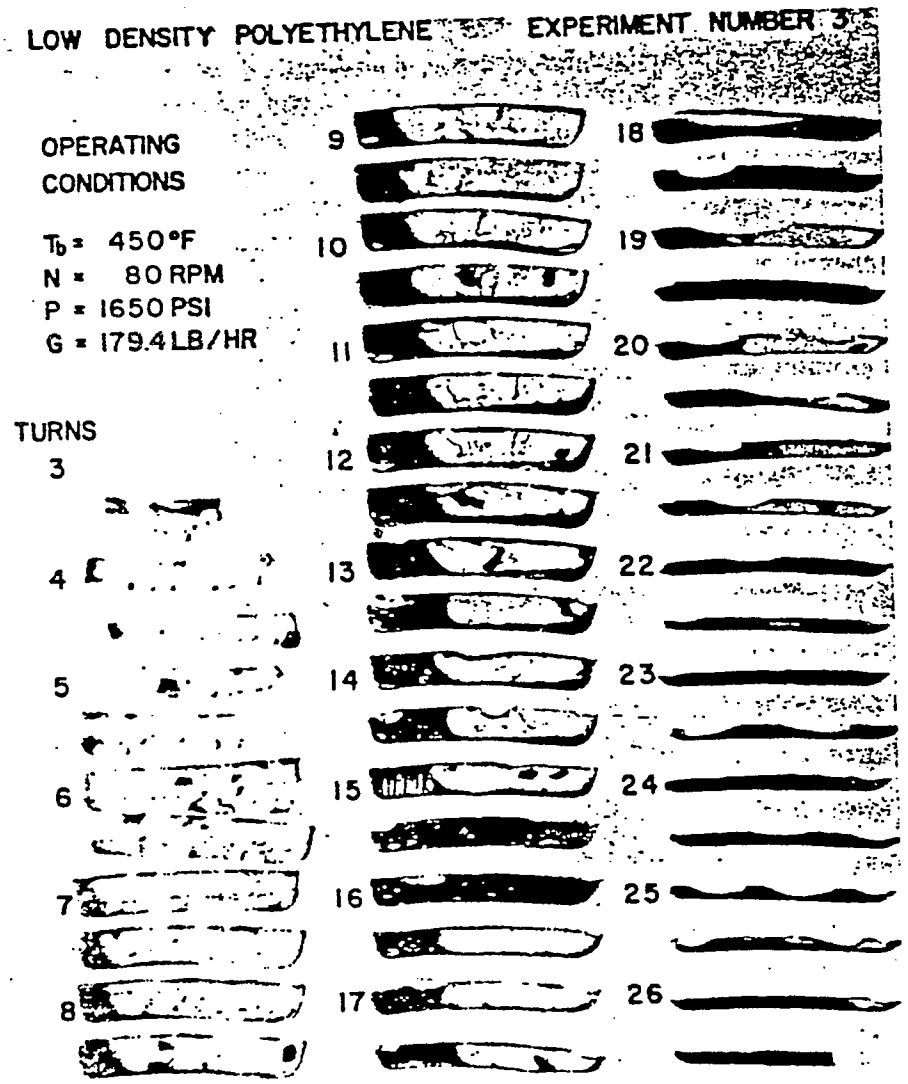

Figure 2.5: Cross–section obtained from cooling experiment. Low density polyethylene was extruded at the conditions listed on the figure.

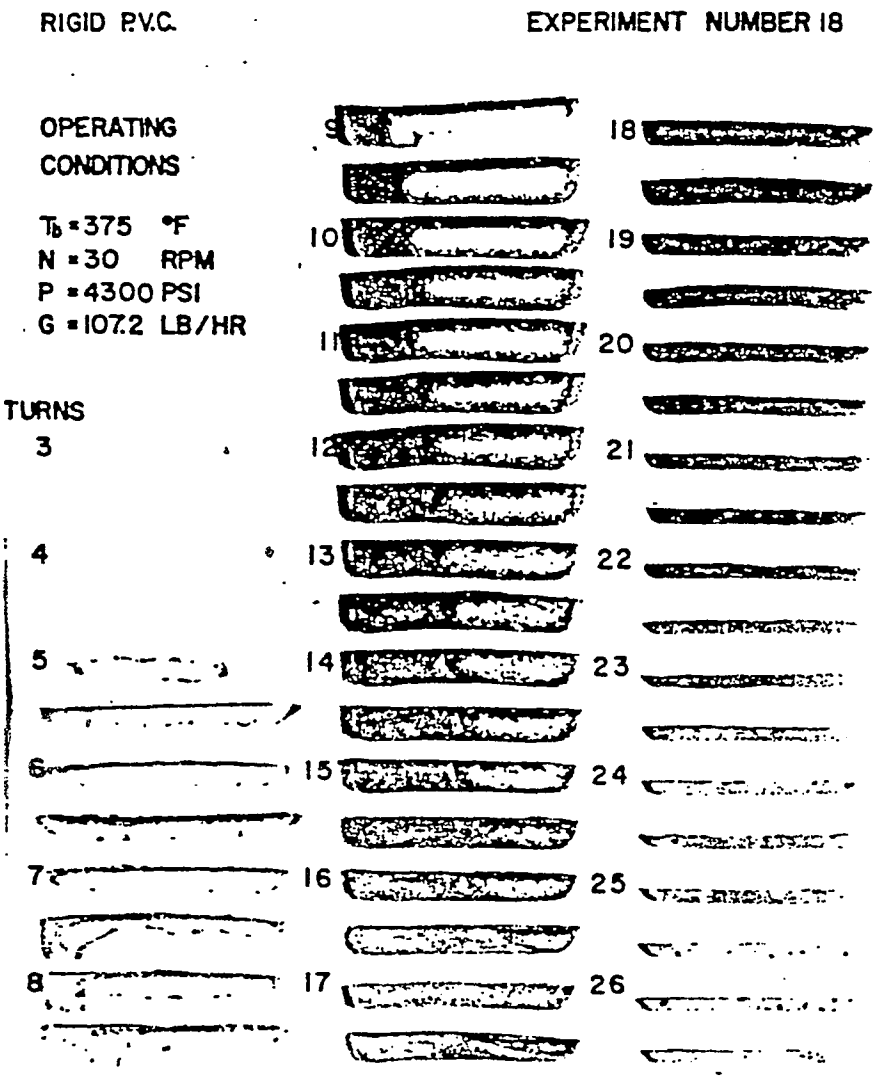

Figure 2.6: Cross–section obtained from cooling experiment. Rigid powered polyvinyl chloride was extruded at the conditions listed on the figure.

more difficult it is for the solid bed to break up. A high taper of the extrusion screw channel in the compression section tends to delay the breaking up process to the beginning of the metering section. Cooling of the screw also stabilizes the solid bed and prevents it from breaking up.[10]

2.4 Barrier Screws

Barrier screws are designed to separate the solid bed from the melt pool. This inhibits solid bed breakup, thereby improving the melting rate and controlling the melting process[11].

An earlier design of this type is Maillefer screw[12]. It has since been modified by many workers. These results have been reviewed by Barr[13].

The first barrier screw employed conventional feed and metering sections and a transition section that incorporated a narrow barrier flight over which only melted resin can pass as shown in Figure 2.7. The barrier clearance is about six times greater than the primary clearance; it rises from the rear of the channel of the main flight where the feed section ends. Because of its greater pitch, it moves closer to the front of the channel as it continues down the transition section until it meets the primary flight at the metering section.

Although a substantial advance, this type of barrier screw has drawbacks. The squeezing action, by which the melted resin is forced from the solid channel over the barrier into the melt channel, is throught by some to cause surging if the rate of change of channel width and depth is not adjusted to each resin type.

In the Hartig MC–3 screw shown in Figure 2.8, the barrier flight has the same helix as the primary flight. Since the widths of both solid and melt channels therefore remain constant, adjustments for the growing volumn ratio of melt to solids are made by changes in channel depth to reduce deformation of the solid bed and thus stabilize the process against surging. The constant width also yields the

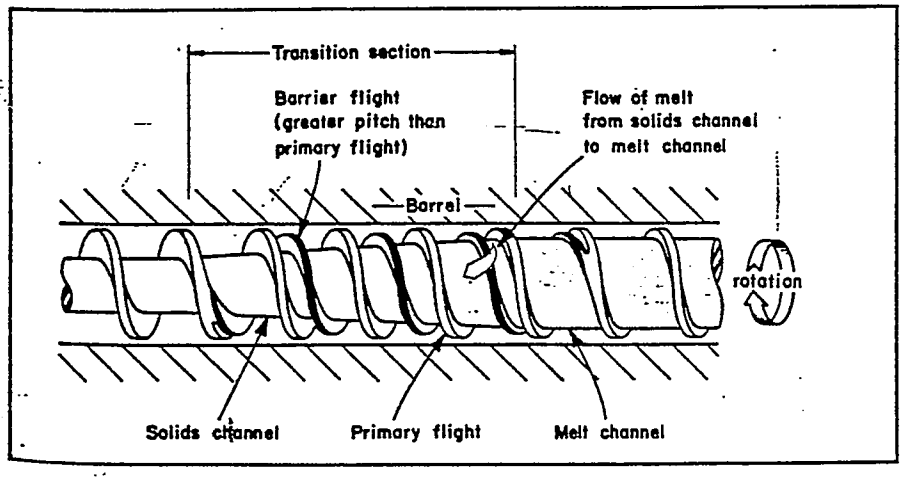

Figure 2.7: To reach the die, material must be able to flow from the solids channel across the barrier to the melt channel. Greater barrier–flight pitch changes the volumn ratio of the two parallel channels as the barrier travels down the screw. (Uniroyal, Inc., N.Y.)

maximum barrel surface area for greater melting. The one remaining problem in both the Hartig and Maillefer screws is that the complete closing of the melt channel at both ends causes high localized shear and the opportunity for melt hangup and degradation. Moreover, the melt channel of the Hartig design, narrow and deep at its outlet, produces cross–channel flow and a considerable melt–temperature gradient.

The Maxmelt screw takes the barrier design one step further shown in Figure 2.9. As in the Hartig model, the parallel melt channel is close–ended, but the barrier flight is created by undercutting the primary flight, and a new primary flight is developed from the trailing edge of the prior one. This allows the resin mass to remain compressed against the rear of the channel, unlike previous designs in which the new barrier flight begins in the rear of the channel and pushes the resin mass to the front of channel, disrupting the flow pattern.

Another barrier screw design, the Barr–2 screw, tries to reduce localized shear with an open–ended melt channel as shown in Figure 2.10. The primary flight terminates in a homogenization section that provides low–shear blending, after melting is complete, to avoid temperature gradients.

An interesting variation in barrier screw with a constant channel width is seen in the "Efficient" screw illustrated in Figure 2.11. Again, the widths of both the melt and solids channels are different yet constant, but the big difference is that the width of the solids channel in the transition section and the width of the channel are alike. This is accomplished by a change in pitch of the primary flight at the end of the feed section. A variant of the "Efficient" screw is the VPS screw, which also has a feed channel and a transition–section solids channel of constant width, and a melt channel of increasing width to accommodate growing amounts of melt shown as Figure 2.12. Constantly increasing helix angles of both flights are used to make these changes.

Pitch changes provide solids with a constant channel width throughout the

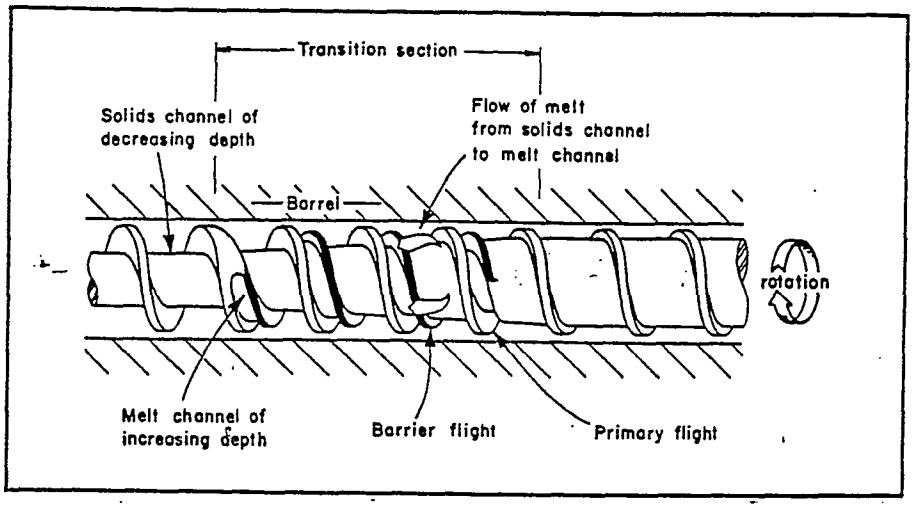

Figure 2.8: The MC–3 barrier screw uses varing channel depth to produce an increasing volume ratio of melt channel to solids channel along the transition section. (Waldron–Hartig Div., Miland–Ross Corp., Cincinnati)

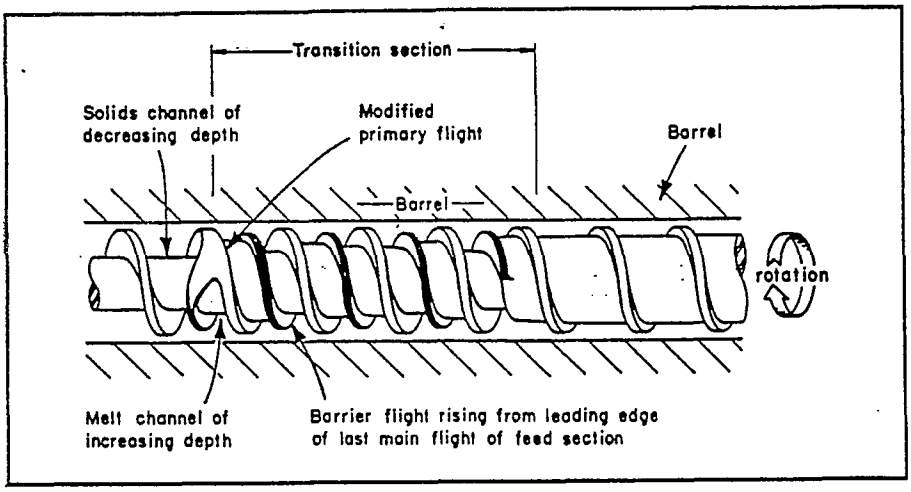

Figure 2.9: In the Maxmelt screw, the barrier flight is created from the rear of the main flight and a new main flights is introduced. The flow path remains undisturbed, and the solid bed moves smoothly from the feed section into the solids channel of the transition. (Hoover Ball and Bearing Co., Saline, Mich.)

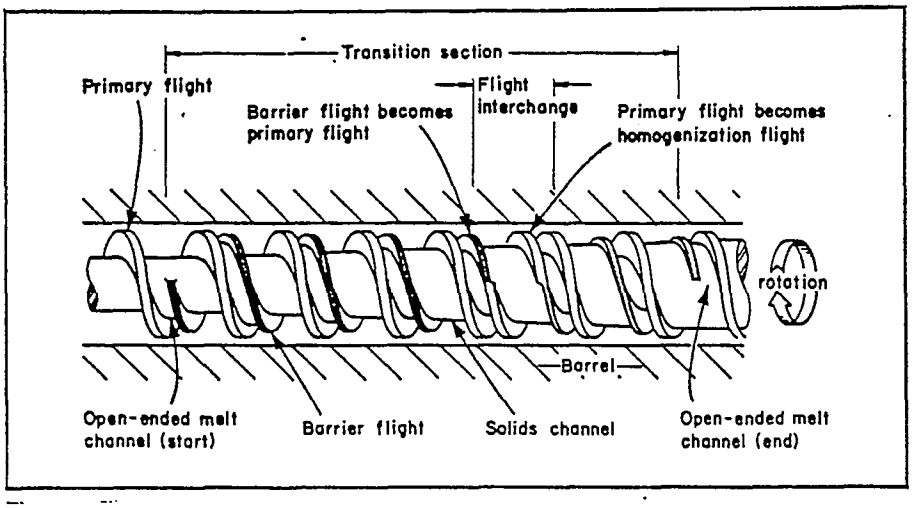

Figure 2.10: The Barr–2 screw uses open–ended melt and solid channels to reduce localized shear, melt hangup, and degradation. A homogenization section has been added at the end of the primary flight (at the start of the metering section) to provide low–shear blending to avoid temperature gradients (Robert Barr, Inc., Virginia Beach, Va.)

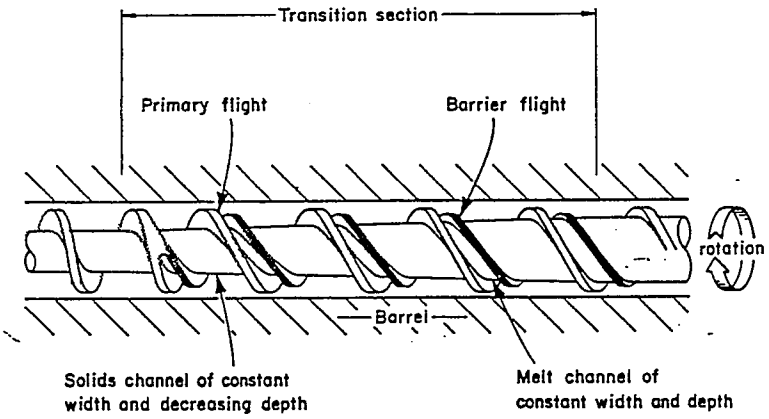

Figure 2.11: The "Efficient" screw uses feed channels and transition–section solids channels of equal and constant width to prevent solid–bed deformation and surging. This is accomplished by a change in pitch of the primary flight at the end of feed section (Feed Screws Div., New Castle Industries, New Castle, Pa.)

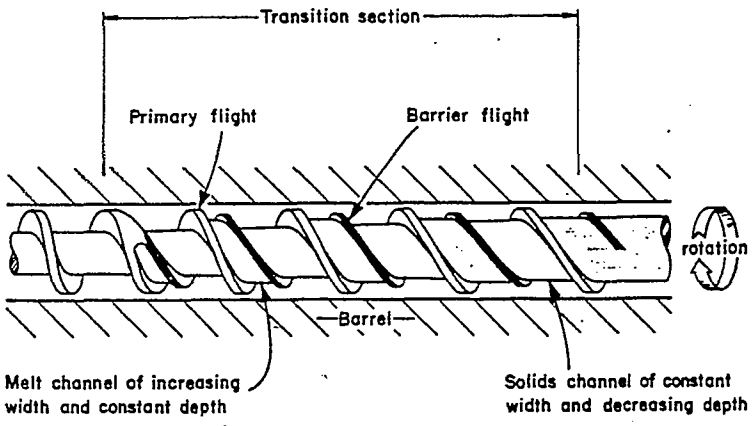

Figure 2.12: The VPB screw also uses feed channels and transition–section solids channels of equal and constant width to prevent surging. An increasing melt channel width accommodates the grpwing volumn of melt. The pitch of both flights changes at the end of the feed section and gradually increase throughout the transition section. (Davis–Stadard Div., Crompton and Knowles Corp., Pawcatuck, Conn.)

feed and transition sections. The greater solid–bed surface and the reduced tendency for surging improves the melting capacity.

Chapter 3

NATURE OF INTERPARTICULATE SOLIDS FRICTION

3.1 Mechanics of Friction

Solid friction is the resistance offered to the sliding of one solid body over another. An idea conceived by De La Hire[14] is that *the surface irregularities or asperities are responsible for the force of friction by interlocking and either deforming, or abrading, each other during relative motion.* From this observation, trilobal and bilobal cross–sections would tends lock each other more tightly than circular cross–sections under the same pressure. Therefore, the IPFC for trilobal and bilobal cross– sections is expected to be superior.

Bowden and Tabor [15] proposed that friction arises from two main factors. *The first, and usually the more important factor, is the adhesion which occurs at the regions of real contact. These adhesions, welds or junctions have to be sheared if sliding is to occur. The second factor arises from the ploughing or cracking of one surface by the asperities on the other.* By neglecting the second factor relative to the first their theory can explain two important experimental observations. The first observation is that friction is independent of apparent contact area. The second observation is that the friction force is proportional to the normal load between

the surfaces known as Admonton's Law [16] illustrated in Figure 3.1. This is the principle by which the IPFC is defined in this thesis.

3.2 The Solids Conveying Zone in Single Screw Extruders

Polymeric particulates in the form of powders, pellets or other shapes is fed into the extruder through a hopper, and then fills, and moves forward, in the helical channel of the screw. The driving force for the movement of the polymer is the friction force between the barrel surface and the solid polymer.

In the plasticating extrusion theory it is assumed that the solid polymer is compacted into a solid plug in the solids conveying zone. The plug is conveyed down channel due to the torque and the frictional force on the barrel surface relative to those on the screw. As this plug advances at a constant velocity, it is subjected to increasing temperature and pressure which can produce changes in the friction between both the screw/polymer and barrel/polymer surfaces.

Particulate solids are made up of loose, discrete particles of more or less uniform size. Brown and Richards[17] defined the properties of solid particulates and their response to external forces as a blend of a) liquidlike behavior b) solidlike behavior, and c) particle–interface dominated behavior. Like liquids, particulate systems take the shape of the container they occupy, exert pressure on container walls, and flow through openings. Yet, like solids, they sustain shearing stress (hence they form piles), possess cohesive strength and exhibit nonisotropic stress distributions upon the application of unidirectional loads rather than the application of rates of deformation. Unlike a solid for particulate solid, the magnitude of the shearing stress is generally indeterminate, and all that can be said is that the following inequality holds,

$$\tau \leq f'\sigma \tag{3.1}$$

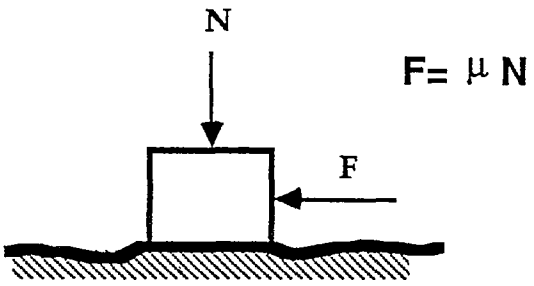

Figure 3.1: The schemetic view of Amonton's Law

where f' is the static interparticulate coefficient of friction and σ represents a range of normal forces (*pressures*) that can be applied to the particulate system before the value of shear stress τ is reached that is high enough to start the particles sliding past one another[18].

Again the inequality given above is also the equation for principle of determining the interparticle static coefficient of friction in this work.

Only the static IPFC not the sliding IPFC has been tested. This difference between static and kinematic coefficient of friction is caused by the *slip–stick* motion that usually occurs during dry sliding. *Slip* occurs when the forces become sufficiently large to shear and plough the material. During *slip*, the area of real contact and the friction rapidly decrease.

3.3 Agglomeration.

Agglomeration means the forming of an aggregate from the individual particles. Agglomeration occurs because of the binding forces between the particles.[19] Agglomeration transforms noncohesive free flowing particulates to cohesive particulates. Solid–solid forces are significantly amplified by increases in pressure and temperature, which induce simultaneously an increase in contact area.

A noncohesive particulate system at fully mobilized friction conditions follows the equation,

$$\tau = tan\beta\sigma = f'\sigma \tag{3.2}$$

where β is the angle of internal friction,

A cohesive particulate system gains strength when pressure is applied. Consequently, their relation between normal forces (*pressure*) and the shear stress is the function of the consolidation pressure and the consolidation time. Although agglomerated particulates will enhance the IPFC, in many instances, the aggomeration will

recur when the particulates should be flowing freely.

3.4 Compaction

In polymer processing, including extrusion, particulate solids are compacted prior to melting. The performance of extruders is greatly influenced by the compaction behavior of the solids[20].

The compaction is obtained by applying an external force. This force is transmitted within the system through the points of contact between the particles. By a process of elastic and plastic deformation, shear deformation and local failure, the points of contact increase, as do the forces holding the particles together. The externally applied force generates an internal stress field, which, in turn, determines the compaction behavior.

Compaction of powders was discussed by Train and Lewis[21], who pointed out that Wollaston[22] was the first scientific worker in this field to realize that high pressures were needed for compaction of dry powders.

Considering an apparently simple situation of compaction in a cylinder as shown in (Figure 3.2). A normal force F_O applied to the top ram generates a certain normal stress as well as a radial stress. The friction shear force due to the latter acts in the opposite direction to the applied force. Hence the transmitted force to the lower ram F_L will be smaller than the applied force.

The response of polymeric particulate solid to compaction was investigated experimentally by Schneider[23] and Goldacker[24]. For polyethylene, for example, a constant radial to axial stress ratio of 0.4 was observed.

3.5 Grooved Feed Throats

Grooved feed throat extruders, with intensively cooled feed sections as shown in Figure 3.3, provide a simple, effective solution to processing tough materials,

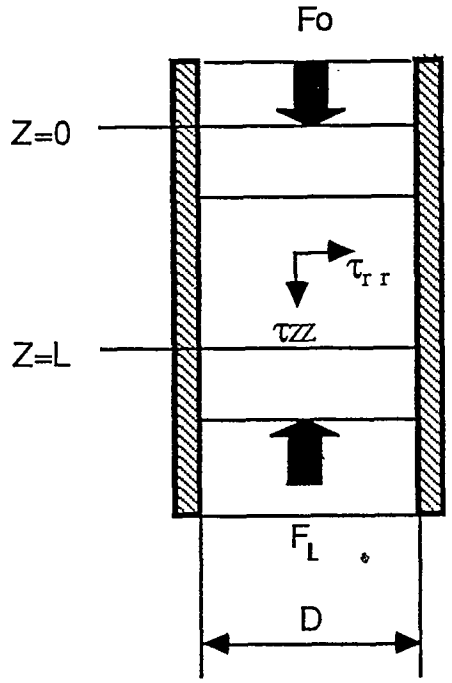

Figure 3.2: Compaction in a cylindrical channel, between frictionless pistons. F_O is the applied force, F_L is the resultant force on the lower piston.

from high molecular weight HDPE to PP and a range of others[25].

The grooved feed sections increase initial compression and increase material turbulence for improved conveying compared with conventional smooth–throat feeds.

Typically, grooved feed sections have axial or helical grooves cut in the throat liner. The grooved sections extend for about three screw diameters beyond the feed opening as shown in Figure 3.3.

For those resins with low or moderate coefficients of friction,the grooved feed section increases feed rates, hence improves outputs. The grooves provide greater improvement in resins with low coeffiients of friction because grooves enable the screw to rotate through the resin mass rather than turning the solid with each revolution and create the friction necessary for high outputs.

Water cooling keeps the resin from overheating and plugging up the grooves. Thus, for most materials, intensive cooling is essential to achieve optimum effects from the grooved feed throats.

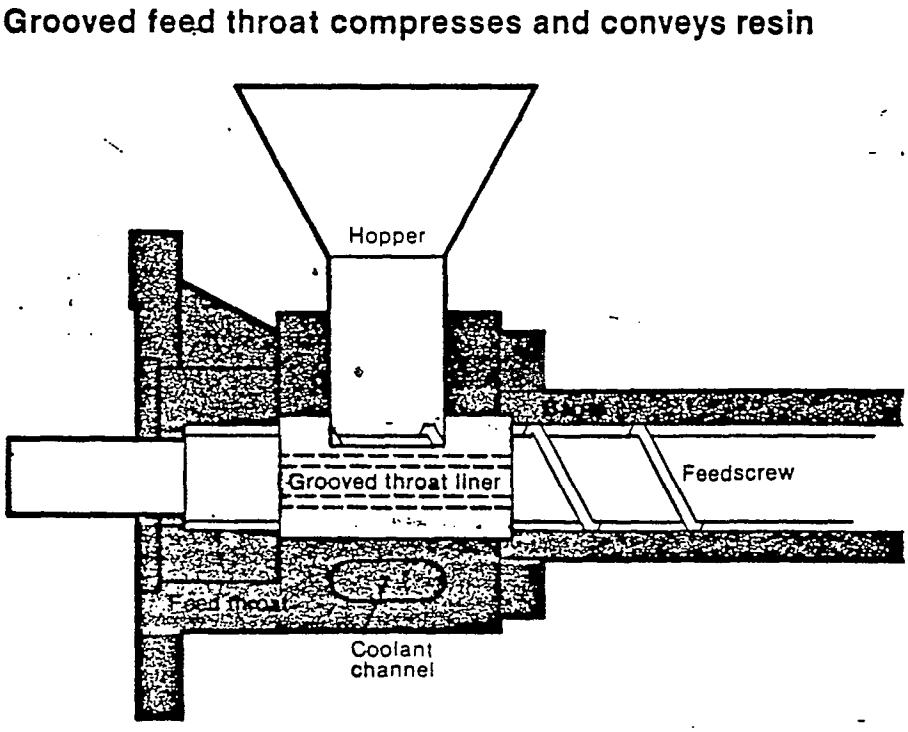

Figure 3.3: The groove liner, inserted in the feed throat section, compresses and conveys difficult to process materilas effectively. The liner typically contains 6–8 longitudinal grooves to provide friction in the feed section. Most applications require intensively cooled feed sections with a heat barrier to seperate the cooled area from the rest of the barrel. (Source, Midland–Ross)

Chapter 4

NATURE OF INTERPARTICULATE SOLIDS FRICTION: PARTICULATES WITH CIRCULAR AND PROFILED CROSS-SECTIONS

4.1 Particulate Configurations

The motivation for this work is provided by considering what may be expected to occur as pellets of bilobal and trilobal cross section contained in solid beds are subjected to shear forces. The cross sections under consideration are shown in Figure 4.1.

Consider the possible arrangements of individual pellets in the shear cell. For pellets with circular cross–sections, there are only four possible arrangements as shown in Figure 4.2.

For pellets with bilobal cross–sections, there are at least seven possible arrangements shown in Figure 4.3.

For pellets with trilobal cross–section, there are at least nine possible arrangements as shown in Figure 4.4.

Clearly the locking action of the multilobal pellets can be produced to exhibit greater IPFC values.

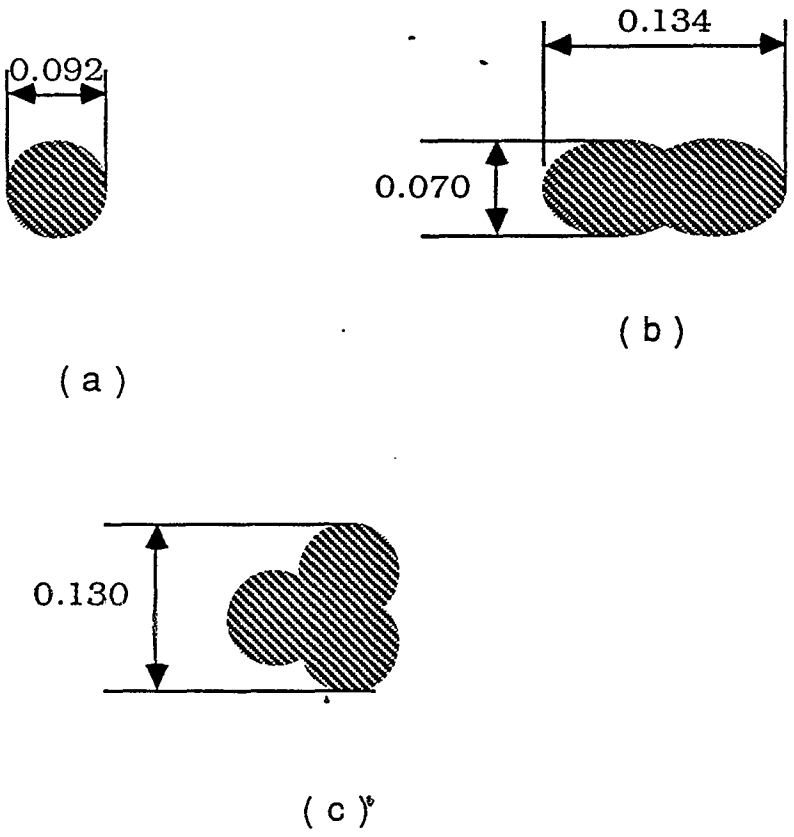

Figure 4.1: Different cross–sections of polymers (a) circular cross–section, (b) Bilobal cross–section, (c) Trilobal cross–section.

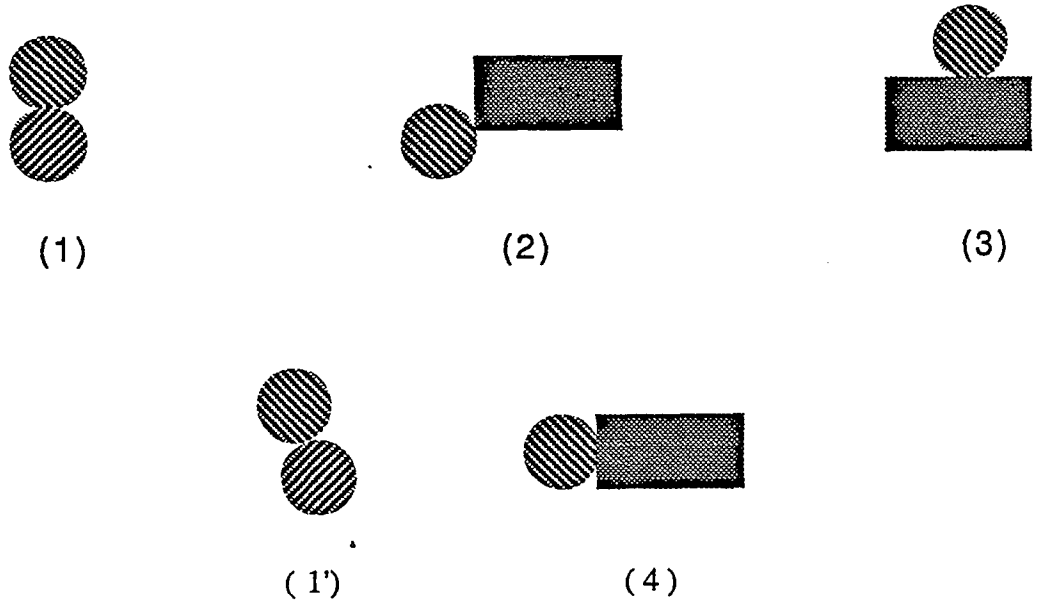

Figure 4.2: Four Possible Arrangements of Circular Cross–section

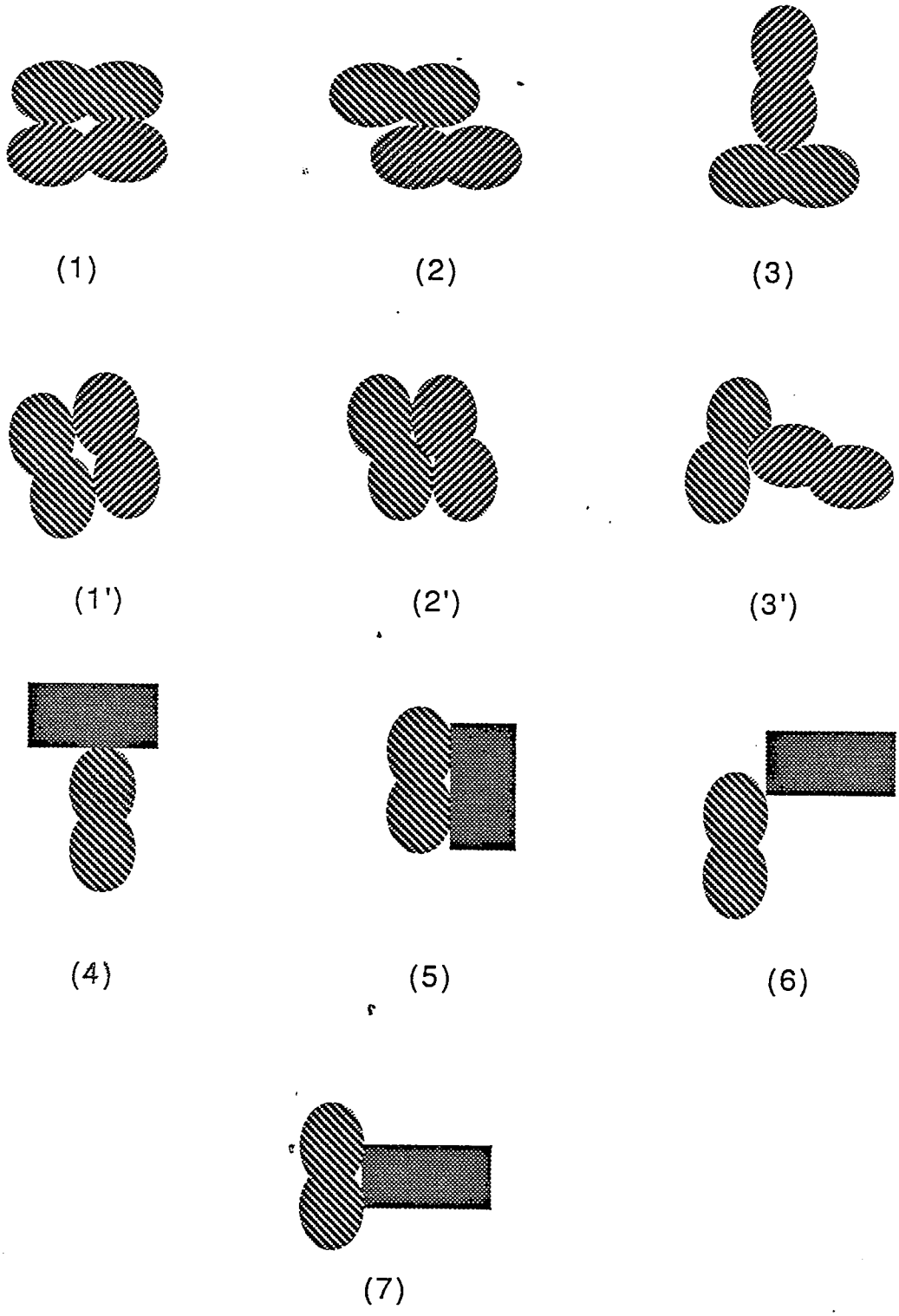

Figure 4.3: Seven Possible Arrangements of Bilobal Cross-section

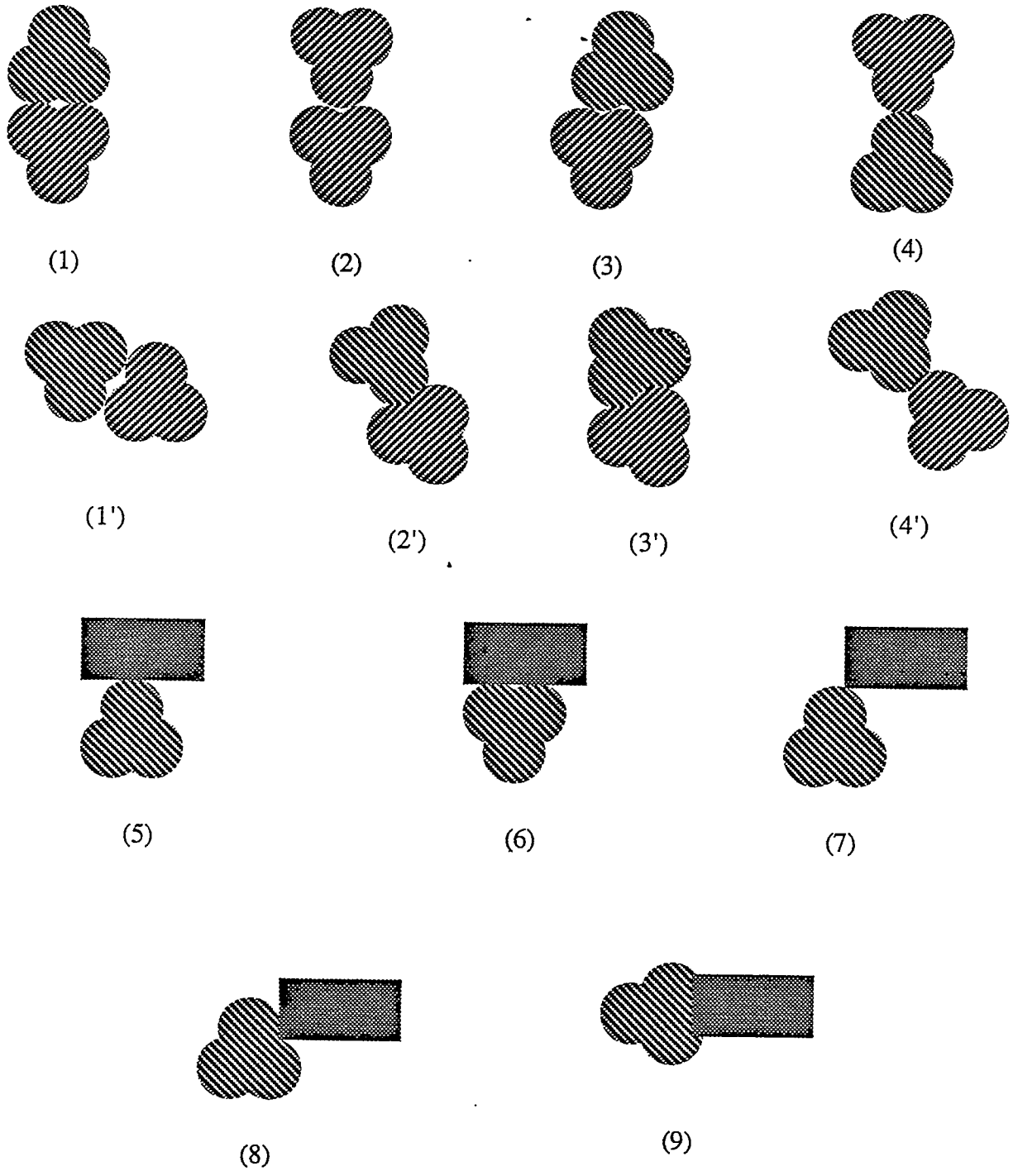

Figure 4.4: Nine Possible Arrangements of Trilobal Cross–section

4.2 Modelling Particulate Beds

Consider, however, what happens in a bed of particulates containing each type of pellet cross sections. First, consider the follow situations.

- Polymer pellets are randomly arranged .
- The internal friction force caused by the external load which is the normal load acting on polymer pellets are the same among all pellets.
- All the pellets are considered to be individual and rigid.

Since pellets are randomly arranged, according to Figure 4.2 the probability of each arrangement for circular cross-section $p_1 = \frac{1}{4}$.

According to Figure 4.3, the probability of bilobal cross–section arrangement $p_2 = \frac{1}{7}$. And according to Figure 4.4, the probability of trilobal cross–section arrangement $p_3 = \frac{1}{9}$.

For circular cross–section, no matter what arrangements are , there is always one contact line (n_1) (or contact point). Therefore the mean value of contact line (or contact point) μ_1 is

$$\begin{aligned} \mu_1 &= n_1 \times p_1 \\ &= 1 \times \frac{1}{4} + 1 \times \frac{1}{4} + 1 \times \frac{1}{4} + 1 \times \frac{1}{4} \\ &= 1.0 \end{aligned}$$

For bilobal cross–section, however, some arrangements have one contact line (or point), some two contact lines (or contact points) as shown in figure 4.3 and figure 4.7. Hence, the mean value of contact lines for bilobol cross–section μ_2 is

$$\begin{aligned} \mu_2 &= n_2 \times p_2 \\ &= 2 \times \frac{1}{7} + 1 \times \frac{1}{7} + 2 \times \frac{1}{7} + \end{aligned}$$

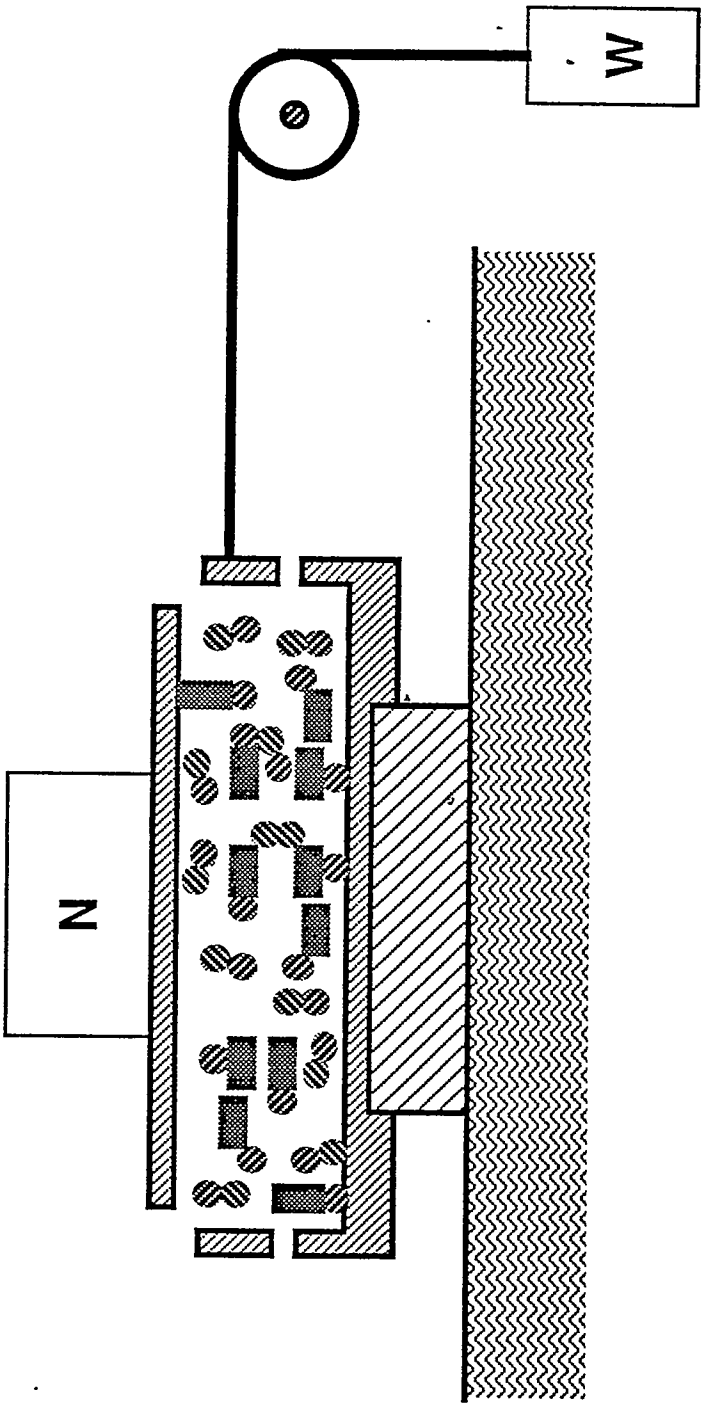

Figure 4.5: The possible arrangements of the circular cross-section in full shear cell.

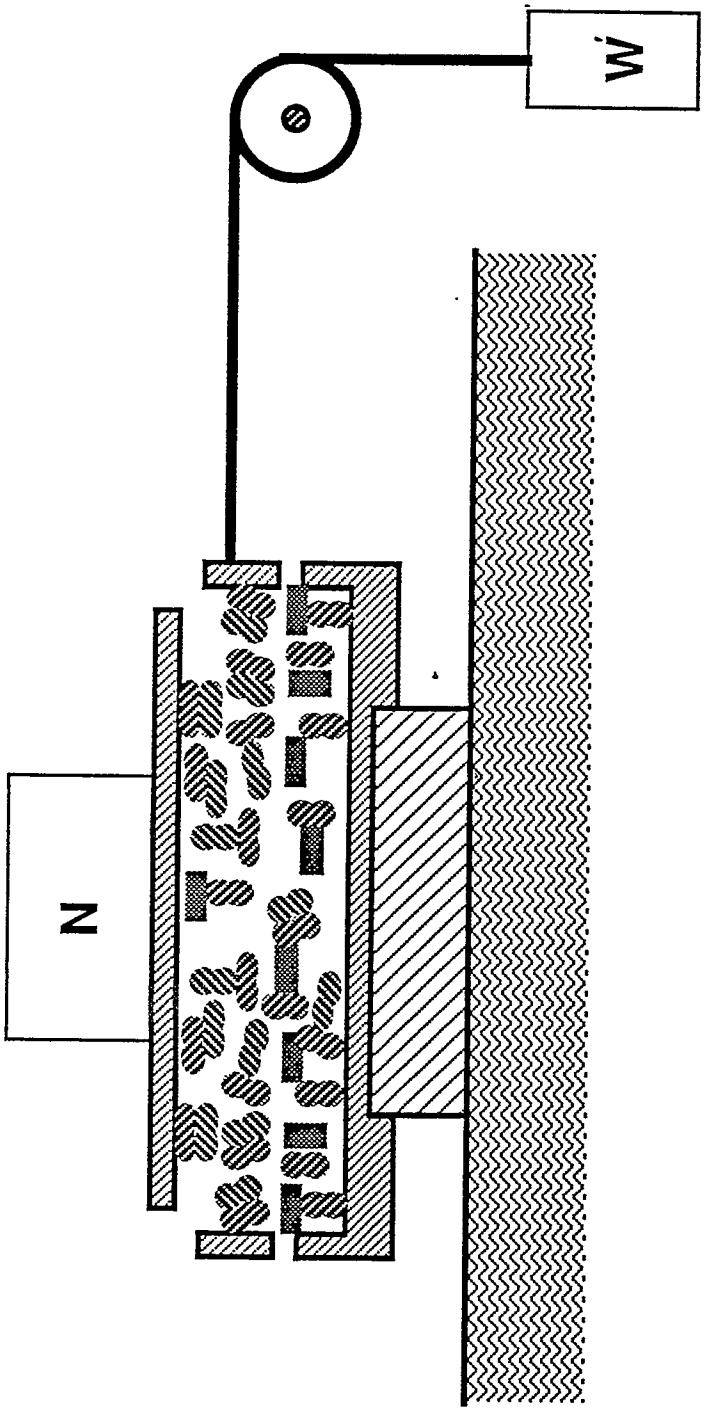

Figure 4.6: The possible arrangements of the bilobal cross–section in full shear cell.

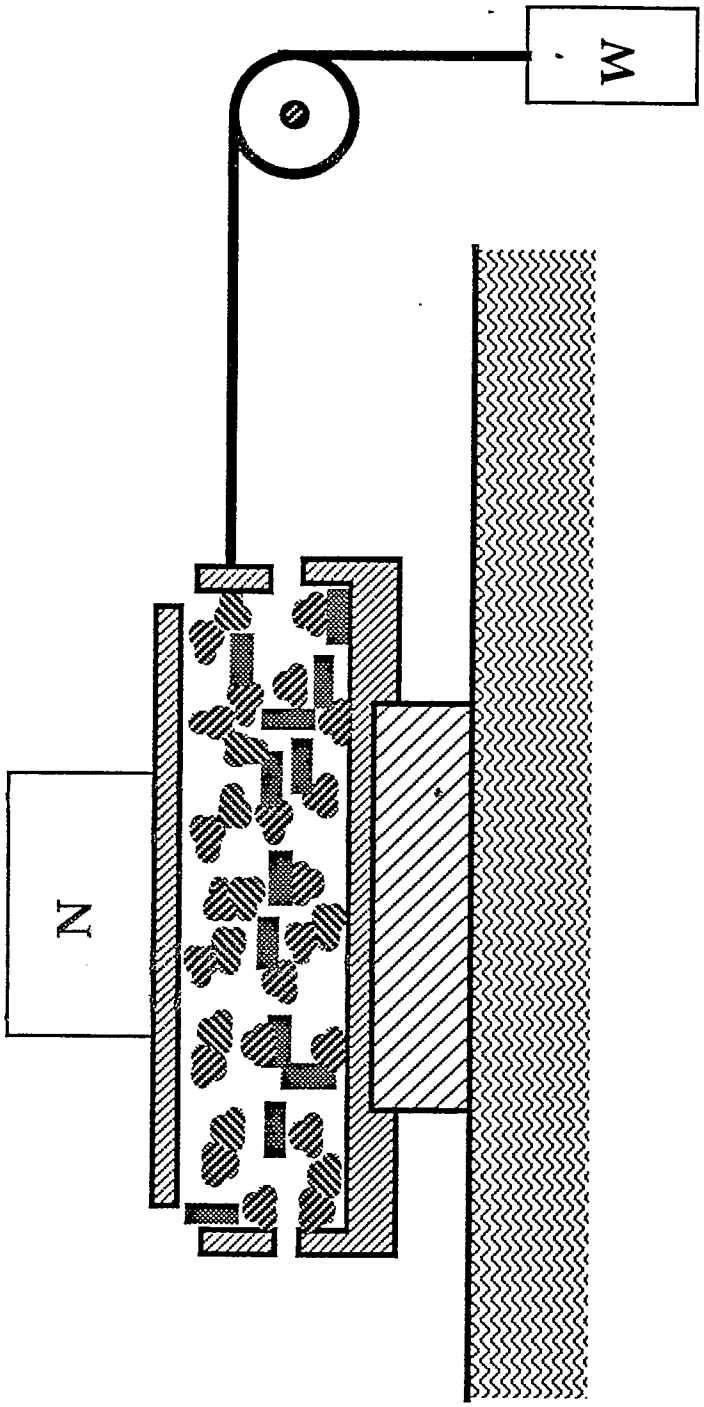

Figure 4.7: The possible arrangements of the trilobal cross–section in full shear cell.

$$1 \times \frac{1}{7} + 2 \times \frac{1}{7} + 1 \times \frac{1}{7} +$$
$$2 \times \frac{1}{7} = 1.571$$

The same assumption as bilobal cross–section, The mean value of contact lines (or points) for bilobal cross–section μ_3 is

$$\begin{aligned} \mu_3 &= n_3 \times p_3 \\ &= 2 \times \frac{1}{9} + 2 \times \frac{1}{9} + 3 \times \frac{1}{9} + \\ &\quad 1 \times \frac{1}{9} + 1 \times \frac{1}{9} + 2 \times \frac{1}{9} + \\ &\quad 1 \times \frac{1}{9} + 1 \times \frac{1}{13} + 2 \times \frac{1}{13} = 1.667 \end{aligned}$$

Therefore the number of contact lines (or points) of trilobal and bilobal pellets is much greater than for circular cross–section pellets.

For the nature of friction discussed in chapter 3, with an individual rigid pellet, the more the contact lines or contact points the greater the total internal friction. In other words, the surface irregularities and asperities would tend to cause the pellets to interlock more because more contact points cause the surface welding together and more contact points represent more real contact area. According to the adhesion theory[26], the frictional force is the product of the true area of contact and the shear strength of the compounds.

4.3 Role of Modulus in IPFC

Since the real contact area is only a fraction of the apparent contact area, the pressure developed is sufficiently high to produce elastic or plastic deformation of the materials. The consequent enlargement of the area of contact which occurs continues until the pressure has fallen to the yield value at which point the area of contact is $A = nP_Y$ [27], where n is the load supported by the individual asperity.

At this stage, the surface materials are in such intimate contact that asperities may for some materials become welded together and the tangential force F required

to break such a contact can be represented as

$$F = SA_. \tag{4.1}$$

where S is the shear strength of the weld. This gives $F = Sn/P_Y$ and as S and P_Y are presumably constants for the system and this results in the local friction law $f = \mu n$ with the constant $\mu = S/P_Y$. If it is assumed that all such contacts break at the same moment under the application of an external shearing force F and all F's are parallel to F, we have

$$F = \sum F = (S/P_Y) \sum n = (S/P_Y)N = \mu N \tag{4.2}$$

where N is the total normal force.

This is the physical picture that frictional resistance is proportional to the normal force and independent to the area of the sliding surface. This accounts satisfactorily for most cases of metallic friction. The solid polymer in various forms are in a state far removed from the ideal for solid just described. The observed frictional force is related to the normal force by the empirical equation

$$F = CN^{\alpha} \tag{4.3}$$

Where C is a constant and α is usually found to lie between 2/3 and unity[28]. It has been suggested that $\alpha = 2/3$ corresponds to the case of pure elastic deformation at the contact points, whereas $\alpha = 1$, to purely plastic (yielding) deformation. Hence, values in between appear to reflect viscoelastic deformation at the contact points.

Chapter 5

TEST APPARATUS AND TEST PROCEDURE

5.1 Design of the Test Apparatus

The experiment test apparatus used for the measurement of the IPFC is shown in Figure 5.1 in a schematic and in Figure 5.2 through Figure 5.5 as photographs. It consists of four pieces with pulley and cable. The pulley is at the edge of table and the shearing cell near the middle of the table.

Before the equation of IPFC being conducted, there are following assumptions.

- The solid polymer is compacted into a solid plug in a solid conveying zone. The plug is conveyed down channel due to the high torque and frictional force on the barrel surface relative to those on the screw as described earlier.
- The friction between the cable and pulley is neglected because the cable does not slip on the pulley and the pulley is free of moving.
- The coefficient of friction of rolling bearings f = 0.0015[29]

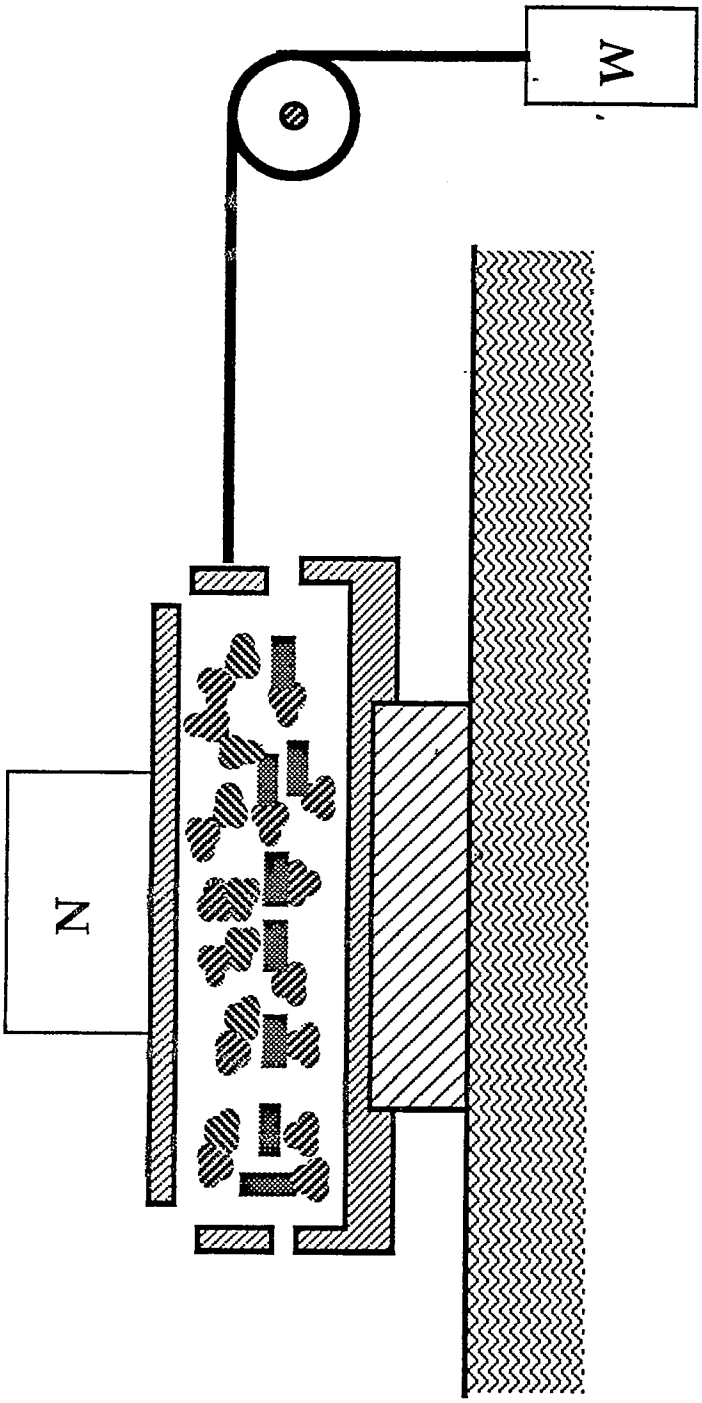

Figure 5.1: Experimental test apparatus

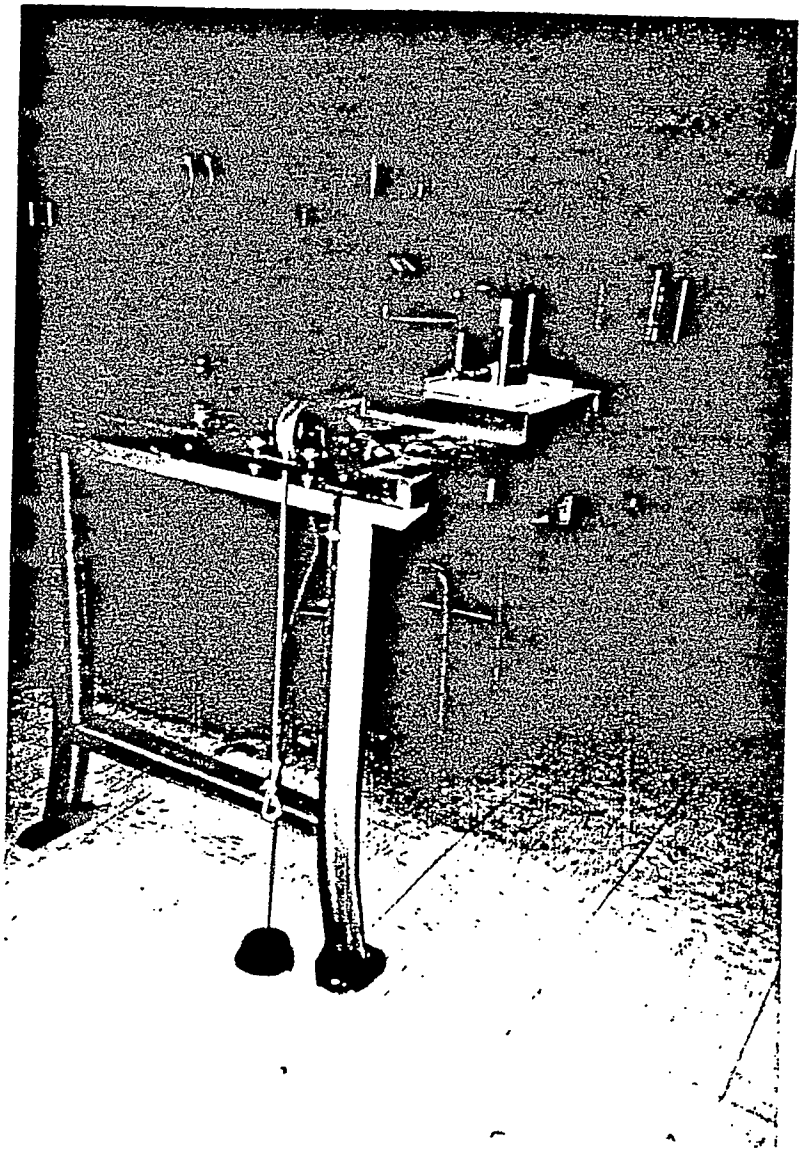

Figure 5.2: Experimental test apparatus with the normal load and weight on

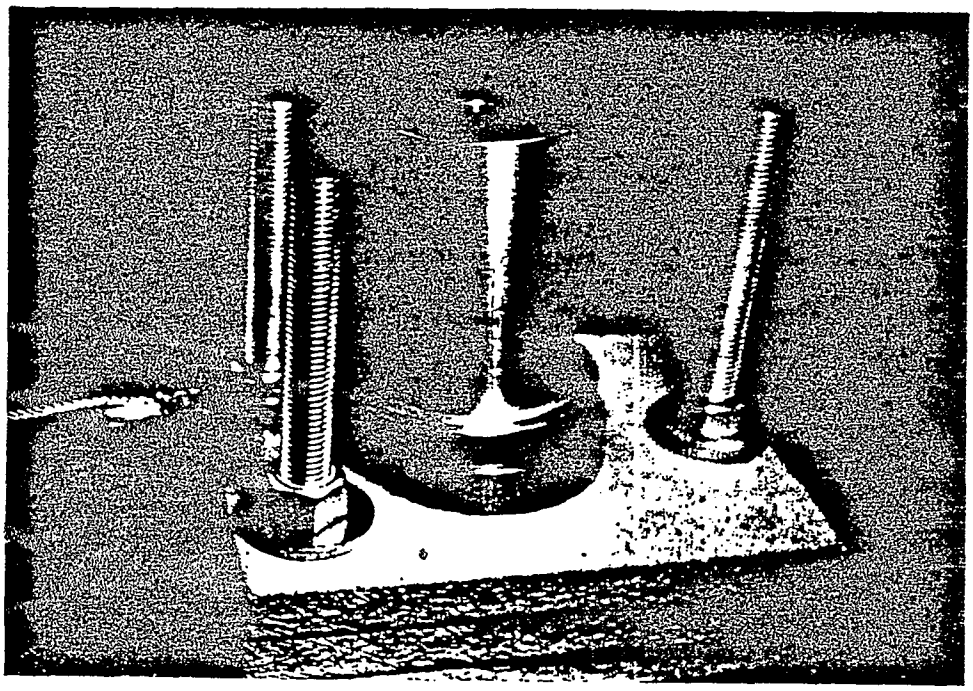

Figure 5.3: The moment the ring starts moving after the weight applied

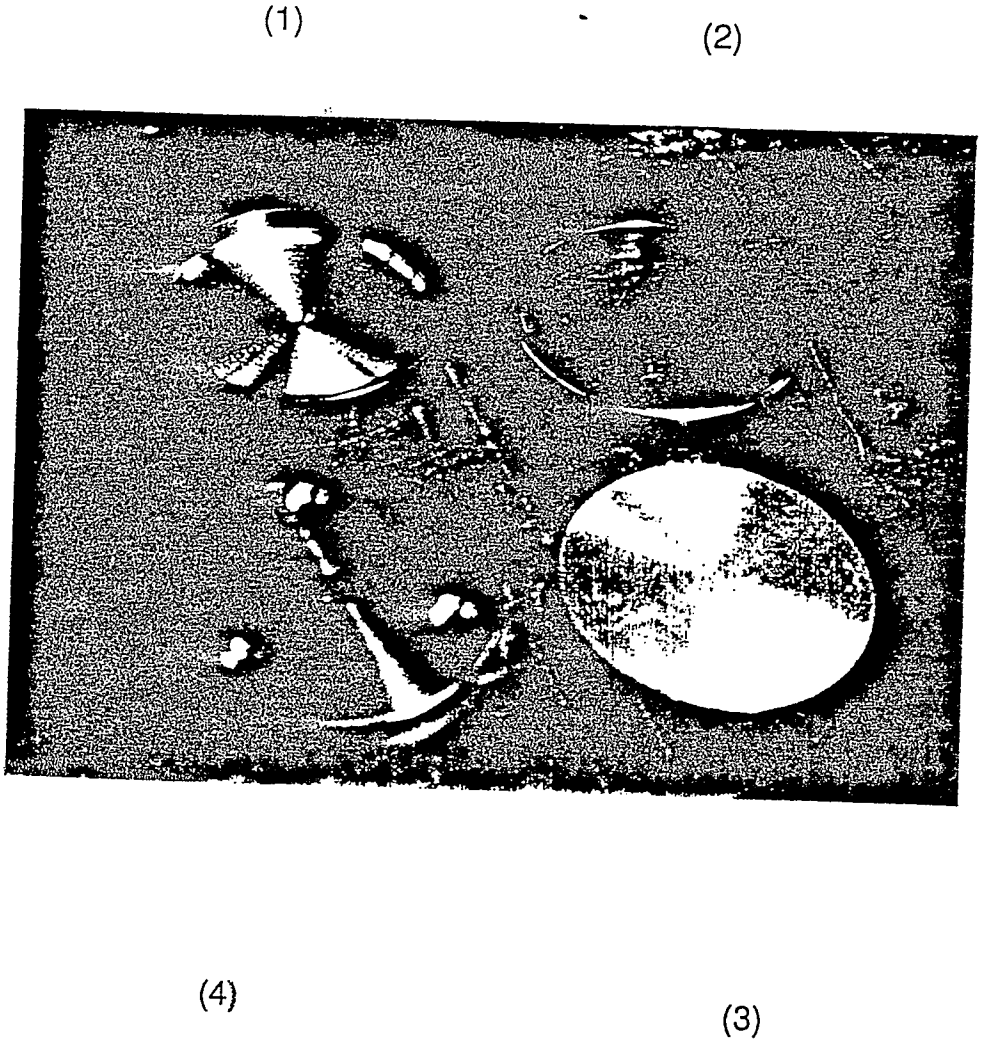

Figure 5.4: The components of experimental test apparatus. 1. Bottem shell cell; 2. Movable Ring; 3. Top plate; 4. Base

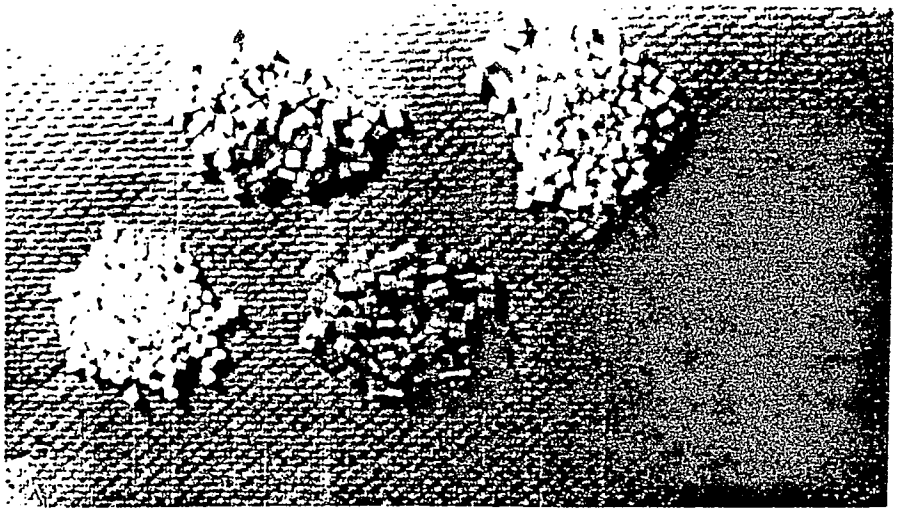

(a)

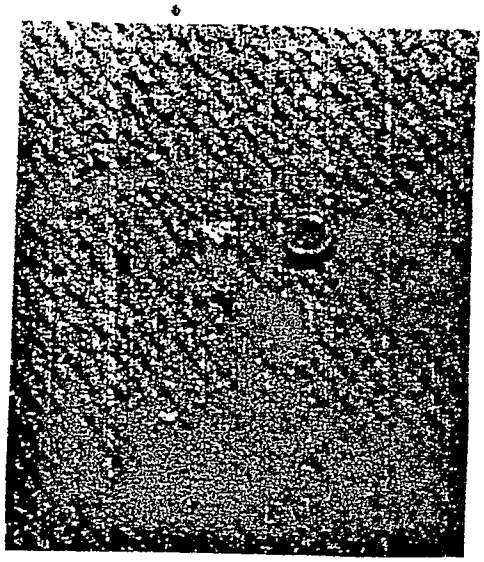

(b)

Figure 5.5: The various pellets forms being tested. (a) Sample pellets, (b) Circular, bilobal, and trilobal pellets

5.2 Test Procedure

As shown in Figure 5.1, the pulley and the shear cell are placed in a consolidating bench where the plastic pellets are consolidated for the required pressure and time. By measuring the shearing strength of the pellet at a number of normal loads below the consolidating pressure, the IPFC is determined. Repeating the test at other consolidating pressure provides the series of IPFC for a particular polymer materials. The more details of testing steps are as follow:

- Apply the required normal load (N_1) on the top of the shear cell.
- Increase the weight (W) vertically just until the movable ring starts moving. Notice that the moment the ring starts moving, stop adding the weight immediately.
- Record the normal force (N) and the weight (W).
- Repeat from step 1 to step 3 four times with the same normal load, and calculate the average weight

$$\overline{W} = \frac{W_i}{4} \tag{5.1}$$

  Where i= 1 ... 4

- Apply another different normal load (N_2) on the top of the shearing cell.
- Repeat from step 2 to step 5 to get another average weight.

According to those assumptions and those detailed test procedure, the interparticulate coefficient friction (IPFC) is calculated by

$$IPFC = \frac{(1-f)W}{N} = \frac{0.985W}{N} \tag{5.2}$$

Now the question is why we only take $n = 4$ as the sample size for evaluating average weight $\overline{W}$ as mentioned in the test steps.

5.3 Validation of the Test Apparatus and Test Method

For the shear cell, the statistical test was made under the following conditions.

test material:	NYLON 1503-2
normal load:	8.373 lb
cross–section of polymer pellets:	round

The 8.373 lb normal load was applied first, then after a second, the vertical weight was added until the ring starts moving.

Then record the weight. Do it again 40 times. Table 5.1 shows the 40 points of weight.

According this table, the histogram and the control chart were constructed, respectively. In the histogram of Figure 5.7, the X–axis represents the recorded weight ranging from 4.0 (lb) to 6.0 (lb) and Y–axis represents the frequency ranging from 0 to 12 in some weight domain.

In the control chart of Figure 5.8 , the X–axis is the number of sample, ranging from 1 to 40, and the Y–axis is the corresponding recorded weight. Three lines appear in the Y–axis, with middle line representing the mean value of weight and between the upper line and lower line is distribution of weight. It is very clear that no point exceeds the upper and lower control limit.

According to statistic theory, suppose we are using $\overline{W}$ to estimate the mean μ of a normal distribution that is known to have variance σ^2. We dicide the sample size n using following equation[30].

Times	Weight (lb)
01	7.070
02	6.940
03	7.057
04	7.052
05	7.060
06	7.055
07	7.051
08	7.070
09	7.066
10	7.047
11	7.051
12	7.032
13	7.033
14	7.038
15	7.041
16	6.812
17	6.927
18	6.932
19	6.929
20	6.923
21	6.924
22	6.784
23	6.896
24	6.895
25	6.932
26	6.929
27	6.932
28	6.780
29	6.895
30	7.010
31	6.900
32	6.895
33	6.897
34	6.790
35	6.905
36	6.901
37	6.910
38	6.902
39	6.794
40	6.909

Table 5.1: Statistic test

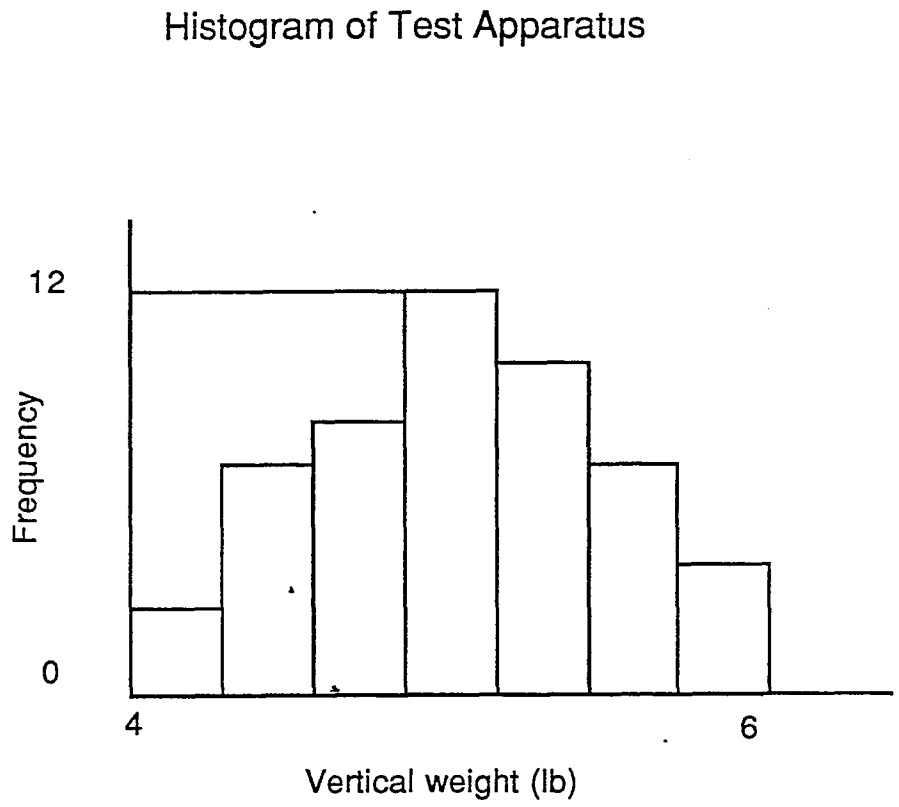

Figure 5.6: Histogram

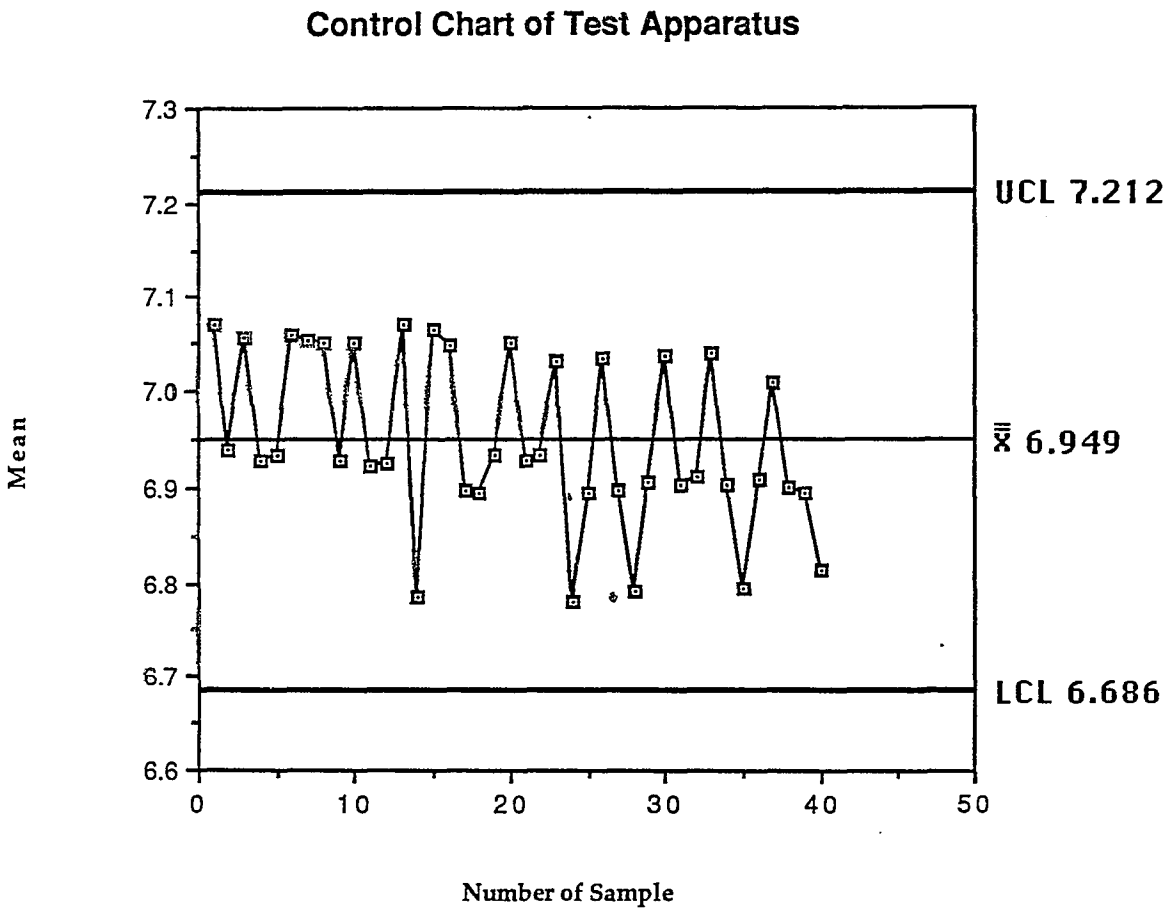

Figure 5.7: Control chart

$$n = [\frac{z_{\alpha/2}\sigma}{e}]^2 \tag{5.3}$$

This equation tells us that when the sample size is n, the confidence is $(1-\alpha)100\%$, the error is less than e.

If we take $\alpha = 0.08$ then according Cumulative Normal Distribution Function[31], we get $z_{\alpha/2} = 1.65$ Therefore, the above equation

$$\begin{aligned} n &= [\frac{(1.65)(0.088)}{0.08}]^2 \\ &= 3.294 \end{aligned}$$

When $n = 4$, the confidence is 92% for the difference of less than 0.08 between μ and $\overline{W}$.

By this time , it has been conclude that the average weight $\overline{W}$ from four points is accurate enough using the above test apparatus to evaluate the IPFC. Therefore, the mean value of vertically applied weight is calculated by

$$\overline{W} = \frac{\sum W_i}{4} \tag{5.4}$$

And the standard deviation is calculated by

$$\sigma = \sqrt{\frac{\sum(W_i - \overline{W})}{4}} \tag{5.5}$$

where i = 1 ... 4

Taken 1σ as the range of weight, then the uppbound of weight $W_{upp} = W + \sigma$, and the lowbound of weight $W_{low} = W - \sigma$

Therefore, the distribution of IPFC is obtained by

$$IPFC_{upp} = \frac{(1-f)W_{upp}}{N} = \frac{0.985W_{upp}}{N} \tag{5.6}$$

$$IPFC_{low} = \frac{(1-f)W_{low}}{N} = \frac{0.985W_{low}}{N} \tag{5.7}$$

Table 5.2 and table 5.3 are the example of how each value is calculated.

Code No.	AC4A201				Test Date:	March 5, 1990
N (lb)	4.756	7.181	8.373	10.798	13.000	15.425
W_1 (lb)	3.496	3.735	5.496	5.540	7.036	9.036
W_2 (lb)	2.735	4.011	5.515	6.036	7.055	9.055
W_3 (lb)	3.220	4.496	5.220	6.091	6.760	9.275
W_4 (lb)	3.000	4.551	5.000	5.760	6.275	8.540
W_5 (lb)	2.735	4.716	5.330	5.650	6.385	8.760
μ_W (lb)	3.037	4.302	5.312	5.815	6.702	8.933
σ_W (lb)	0.293	0.368	0.190	0.215	0.323	0.256
W_{Upp} (lb)	3.330	4.670	5.503	6.030	7.025	9.189
W_{Low} (lb)	2.745	3.934	5.122	5.601	6.379	8.678

Table 5.2: Example of how average weight, IPFC, and distribution of IPFC was calculated

N (lb)	μ_W	W_{Upp}	W_{Low}	σ (psi)	μ_{IPFC}	$IPFC_{Upp}$	$IPFC_{Low}$
4.756	3.037	3.330	2.745	0.432	0.629	0.690	0.569
7.181	4.302	4.670	3.934	0.653	0.590	0.641	0.540
8.373	5.312	5.503	5.122	0.761	0.625	0.647	0.603
10.798	5.815	6.030	5.601	0.982	0.530	0.550	0.511
13.000	6.702	7.025	6.379	1.182	0.508	0.532	0.483
15.425	8.933	9.189	8.678	1.402	0.570	0.587	0.554

Table 5.3: Example of how average weight, IPFC, and distrubition of IPFC was calculated

Chapter 6

TEST MATERIALS

The materials being tested here represent a cross section of resins grades currently being extruded, that is polyester, polypropylene, polystyrene, nylon, polycarbonate, and acetal copolymer. Some have high modulus and some low. Some are normal. All resin families are represented.

High modulus polymers are potential materials of choice in applications requiring high mechanical properties and light weight. High modulus is achieved only in the direction of molecular chain orientation. Properties normal to the molecular axis tend to be an order of magnitude or more lower than the longitudinal values resulting in low compressive and/or shear properties. Compensation for the low shear properties is accomplished through composite design concepts. According to Encyclopedia of Polymer Science and Engineering[32], modulus is taken to mean the tensile modulus as defined by the slope of the initial linear portion of the load extension response (stress–strain curve) of a specimen deformed at room temperature. Table 6.1 lists the modulus of some typical polymers.

Besides, these materials prove useful in more and more areas and bring a unique set of properties that fill a lot of application requirements. They are also versatile enough to accept fillers and reinforcements, and can be blended or alloyed to extend their property ranges.

New grades, offshoots, blends and alloys of these engineering resins offer a

myriad of new replacement materials for metal and glass components, as well as for more expensive polymers that are either overengineered or that fail to meet specific requirements. Many of these polymers are moving beyond their original niche of replacing glass and metal and entering into inter–polymer rivalries.

Taken an example, a thermoplastic polyester was recently used for the housing of a new sump pump to provide both corrosion resistance and impact strength at a reasonable cost[34].

Also, a tire–traction device, offered as an alternative to chains or heavy bags of sand for rescuing cars stuck in snow, consists of Celcon M–90, an acetal copolymer from Hoechst Celanese. This materila not only proved to be strong enough to withstand the force of tires bearing down on the clips, but also remained flexible in the cold[34].

Polyester packing film has excellent clarity, stiffness, and dimentional stability. Because of high permeability to water vapor and gases, it is well suited for packaging fresh produce requiring the presence of oxygen. In addition, the tear resistance is low.

Nylon is the designation for a family of thermoplastic polyamide materials, which in film form are moderate–oxygen barriers. The gas–barrier properties are equal to odor– and flavor–barrier properties important in food applications. Nylon films are usually tough and thermoformable, but only fair moisture barriers.

The applications of those polymer are unlimited. The sole purpose in this work is to find out how the IPFC varies for different profiled cross section in order to increase the output of the extrusion process and to improve the quality of products.

	tensile modulus (MPa)
Acrylonitrile–butadiene–styrene	1660–2200
Nylon	1170–2760
Polyesters	2760–4140
Polypropylene	1100–1520
Polystyrene	3100
Poly(vinylchloride)	2410

Table 6.1: Tensile modulus of typical polymer materials

Chapter 7

EXPERIMENTAL RESULTS

The results for the measurement of the IPFC, using the procedure described in chapter V and the the materials described in chapter VI are presented here. The X–axis is the pressure (psi) obtained by normal load (lb) divided by cross–section area of shear cell $(inch)^2$. Y–axis is the IPFC obtained from

$$IPFC = \frac{0.985W}{N} \tag{7.1}$$

In the graph, the average IPFC is obtained from

$$\overline{IPFC} = \frac{0.985\overline{W}}{N} \tag{7.2}$$

The upper bound of the IPFC is obtained from

$$IPFC_{upp} = \frac{0.985W_{upp}}{N} \tag{7.3}$$

And the lower bound of the IPFC is obtained from

$$IPFC_{low} = \frac{0.985W_{low}}{N} \tag{7.4}$$

Therefore, the IPFC of circular cross section, bilobal cross section and trilobal cross section with different materials is plotted for each test. The code number identification for material and die is presented in the Appendix A and Appendix B, respectively.

7.1 Circular Cross Section

Figure 7.1 shows the IPFC of circular cross section for Acetal Copolymer with grade U10–01. The variety of IPFC is appoximately within 0.5 and 0.6 for the pressure between 0.4 (psi) and 1.4 (psi).

Figure 7.2 shows the IPFC of circular cross section for Acetal Copolymer with grade M25. The variety of the IPFC is approximately within 0.5 and 0.58 for the pressure between 0.4 (psi) and 1.4 (psi).

Figure 7.3 shows the IPFC of circular cross section for Acetal Copolymer with grade M90. The IPFC decreases when pressure is approximately between 0.4 (psi) and 1.0 (psi) and remains almost constant when pressure is larger than 1.0 (psi). And the tendency of IPFC is decreasing.

Figure 7.4 shows the IPFC of circular cross section for Acetal Copymer with grade M270. The IPFC decreases when the pressure is approximately between 0.4 and 1.0 (psi) and remains almost constant when pressure is larger than 1.0 (psi). And the tendency of the IPFC is decreasing.

Figure 7.5 shows the IPFC of circular cross section for Acetal Copolymer with grade M450. The IPFC also decreases when pressure is approximately between 0.4 and 1.0 (psi) and again remains constant when pressure is larger than 1.0 (psi). And the tendency of the IPFC is decreasing.

Figure 7.6 shows the IPFC of circular cross section for Nylon. The variety of the IPFC is approximately within 0.63 and 0.76 for the pressure between 0.4 and 1.2 (psi).

Figure 7.7 shows the IPFC of circular cross section for Polystyrene. The IPFC decreases constantly from 0.58 to 0.5 when the pressure increases.

Figure 7.8 shows the IPFC of circular cross section for Polyester. The IPFC varies and the variety are within 0.58 to 0.65 with no increasing and decreasing tendency.

Figure 7.9 shows the IPFC of circular cross section for Polypropylene. The IPFC also varies and the variety are within approximately 0.48 to 0.56 with no increasing and decreasing tendency.

Figure 7.10 shows the IPFC of circular cross section for ABS. The IPFC varies greatly within approximately 0.47 to 0.58 and no increasing and decreasing tendency.

7.2 Bilobal Cross Section

Figure 7.11 shows the IPFC of bilobal cross section for Acetal Copolymer with grade U10–01. The IPFC varies but its variety constantly decreases.

Figure 7.12 shows the IPFC of bilobal cross section for Acetal Copolymer with grade M25. The IPFC decreases greatly from approximately 0.85 to 0.6 when the pressure increases.

Figure 7.13 shows the IPFC of bilobal cross section for Acetal Copolymer with grade M90. The IPFC also decreases from approximately 0.72 to 0.64 when the pressure increases.

Figure 7.14 shows the IPFC of bilobal cross section for Acetal Copolymer with grade M270. The IPFC varies but also decreases from 0.76 to 0.69.

Figure 7.15 shows the IPFC of bilobal cross section for Acetal Copolymer with grade M450. The IPFC decreases greatly when the pressure is larger than approximately 1.0 (psi).

Figure 7.16 shows the IPFC of bilobal cross section for Polystyrene. The IPFC remains almost constant when the pressure is more than approximately 0.72 (psi).

Figure 7.17 shows the IPFC of bilobal cross section for Polyester. The IPFC decreases from 0.86 to 0.7 when pressure increases.

Figure 7.18 shows the IPFC of bilobal cross section for Polypropylene. The IPFC decrease from approximately 0.8 to 0.72 when pressure increases.

Figure 7.19 shows the IPFC of bilobal cross section for ABS. The IPFC varies and the variety is between 0.62 to 0.68 with no increasing and decreasing tendency.

Figure 7.20 shows the IPFC of bilobal cross section for Nylon. The IPFC varies greatly with decreasing tendency.

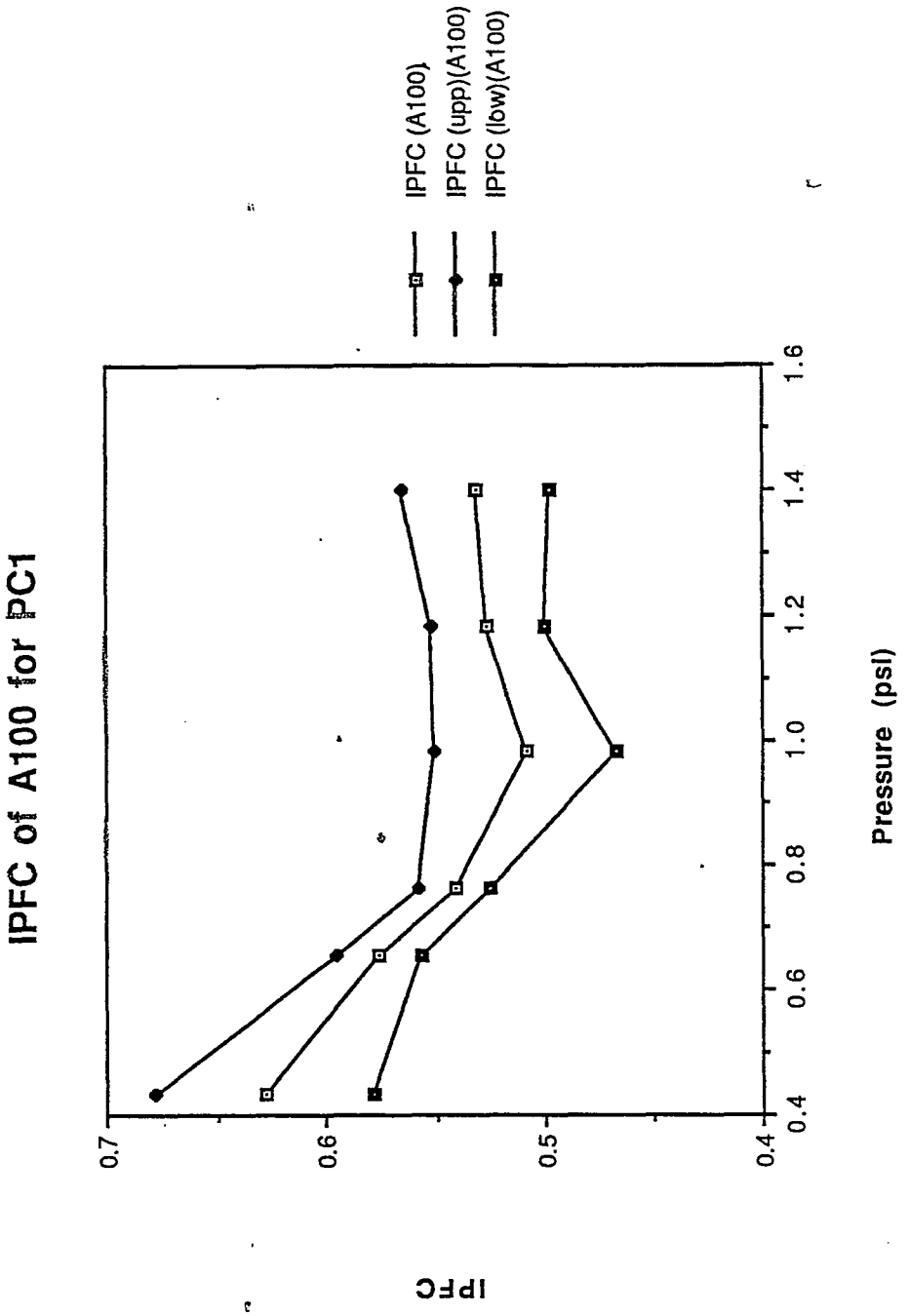

Figure 7.1: IPFC of circular cross section for PC1

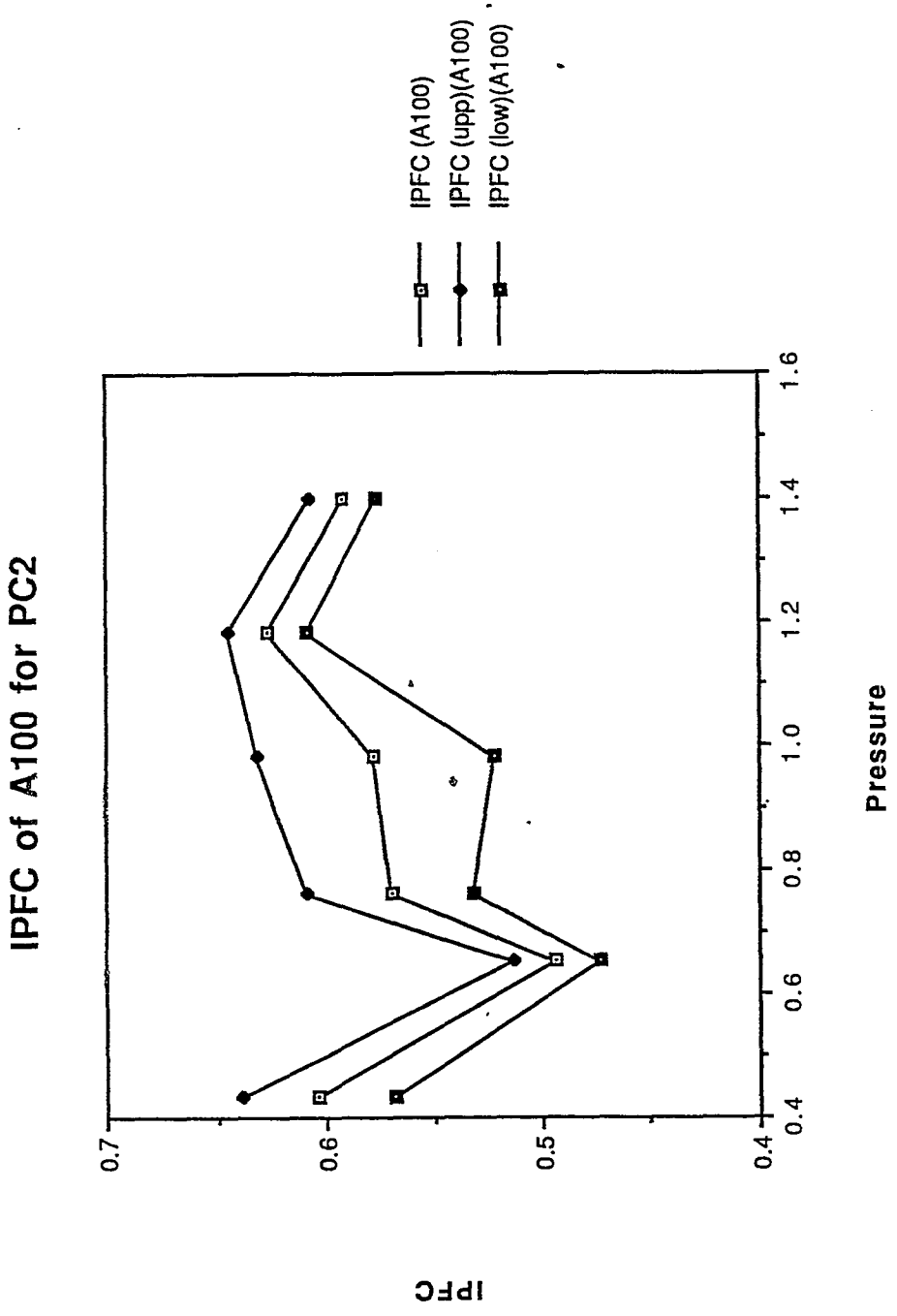

Figure 7.2: IPFC of circular cross section for PC2

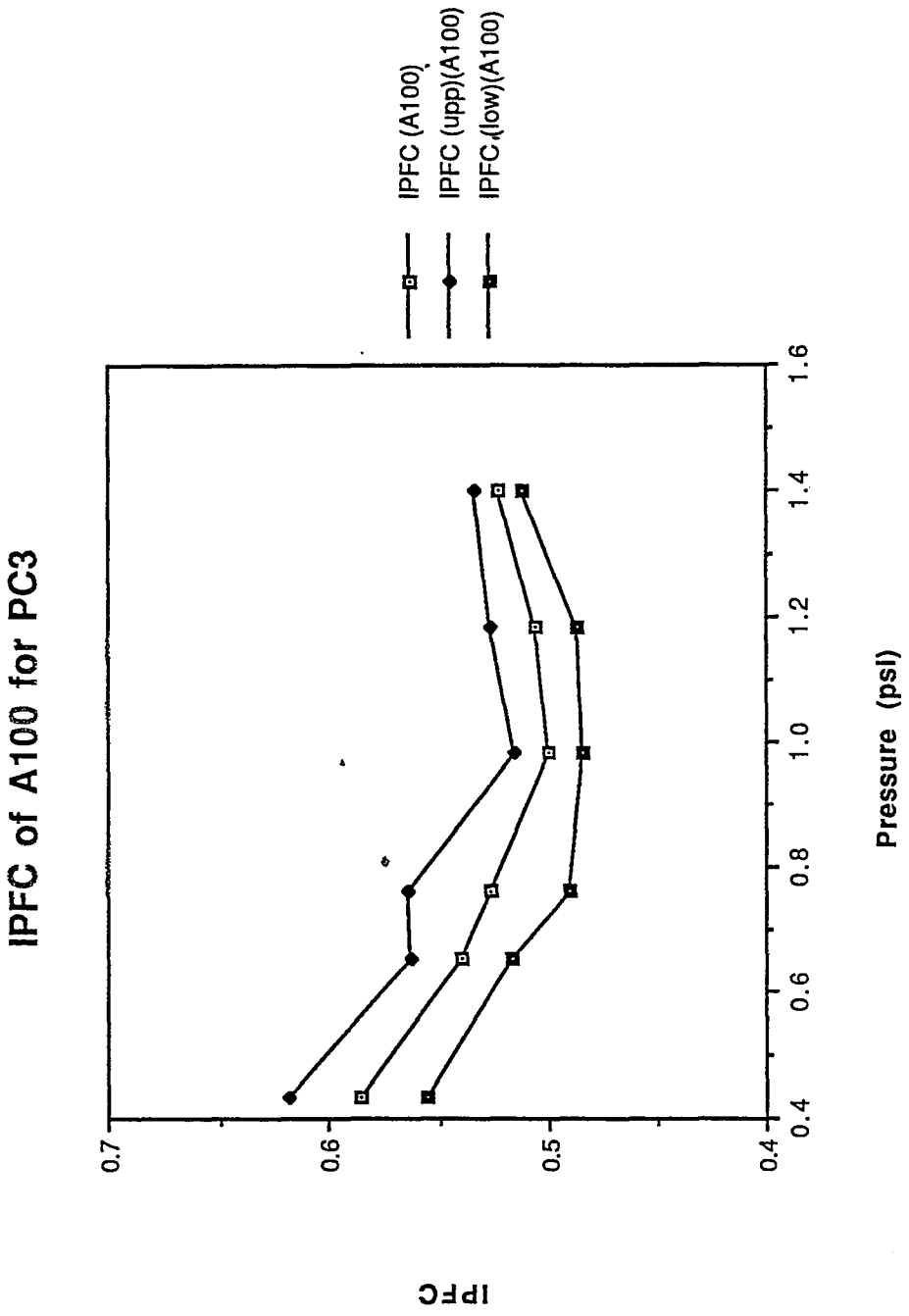

Figure 7.3: IPFC of circular cross section for PC3

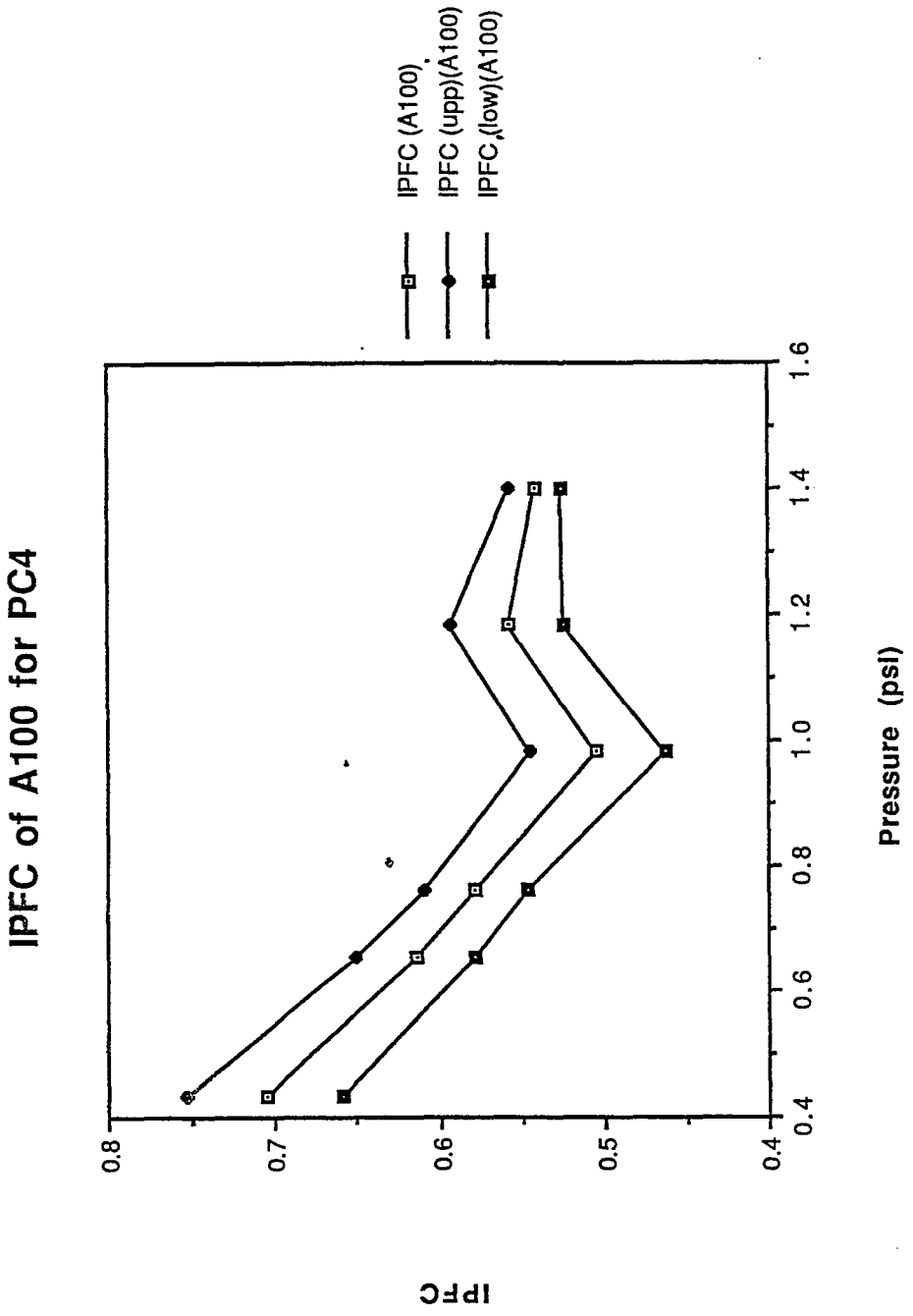

Figure 7.4: IPFC of circular cross section for PC4

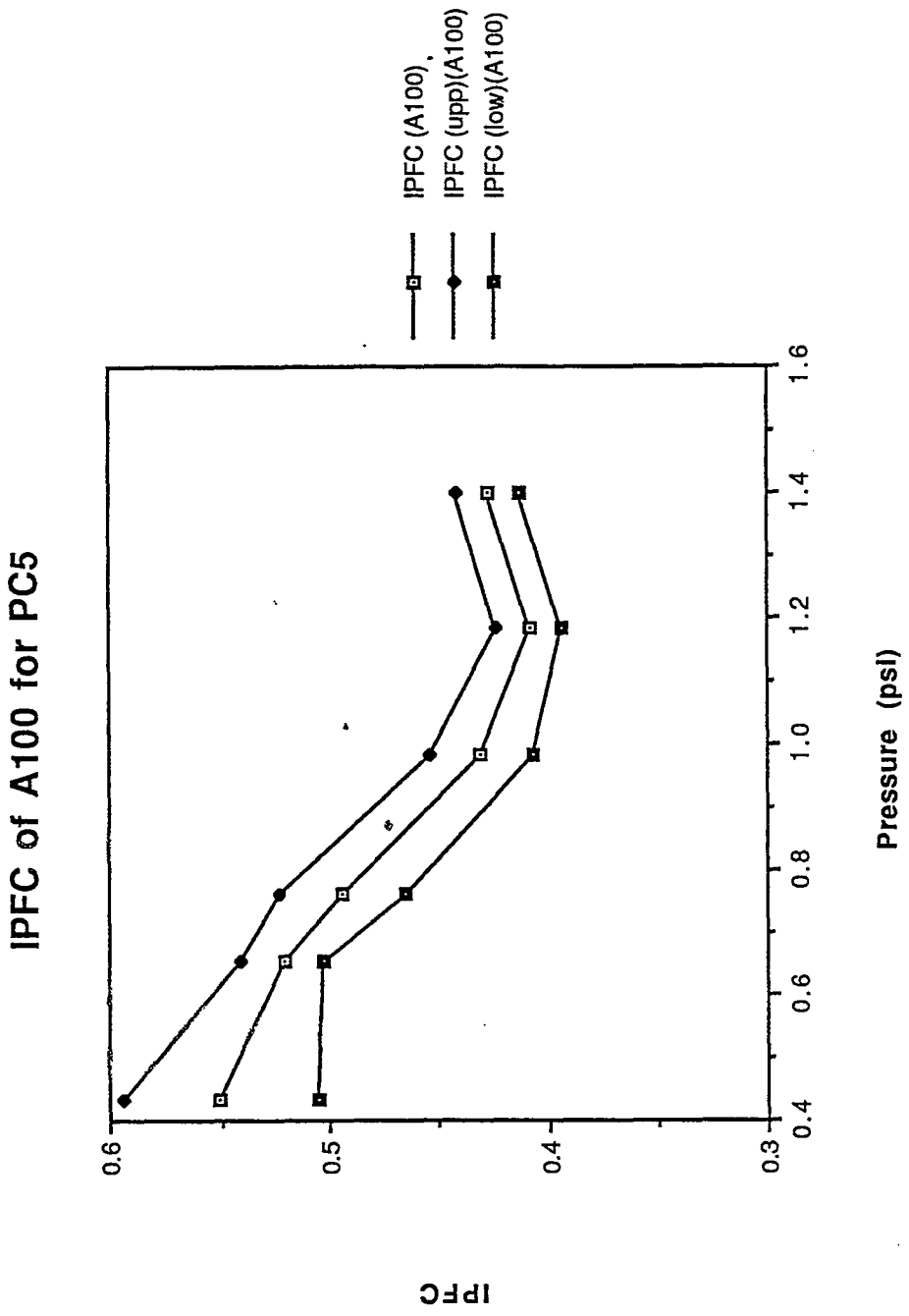

Figure 7.5: IPFC of circular cross section for PC5

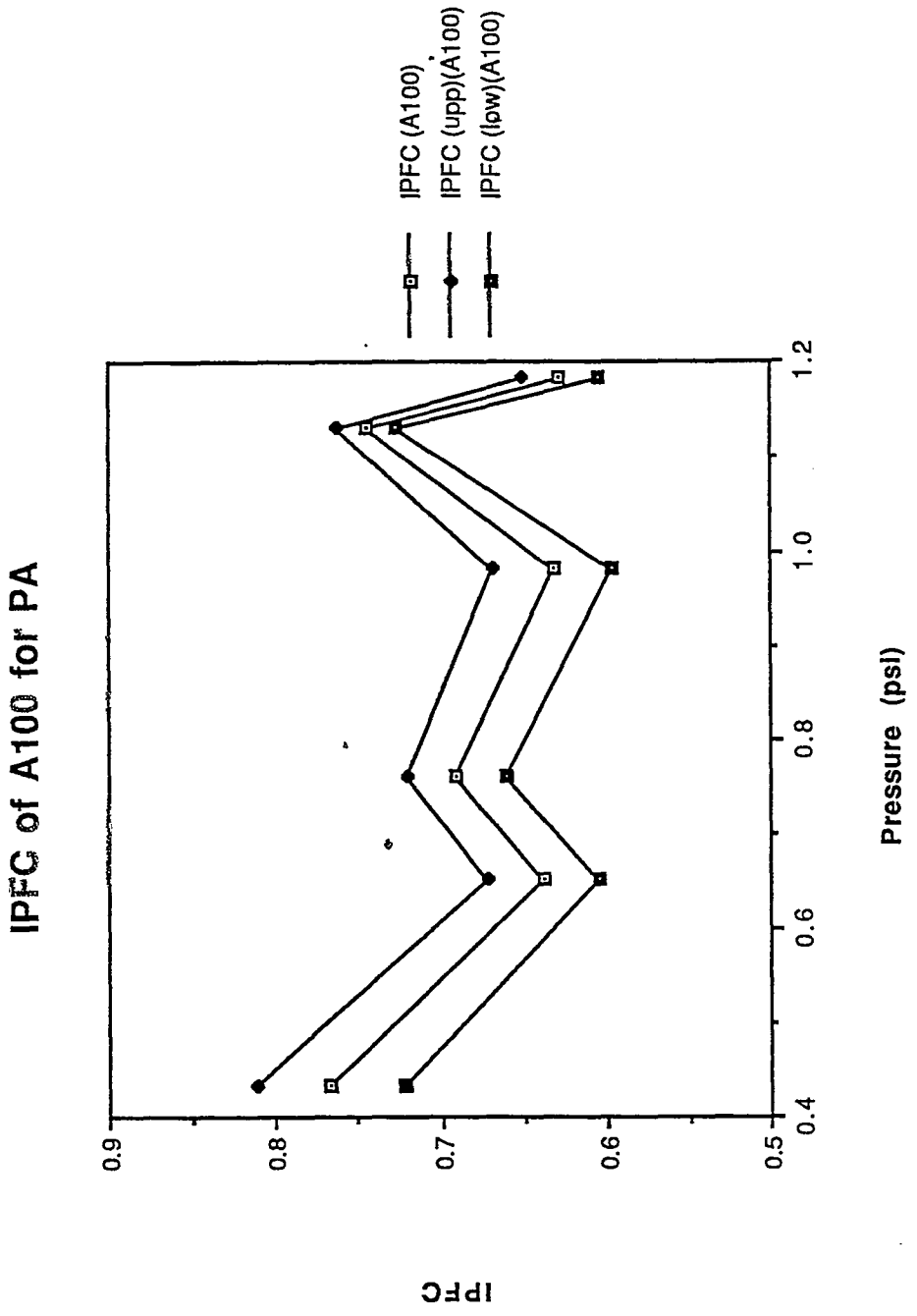

Figure 7.6: IPFC of circular cross section for PA

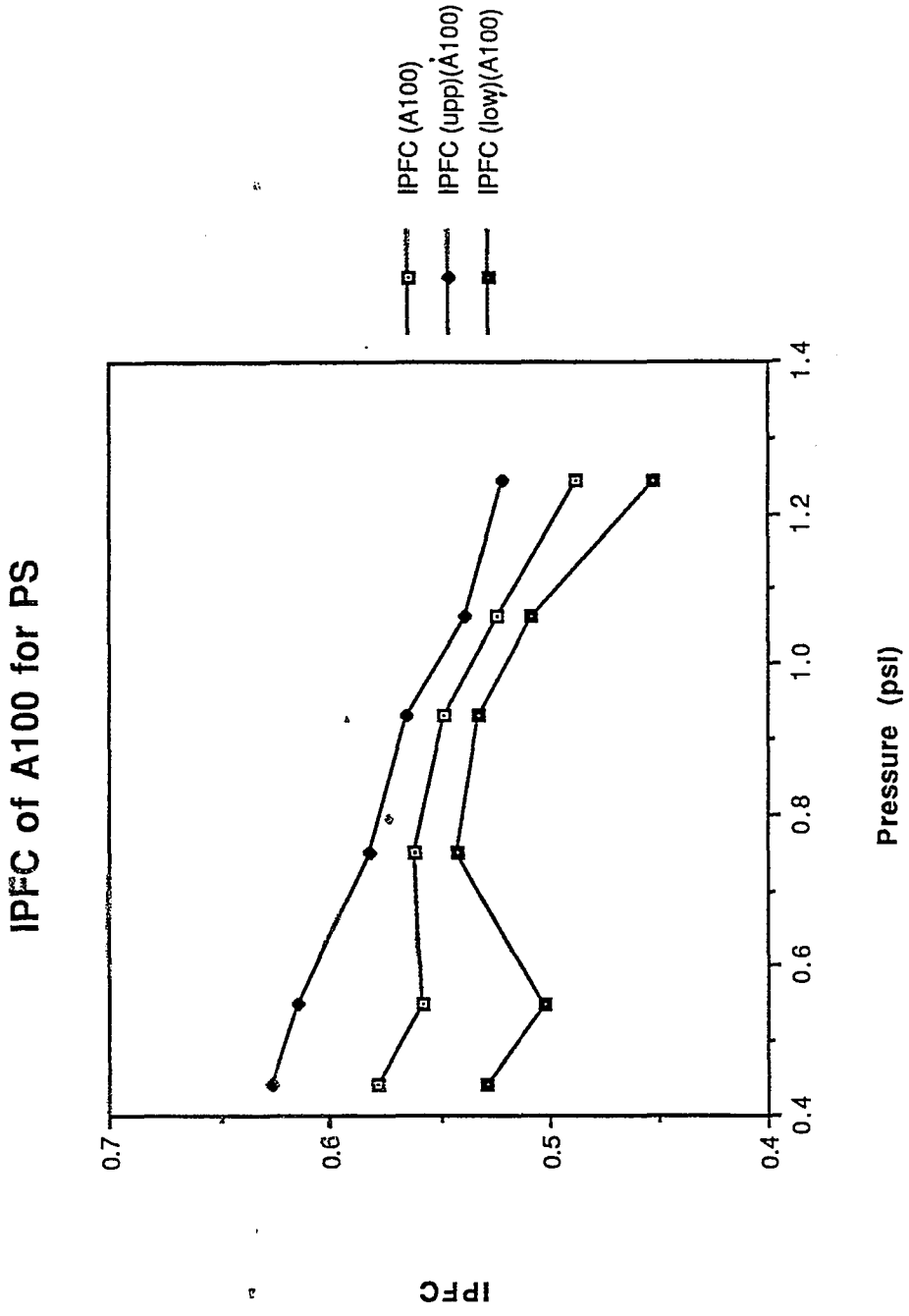

Figure 7.7: IPFC of circular cross section for PS

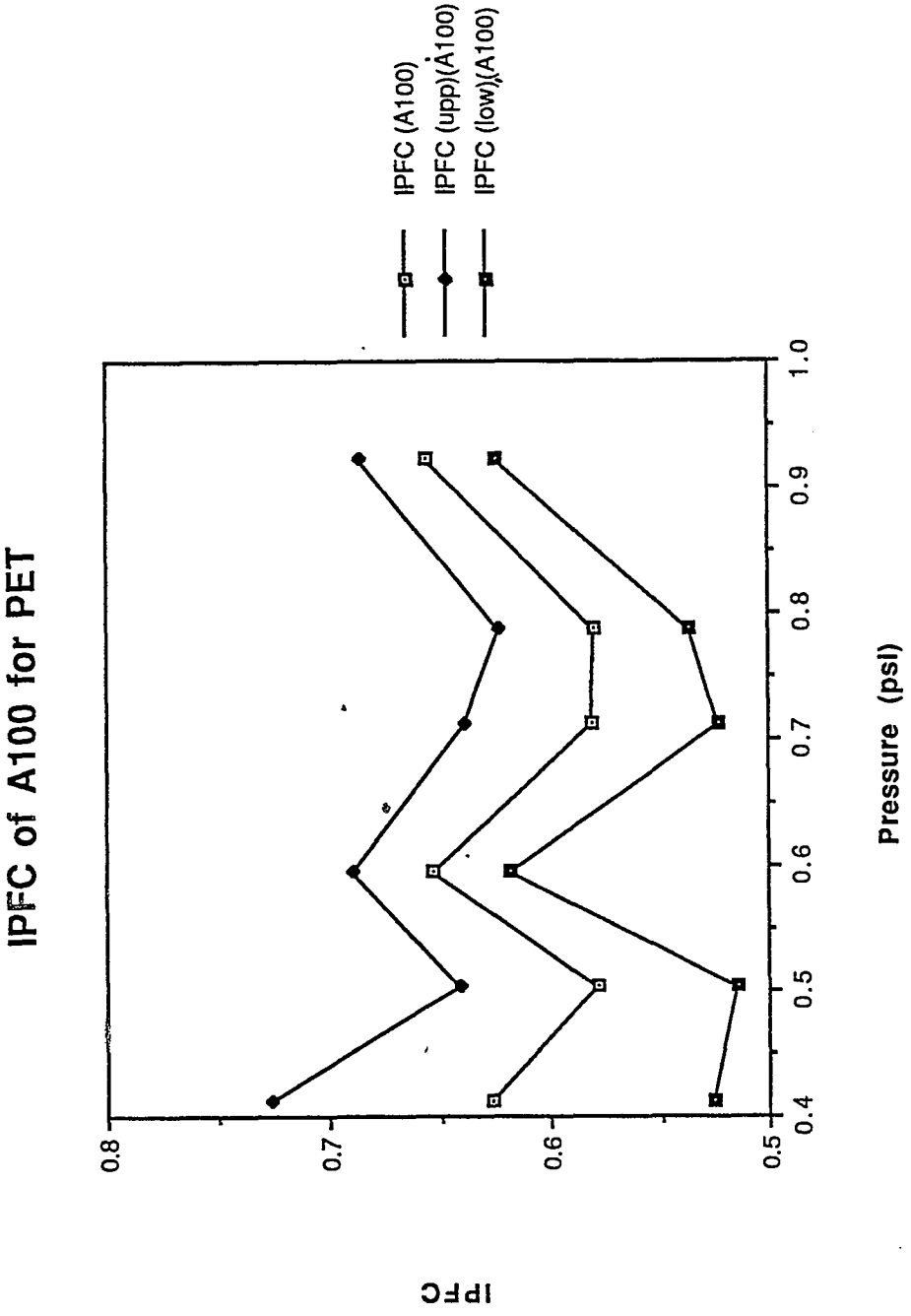

Figure 7.8: IPFC of circular cross section for PET

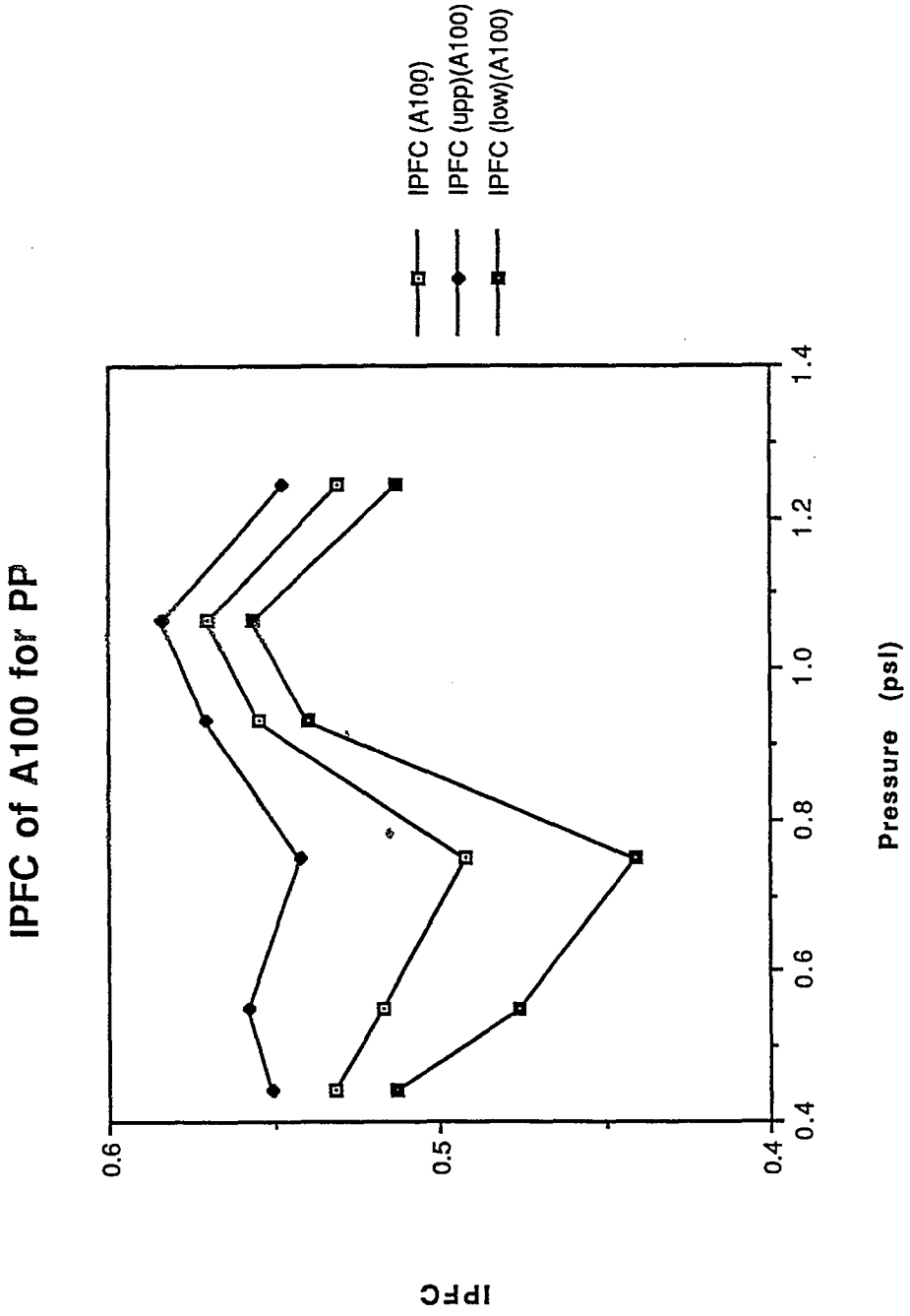

Figure 7.9: IPFC of circular cross section for PP

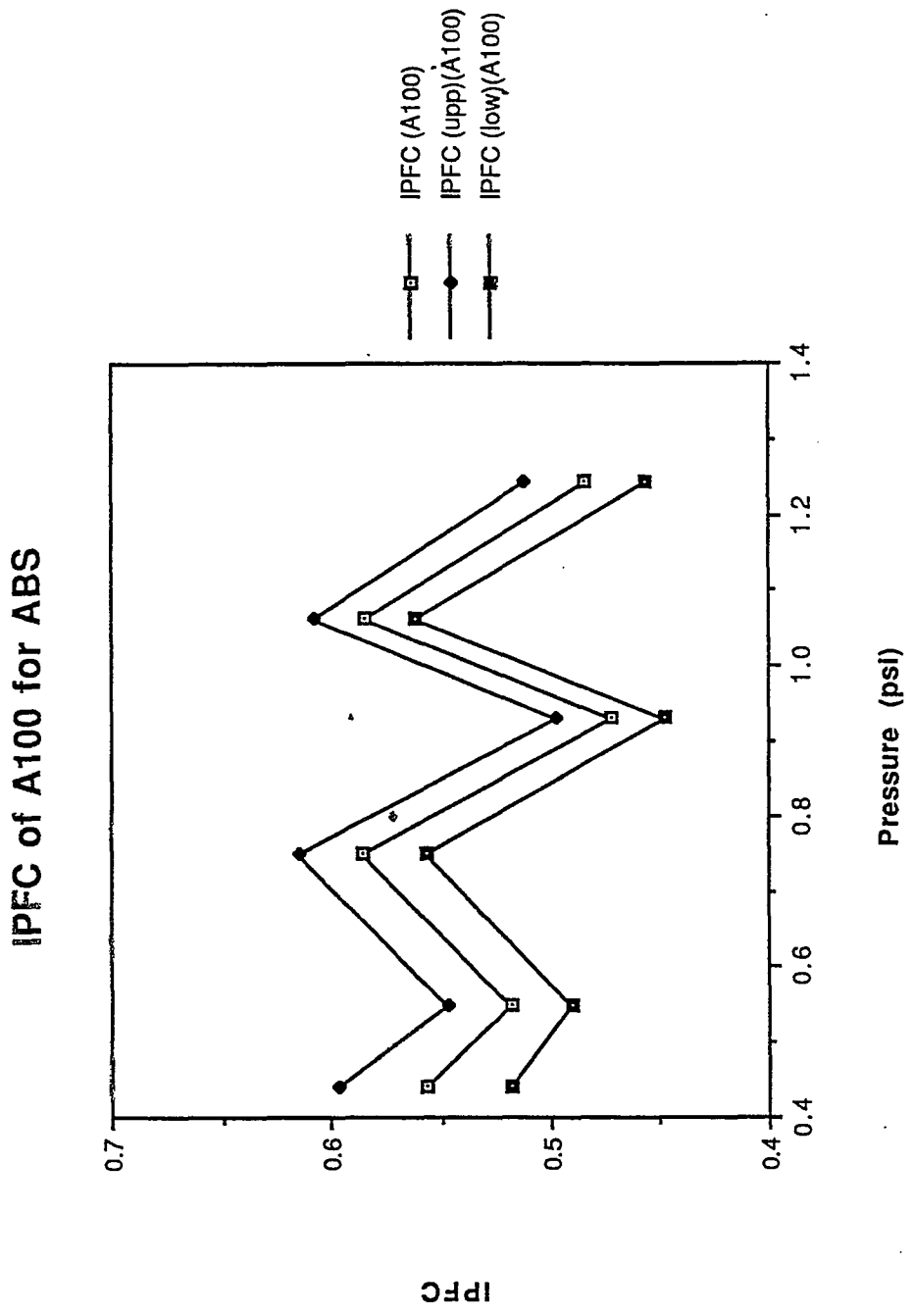

Figure 7.10: IPFC of circular cross section for ABS

7.3 Trilobal Cross Section

Figure 7.21 shows IPFC of the trilobal cross section with high density of Polyethlene. The IPFC varies with decreasing tendency and the variety is approximately within 0.62 to 0.48.

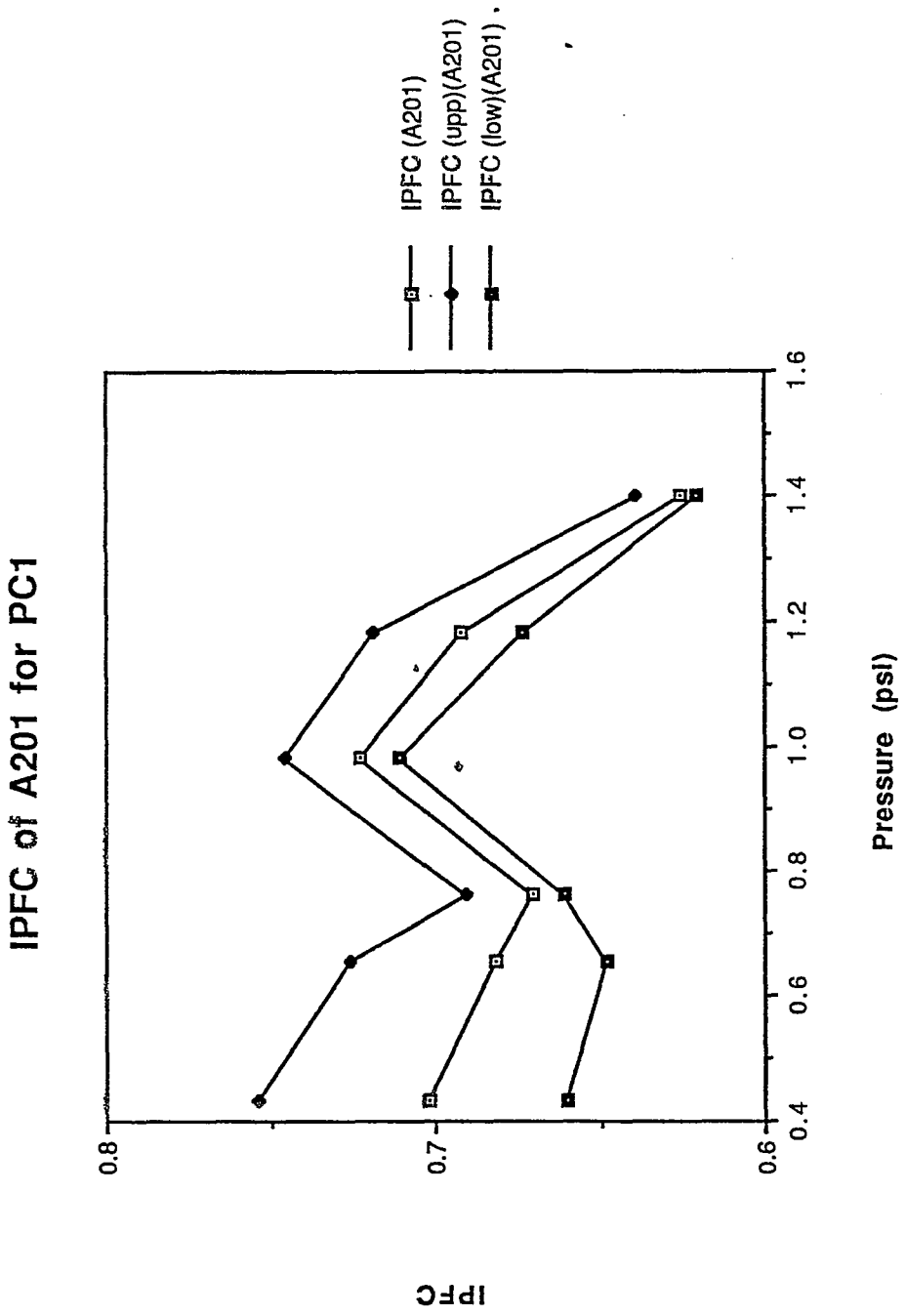

Figure 7.11: IPFC of bilobal cross section for PC1

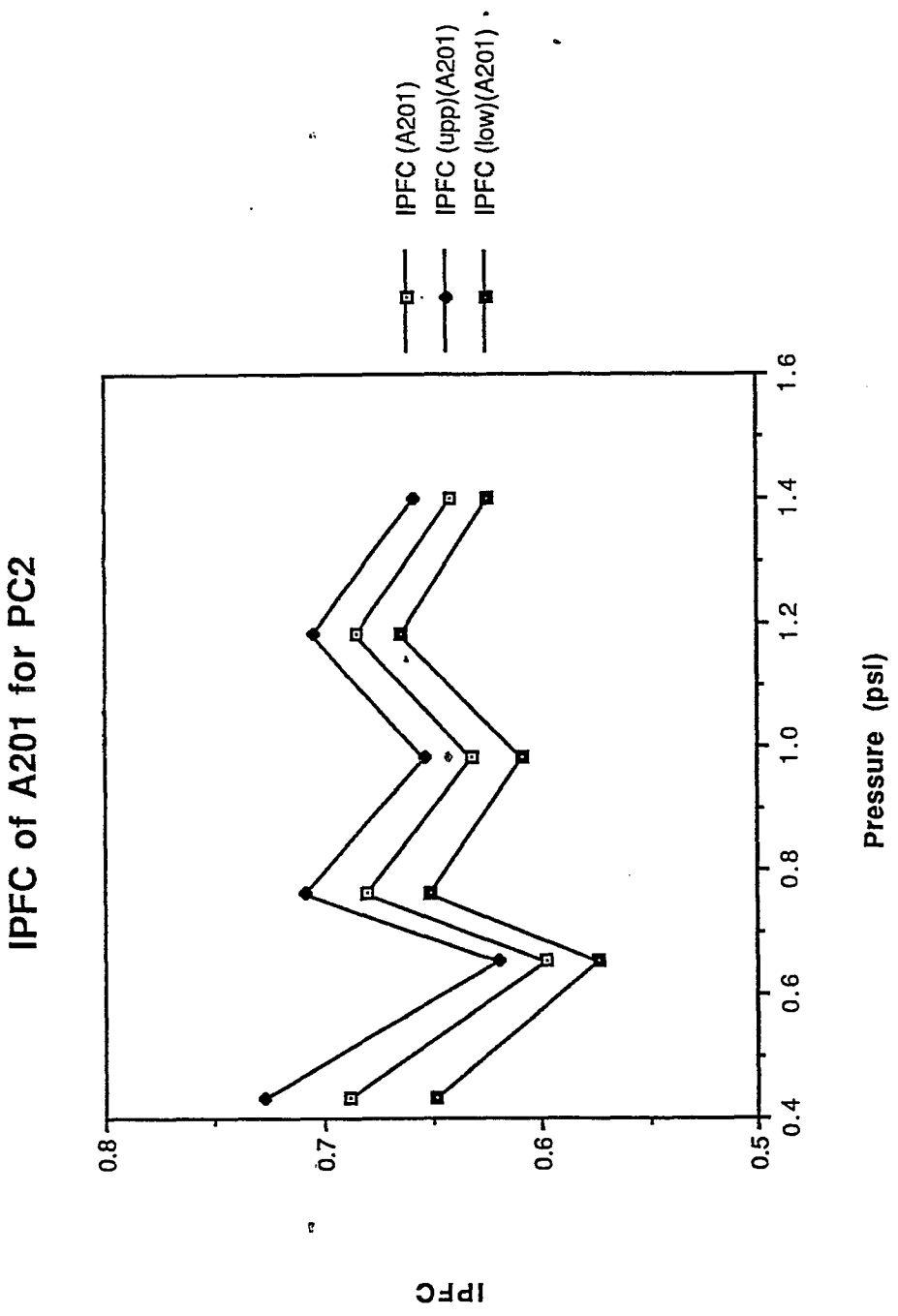

Figure 7.12: IPFC of bilobal cross section for PC2

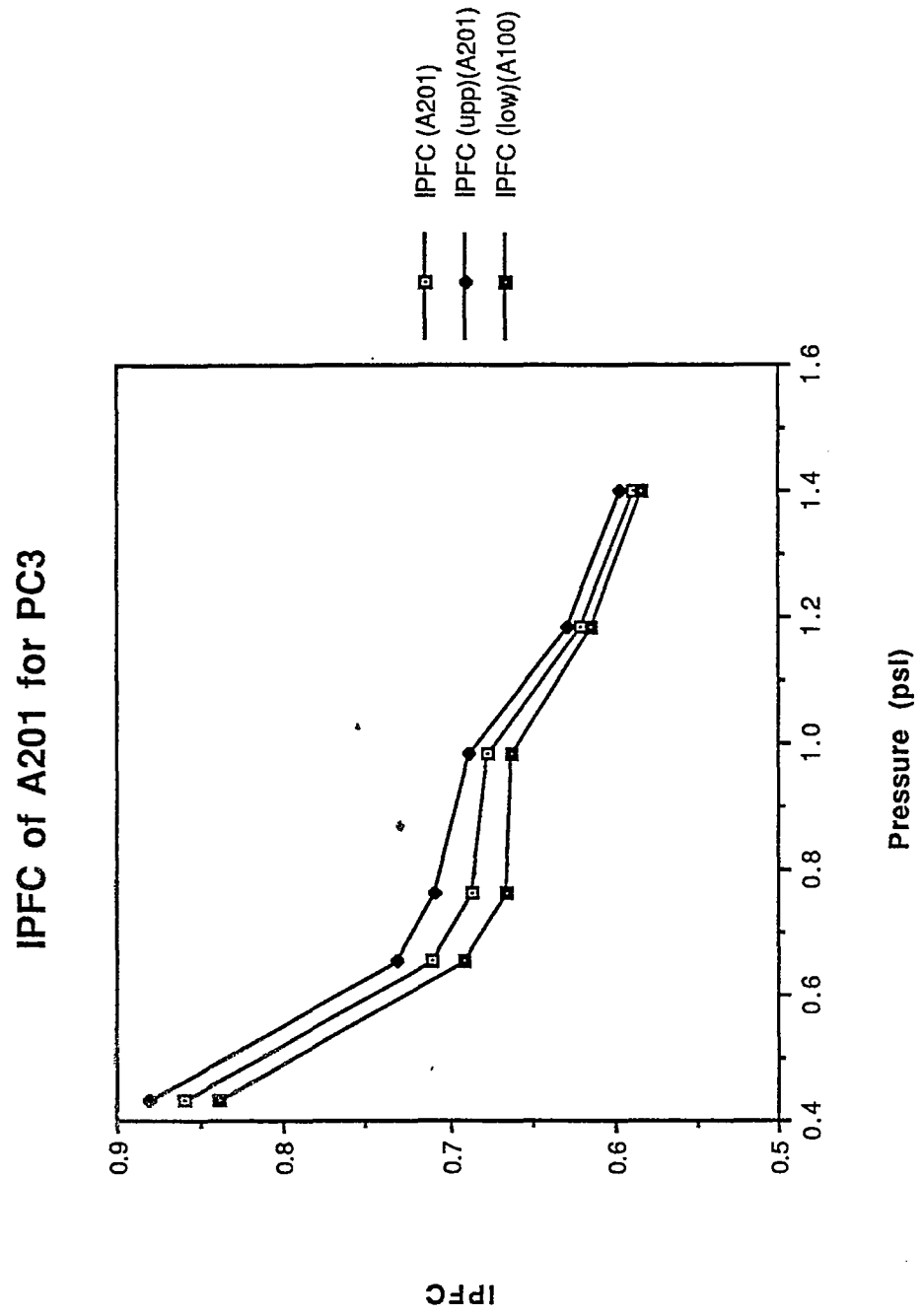

Figure 7.13: IPFC of bilobal cross section for PC3

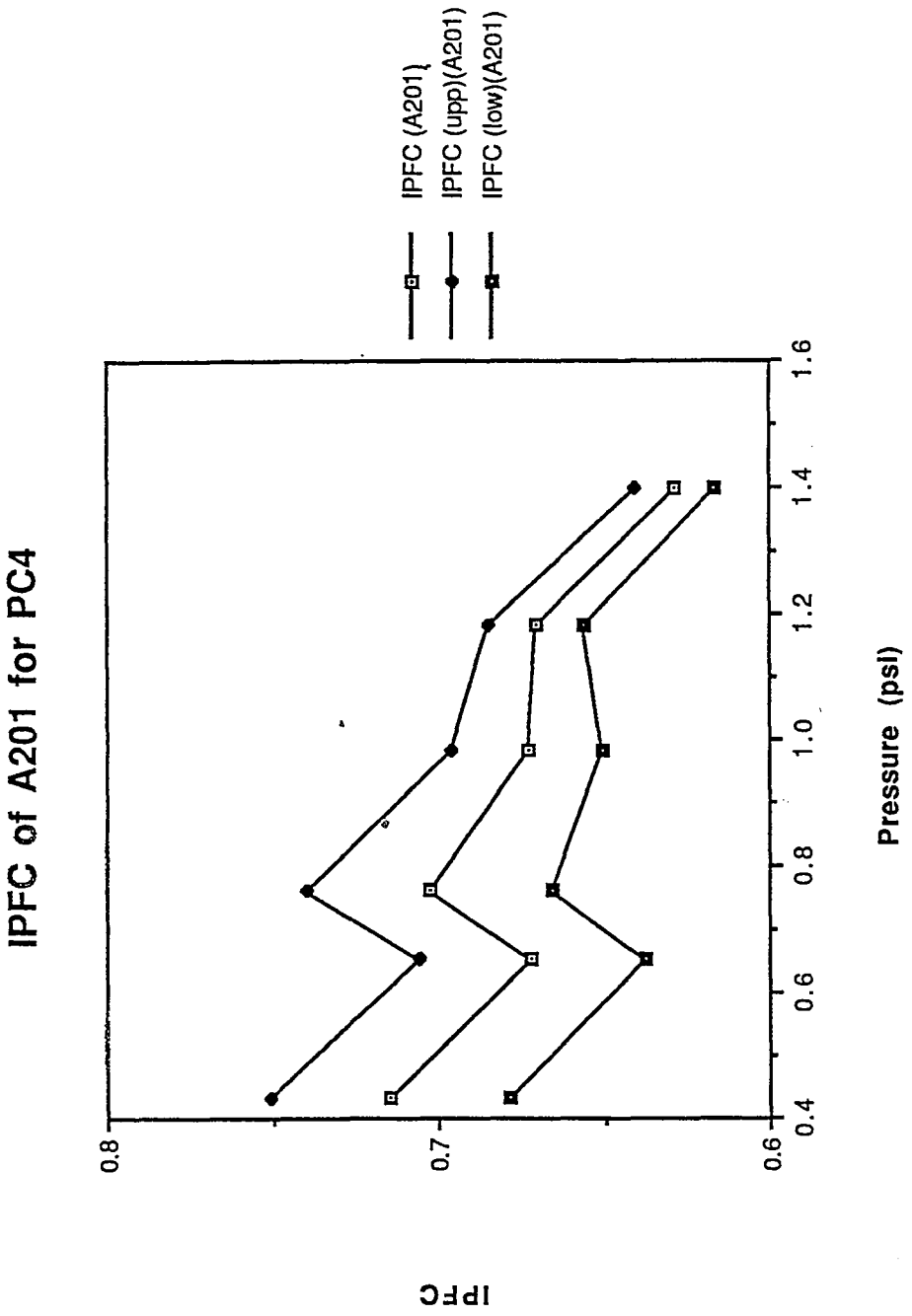

Figure 7.14: IPFC of bilobal cross section for PC4

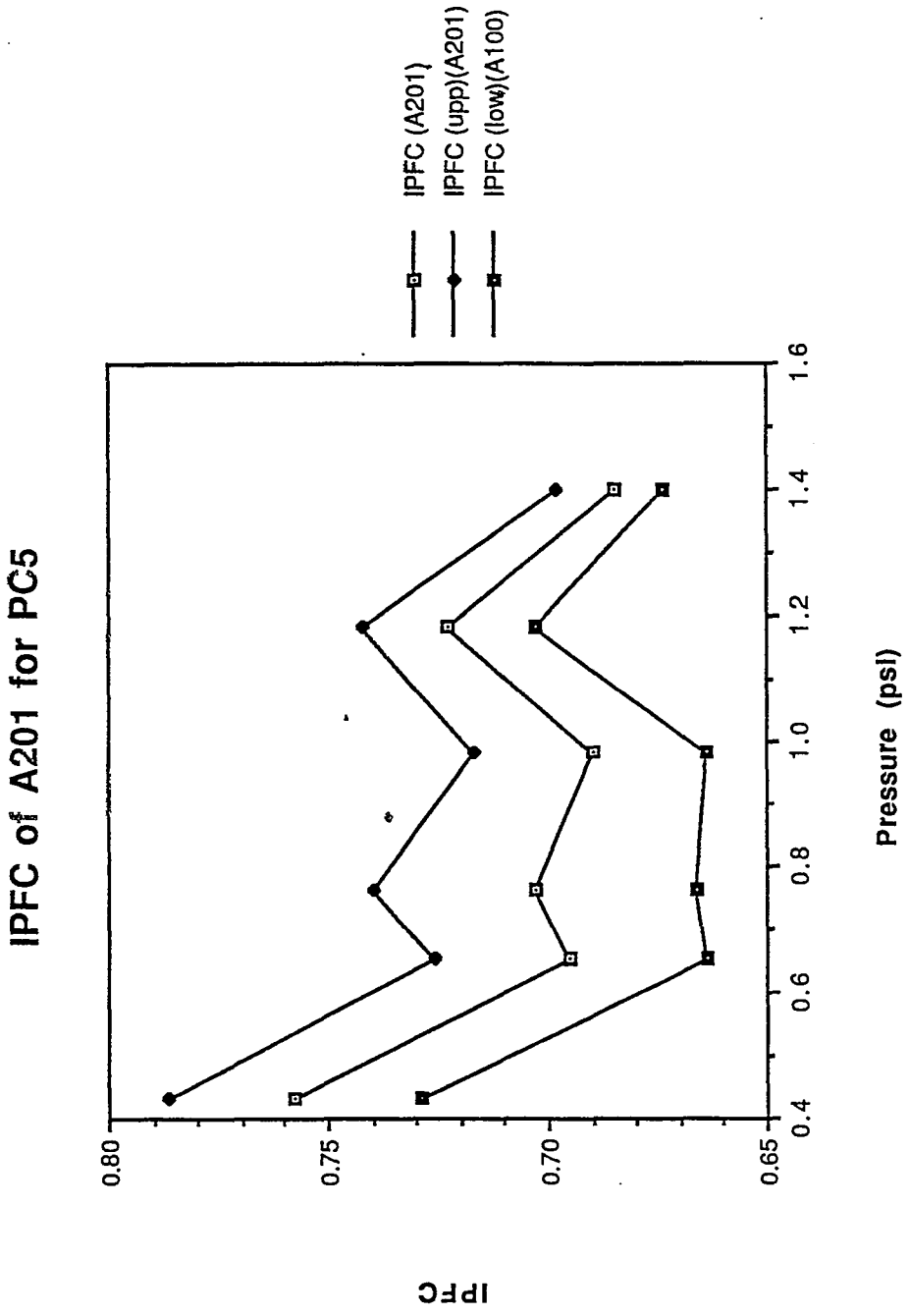

Figure 7.15: IPFC of bilobal cross section for PC5

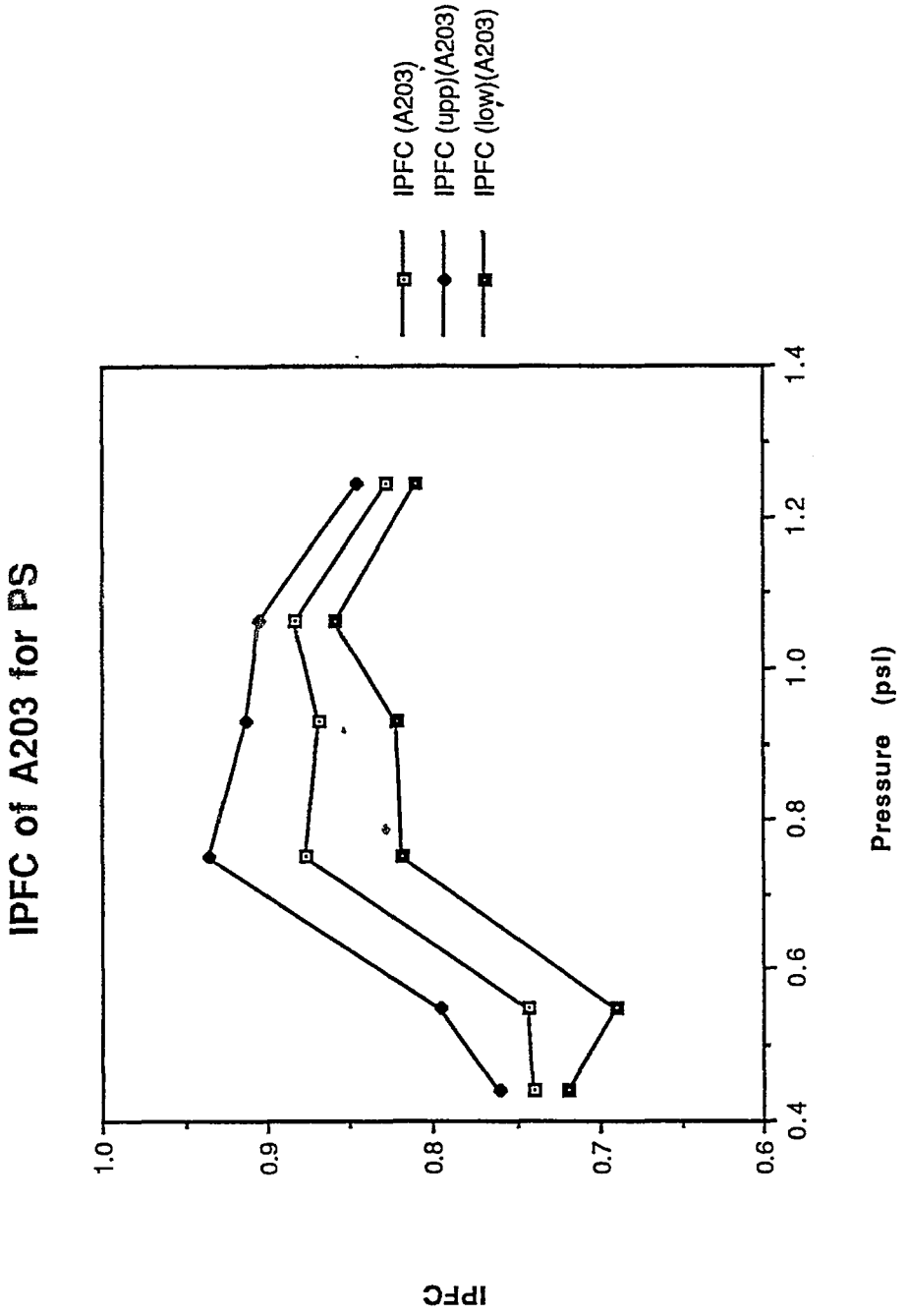

Figure 7.16: IPFC of bilobal cross section for PS

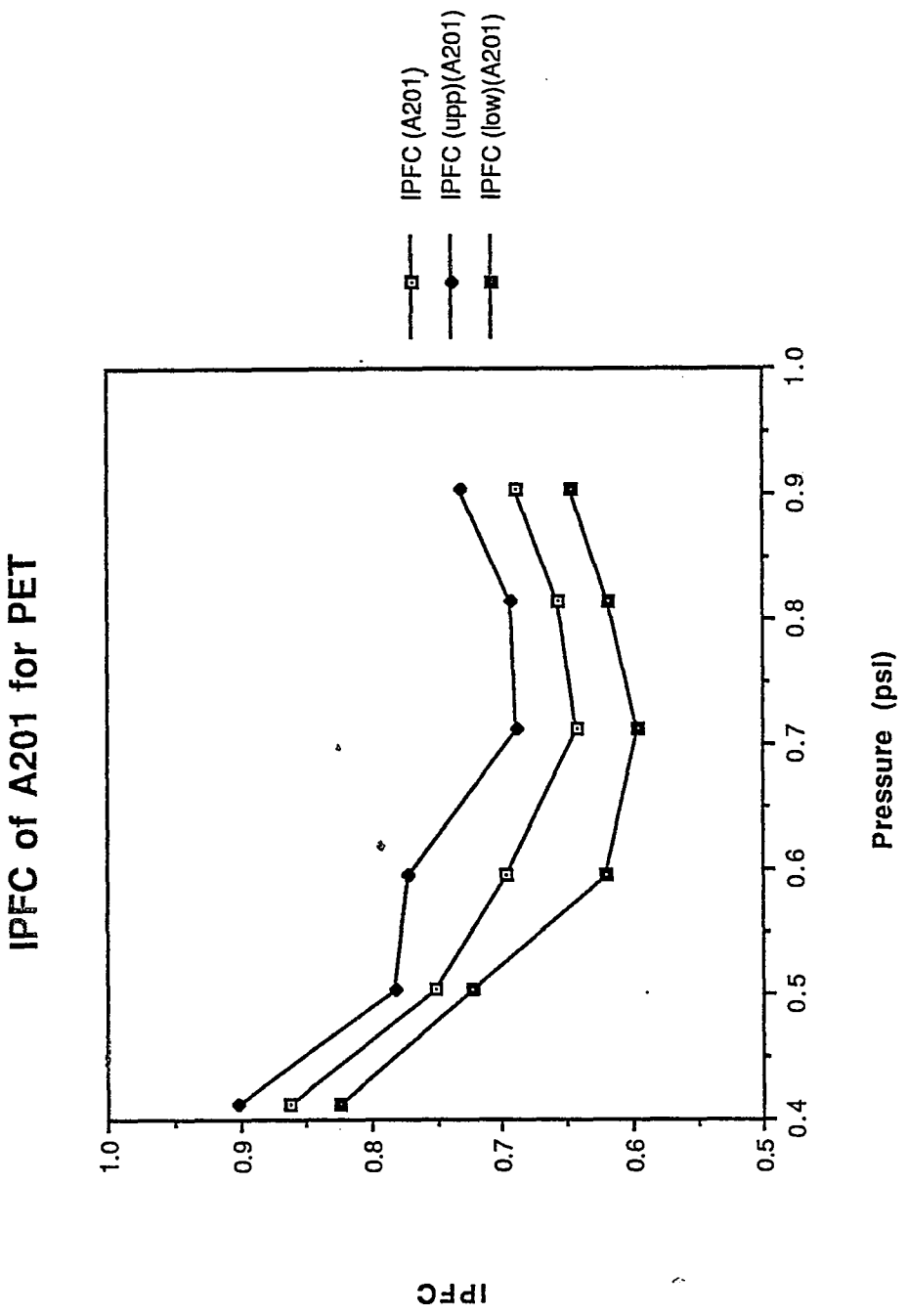

Figure 7.17: IPFC of bilobal cross section for PET

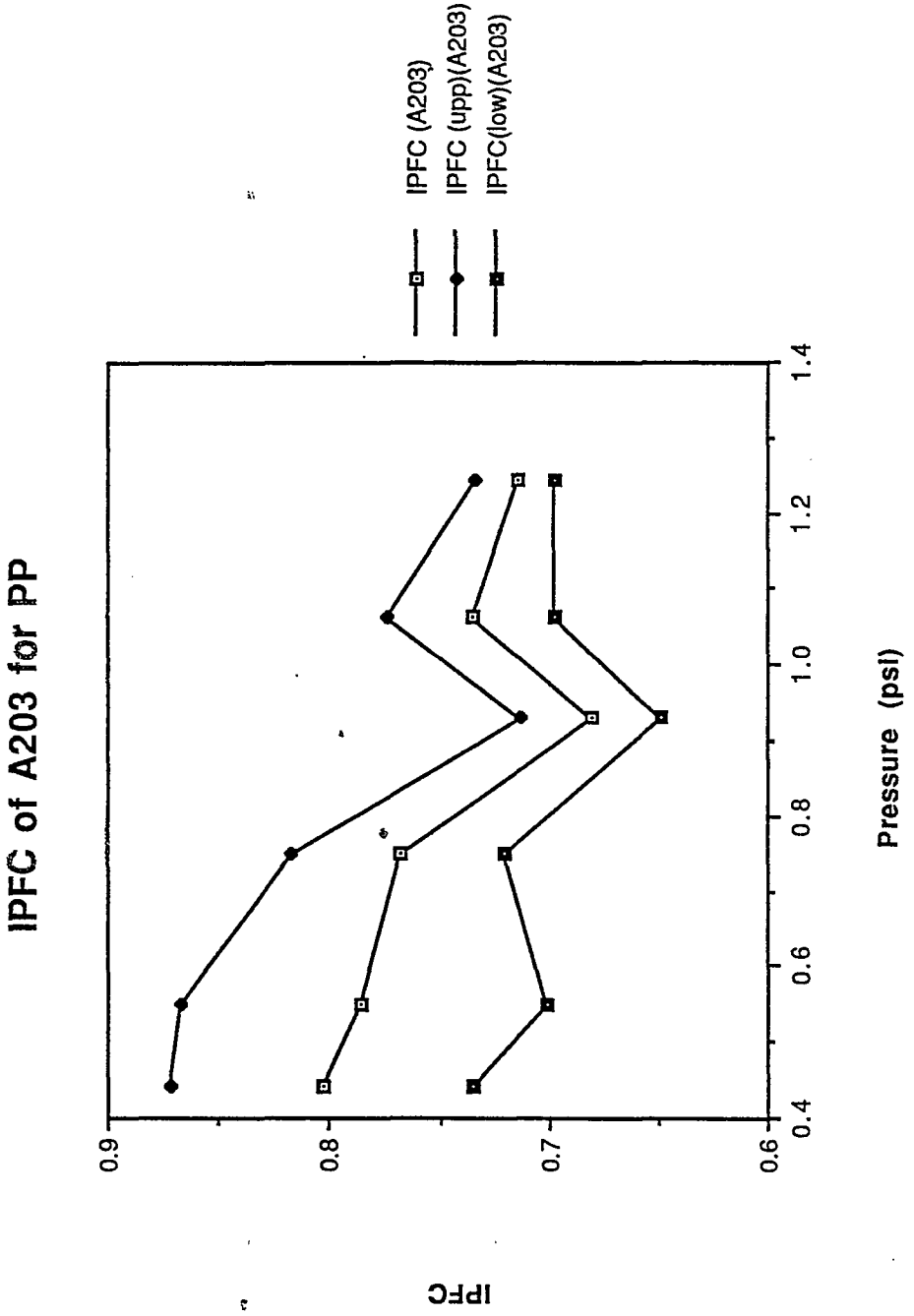

Figure 7.18: IPFC of bilobal cross section for PP

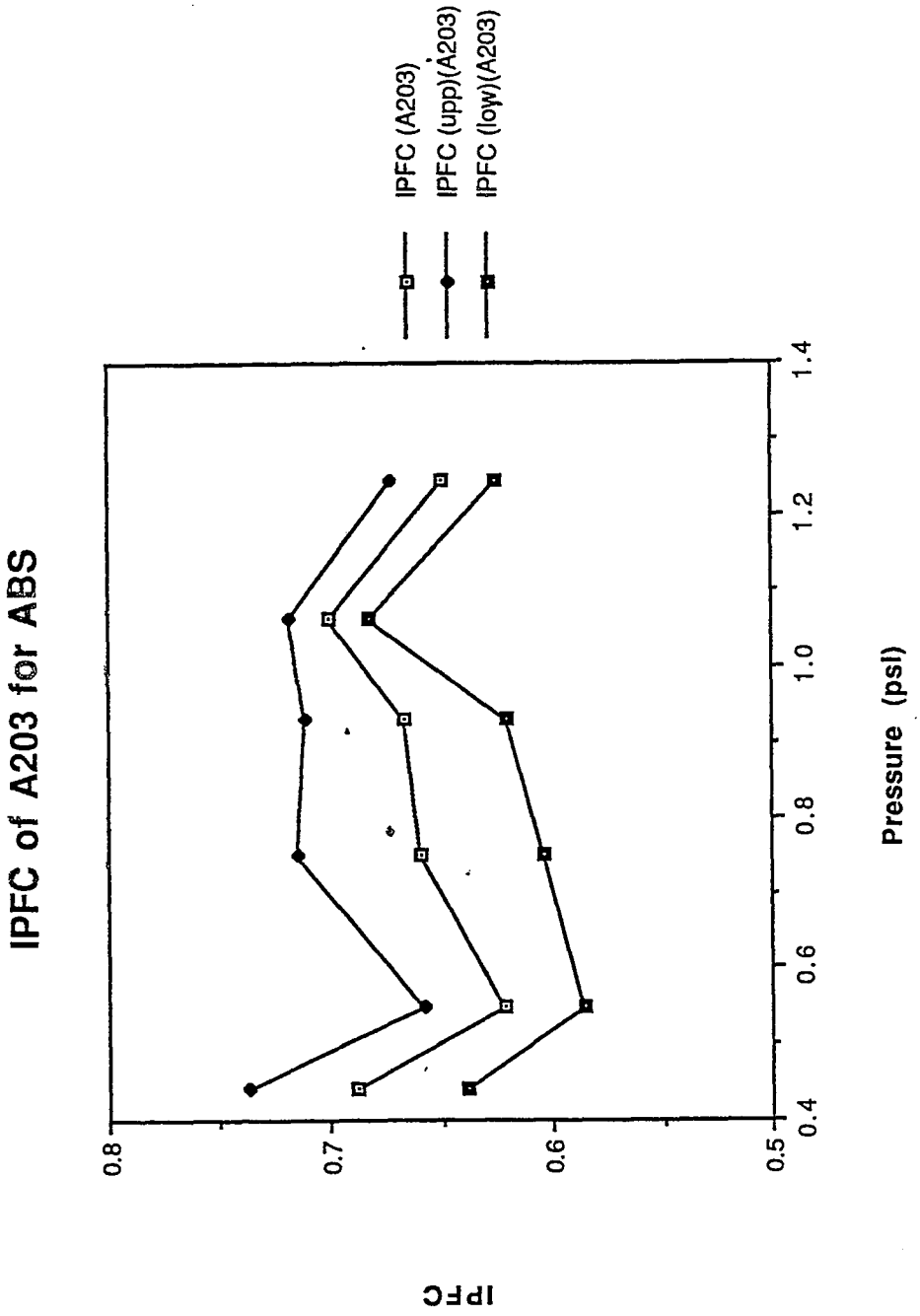

Figure 7.19: IPFC of bilobal cross section for ABS

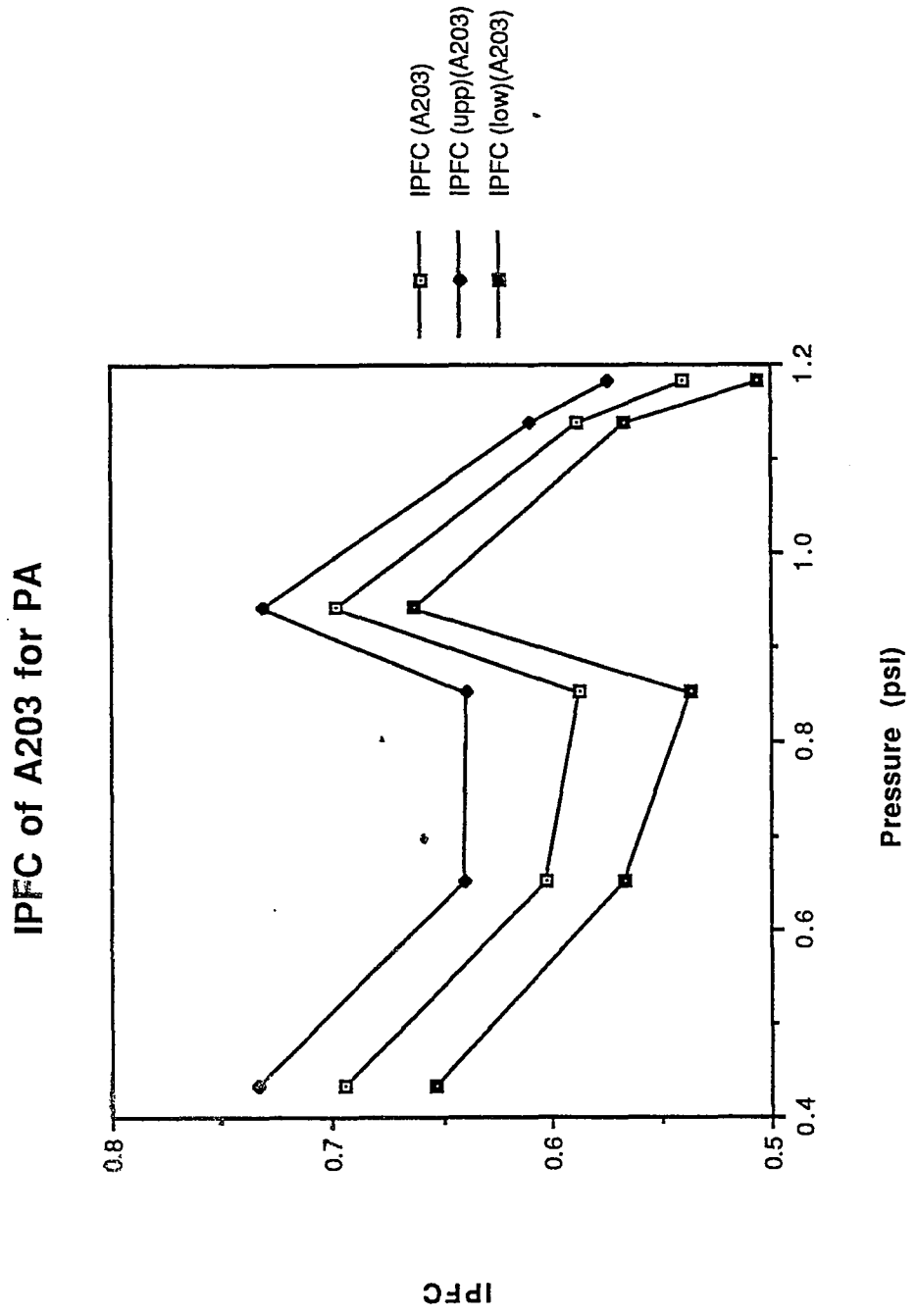

Figure 7.20: IPFC of bilobal cross section for PA

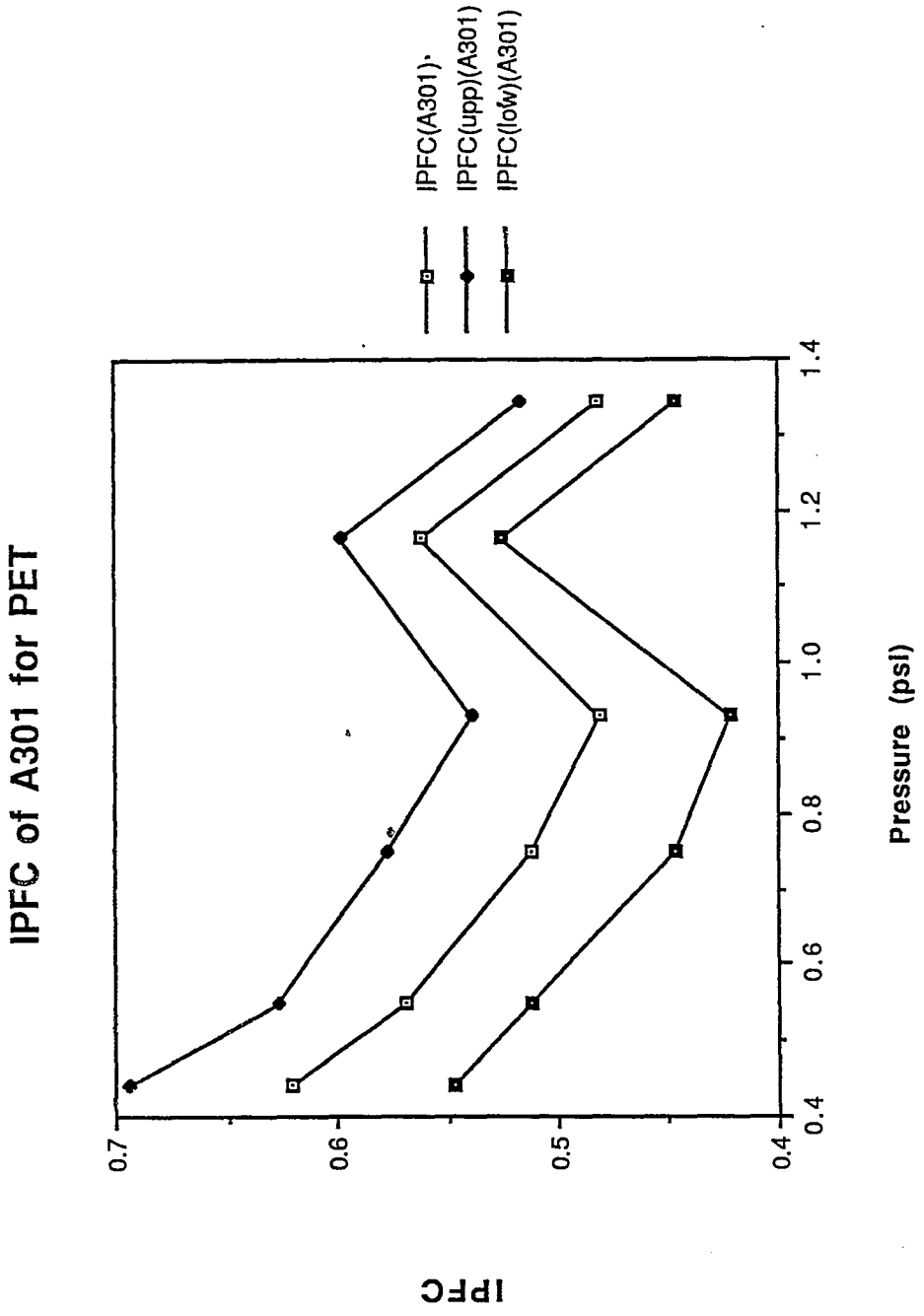

Figure 7.21: IPFC of trilobal cross section for HDPE

Chapter 8

DISCUSSION OF THE RESULTS

8.1 Comparison of the IPFC for Circular and Bilobal Cross Sections

The comparison of IPFC between circular cross section pellets and bilobal cross section pellets for different test materials are plotted shown in Figure 8.1, Figure 8.2, Figure 8.3, Figure 8.4, Figure 8.5, Figure 8.6, Figure 8.7,Figure 8.8, and Figure 8.9.

Figure 8.1 shows the comparison between bilobal cross section pellets and circular cross section pellets for acetal copolymer with grade U10–01. Both of their IPFC variety are decreasing as pressure increases. Further more, the IPFC of bilobal cross section pellets is greater than of circular cross section for each corresponding pressure.

Figure 8.2 shows the comparison between bilobal cross section pellets and circular cross section pellets for acetal copolymer with grade M25. For bilobal cross section, the IPFC decreases when pressure increases, while for circular cross section, the IPFC remains almost constant. In addition, the IPFC of bilobal cross section is greater than circular cross section for each corresponding pressure.

Figure 8.3 shows the comparison between bilobal cross section pellets and circular cross section pellets for acetal copolymer with grade M90. Their IPFC

both decrease when pressures increase. Also for bilobal cross section pellets, its IPFC is greater than circular cross section for each corresponding pressure.

Figure 8.4 shows the comparison between bilobal cross section pellets and circular cross section pellets for acetal copymer with grade M270. The IPFC of bilobal cross section remains constant while the IPFC of circular pellets is decreasing when pressure increases. Moreover, the IPFC for bilobal is much greater than for circular pellets for each corresponding pressure.

Figure 8.5 shows the comparison between bilobal cross section pellets and circular cross section pellets for acetal copymer with grade M450. Both of the IPFC decrease with circular pellets decreased more apparently. In addition, for the bilobal cross section, the IPFC is much larger than for the circular pellets.

Figure 8.6 shows the comparison between bilobal cross section pellets and circular cross section for ABS material. Even though both of their IPFC are varying the IPFC is greater for bilobal pellets than for circular pellets with each corresponding pressure.

Figure 8.7 shows the comparison between bilobal cross section pellets and circular cross section pellets for Polypropylene. Clearly, the IPFC is greater for bilobal pellets than for circular cross section for each corresponding pressure though their IPFC are varing.

Figure 8.8 shows the comparison between bilobal cross section pellets and circular cross section pellets for Polyester. Clearly, the IPFC of bilobal pellets is greater than of circular cross section for each corresponding pressure though both of their IPFC vary for the whole range of test pressure.

Figure 8.9 shows the comparison between bilobal cross section pellets and circular cross section pellets for Polystyrene. Obviously, the IPFC for bilobal cross section is greatly larger than for circular cross section even with their different varying tendency.

On the whole, From Figure 8.1 to Figure 8.5, for all acetal copolymer with different grades, their IPFC of bilobal cross section is greater than its circular cross section despite of their varying tendency. From Figure 8.6 to Figure 8.9, for ABS, PP, PET, PS, and PA, their IPFC of bilobal cross section is also greater than its circular cross section.

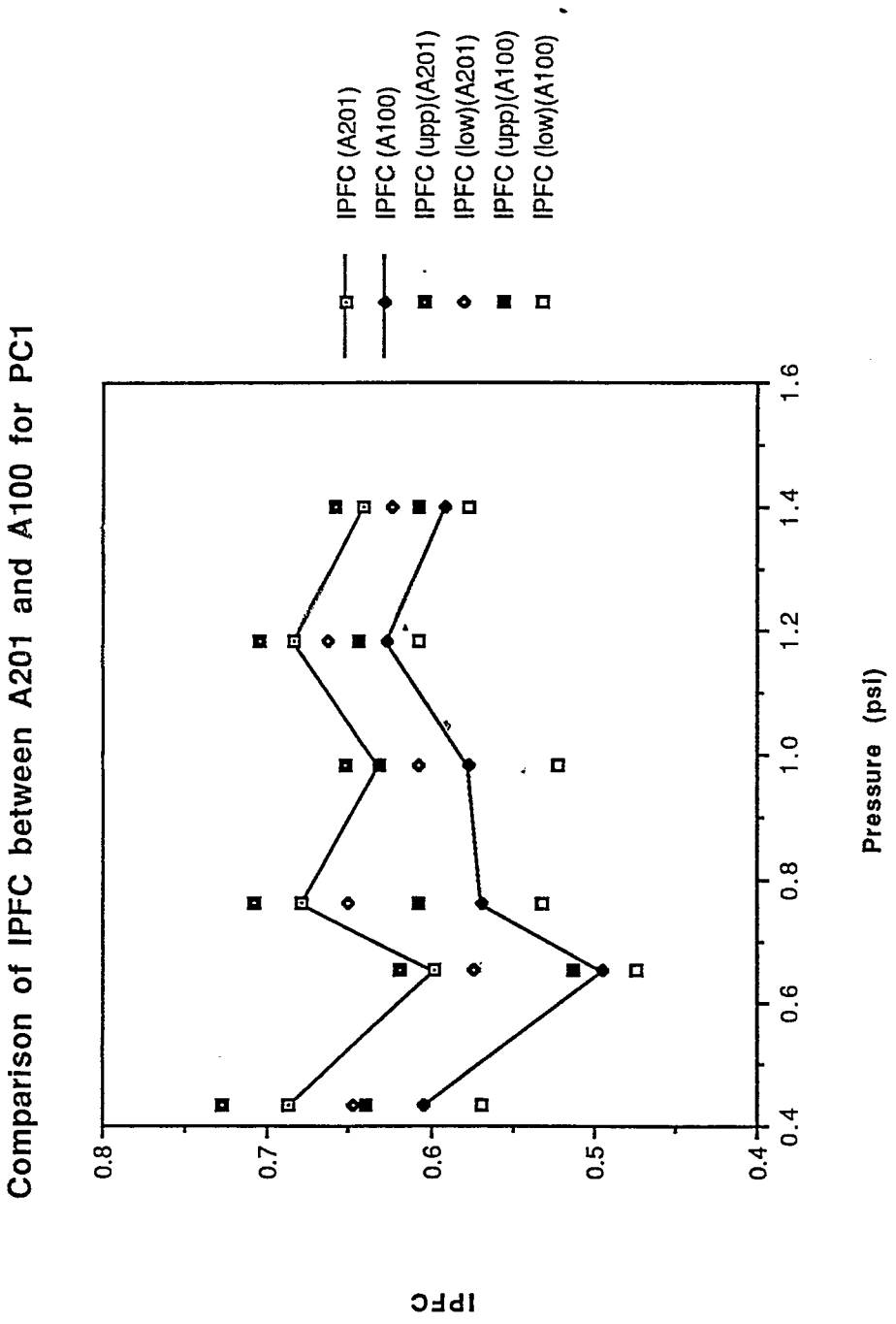

Figure 8.1: Comparison of IPFC between PC1A201 and PC1A100

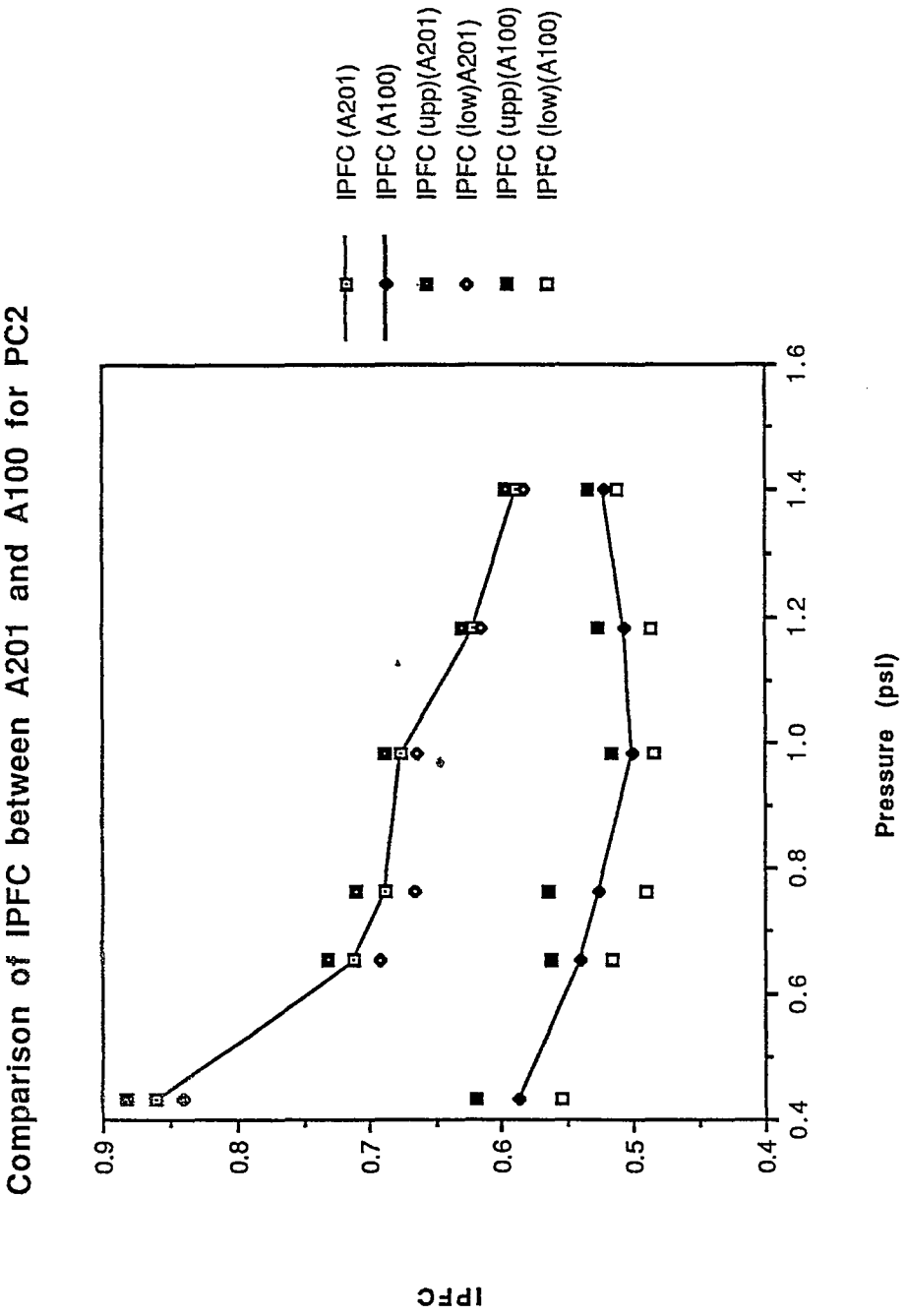

Figure 8.2: Comparison of IPFC between PC2A201 and PC2A100

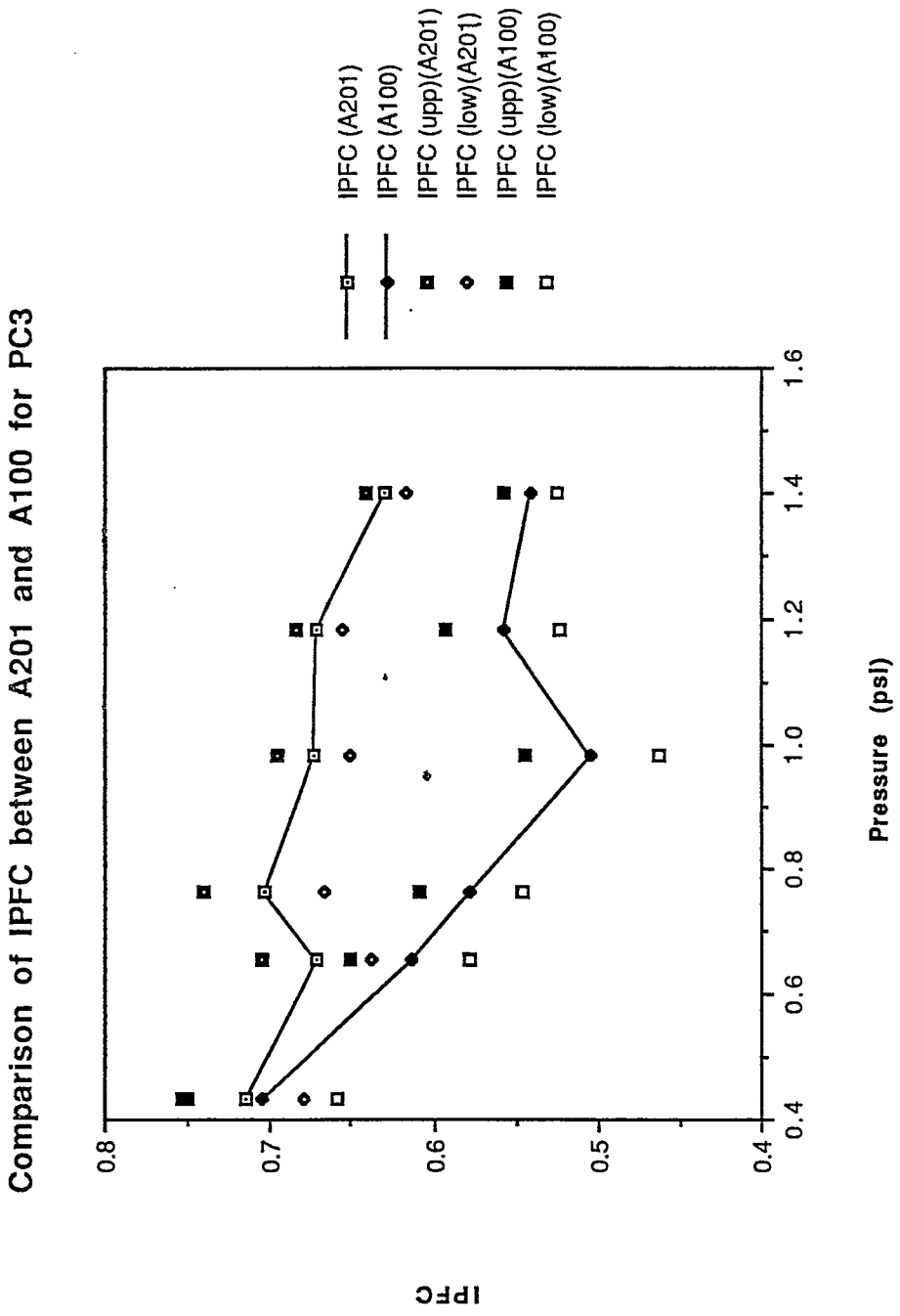

Figure 8.3: Comparison of IPFC between PC3A201 and PC3A100

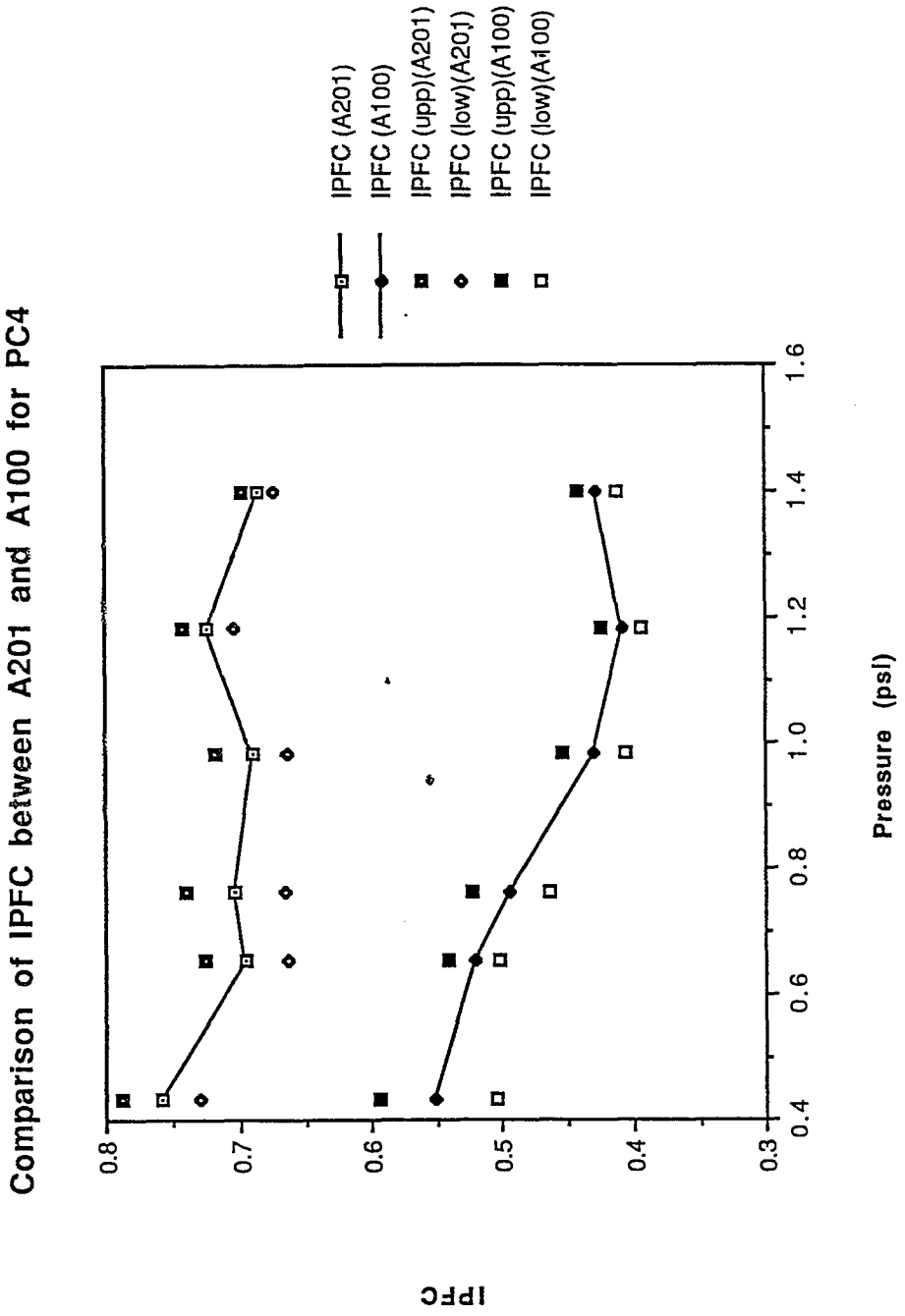

Figure 8.4: Comparison of IPFC between PC4A201 and PC4A100

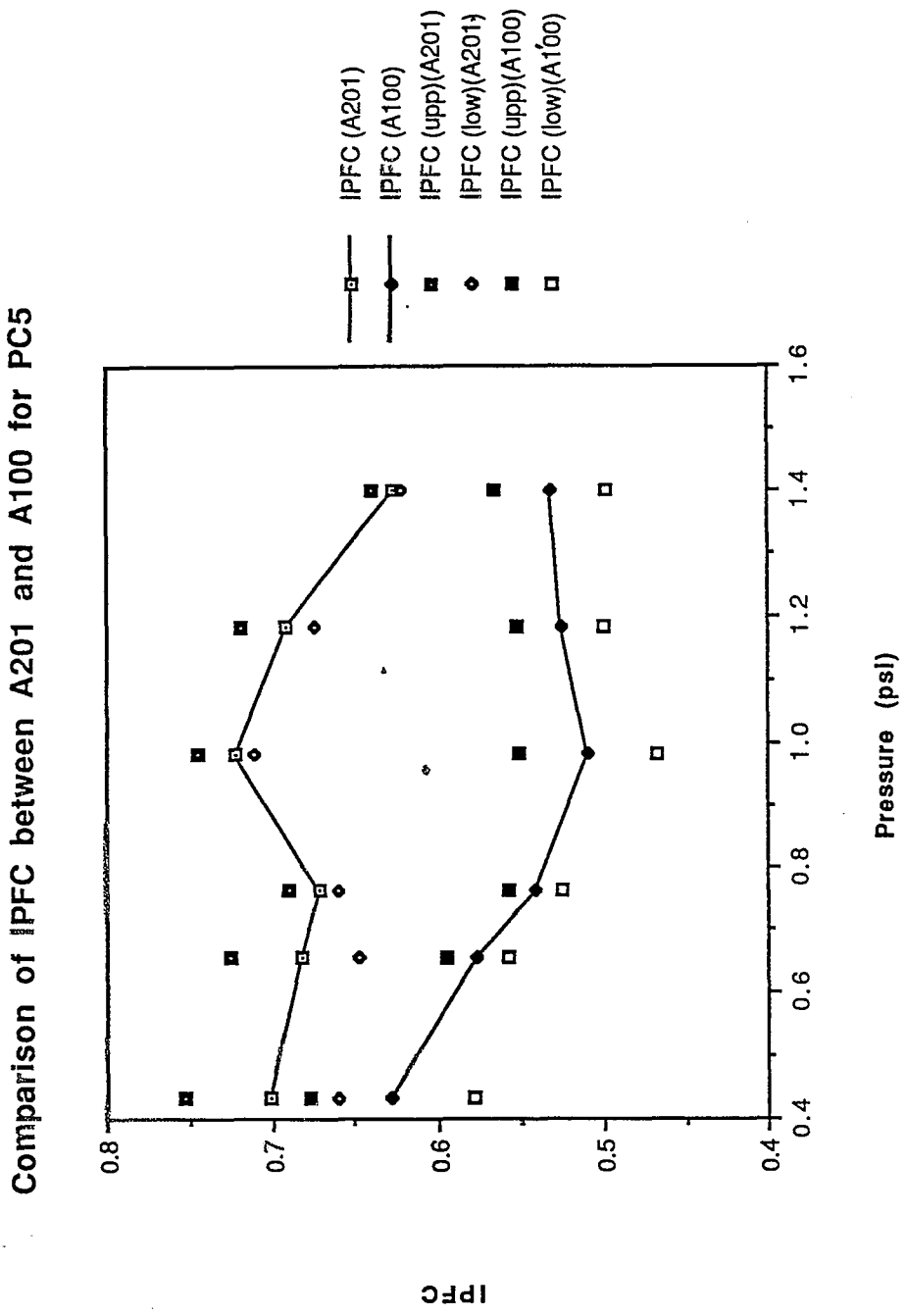

Figure 8.5: Comparison of IPFC between PC5A201 and PC5A100

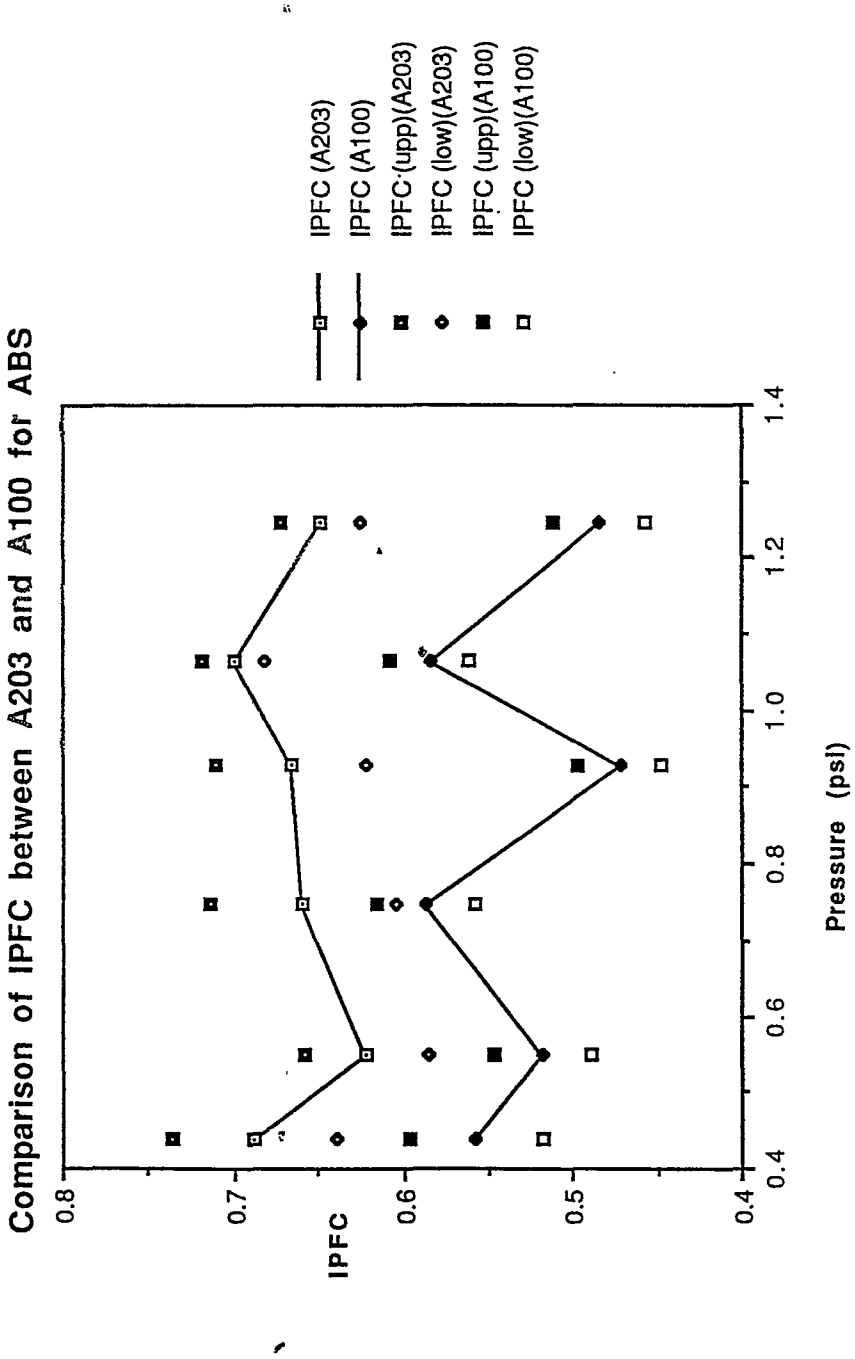

Figure 8.6: Comparison of IPFC between ABSA203 and ABSA100

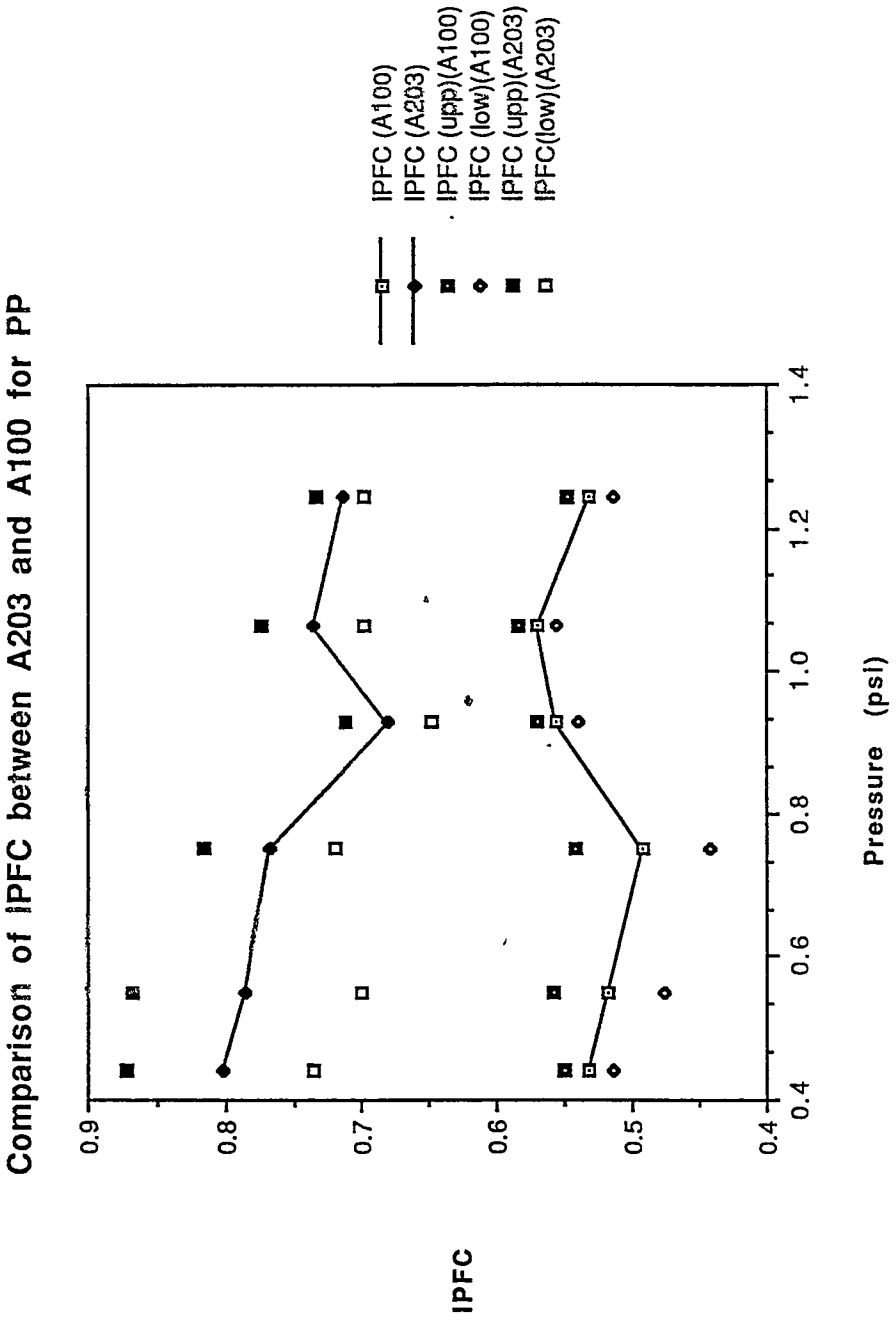

Figure 8.7: Comparison of IPFC between PPA203 and PPA100

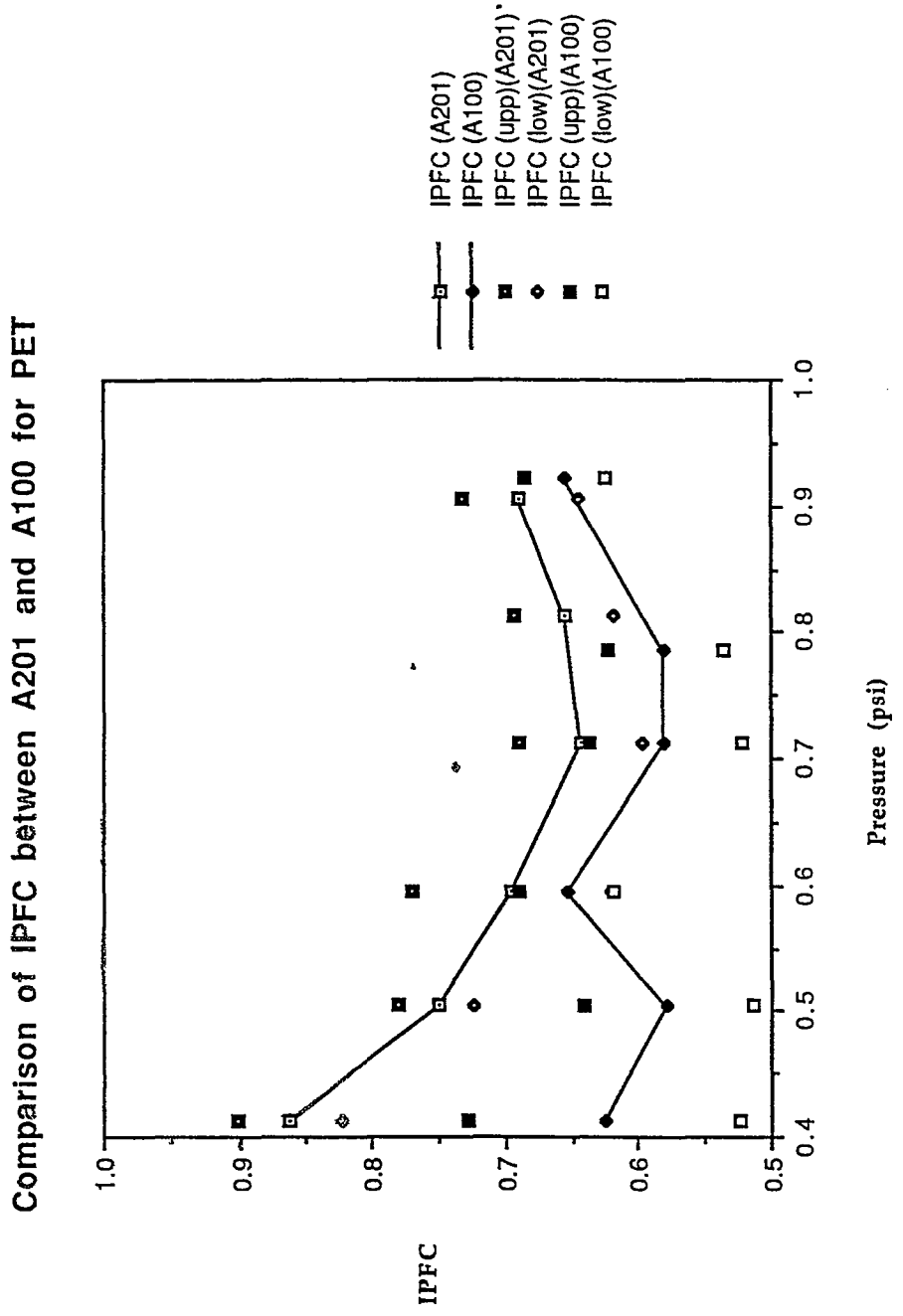

Figure 8.8: Comparison of IPFC between PETA203 and PETA100

8.2 Comparison of Low Modulus Pellets to High Modulus Pellets of Both Circular Cross Sections

Figure 8.14 shows the comparison of the IPFC for circular cross section between Polystyrene (PS) and Nylon (PA). Clearly, the IPFC for PA is greater than for PS for each corresponding pressure even though the varieties for PA is greater than for PS. However, the modulus of PA is lower than of PS as discussed in chapter 6.

Figure 8.15 shows the comparison of the IPFC for circular cross section between Polypropylene (PP) and Polystyrene (PS). The IPFC of PP is greater than of PS when the pressure is more than approximately 0.9(psi) and lower than of PS when pressure is less than 0.9(psi). However, the modulus of PS is higher than of PP.

Figure 8.16 shows the comaprison of the IPFC for circular cross section between Polypropylene and ABS. Because of great variety which one is greater for IPFC between PP and ABS is not clear. The same as in Figure 8.17.

Therefore, for those circular cross section pellets, the correlation between IPFC and modulus is not clear.

8.3 Comparison of Low Modulus Pellets to High Modulus Pellets of Both Bilobal Cross Sections

Figure 8.18 shows the comparison of the IPFC for bilobal cross section between Nylon (PA) and Polystyrene (PS). Obviously, the IPFC for PS is higher than for PA for each corresponding pressure even though their tendencies of variety are different. In addition the modulus for PS is greater than for PA.

Figure 8.19 shows the comparison of the IPFC for bilobal cross section be-

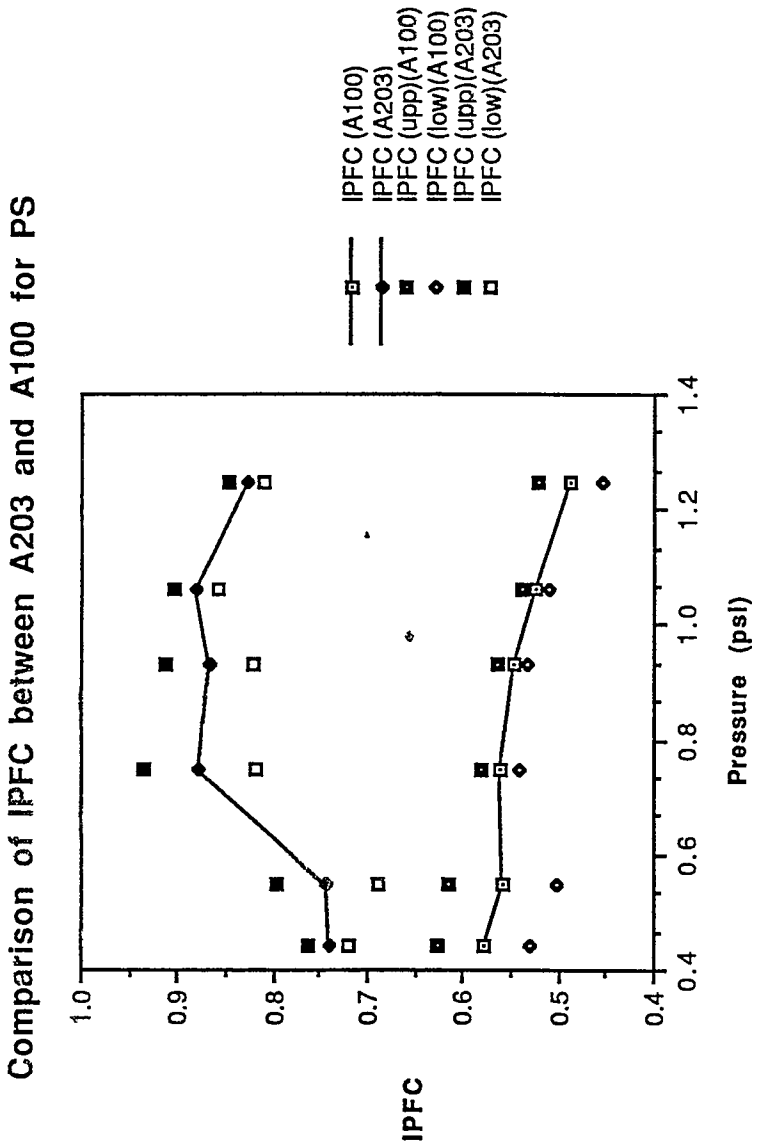

Figure 8.9: Comparison of IPFC between PSA203 and PSA100

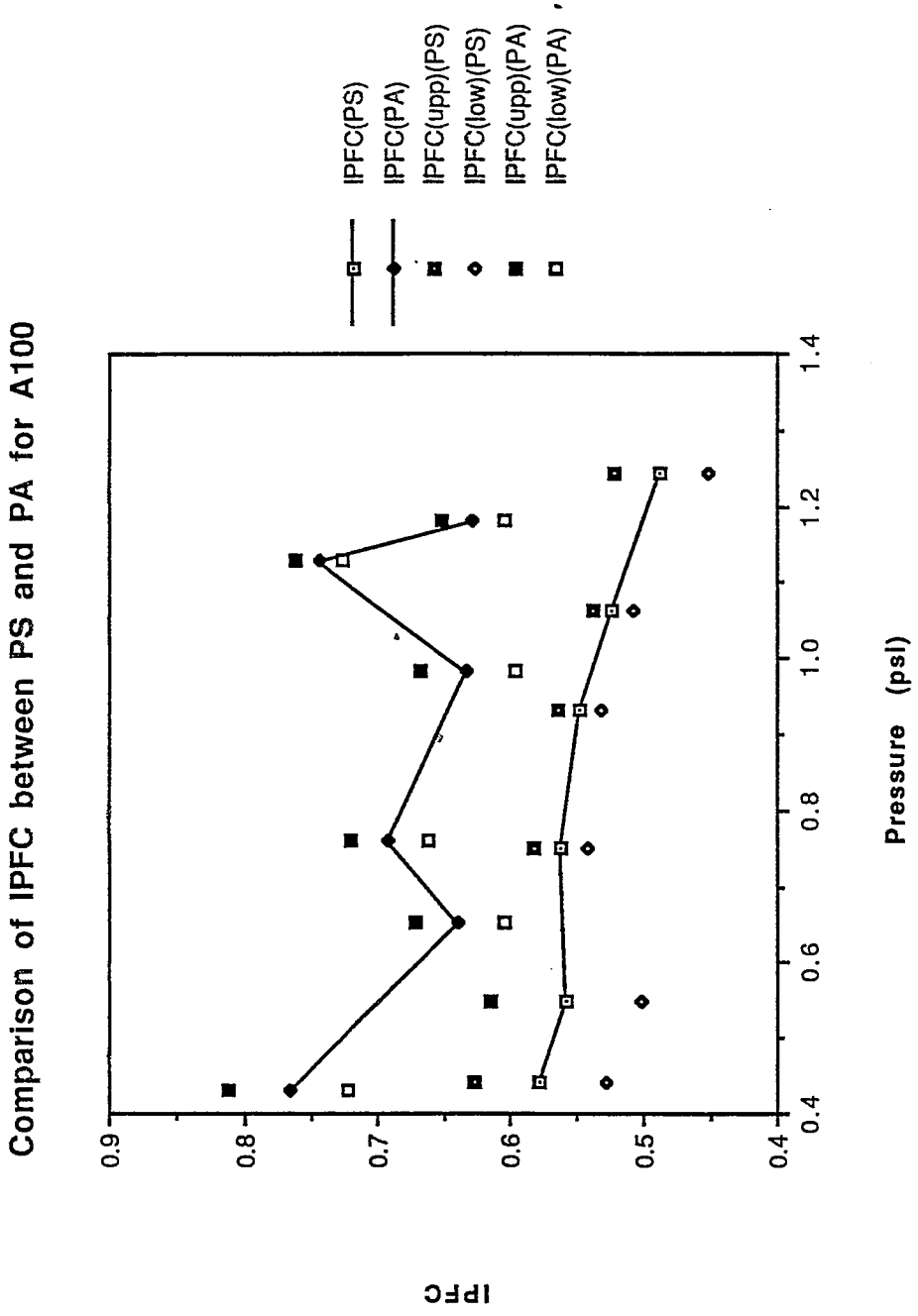

Figure 8.10: Comparison of IPFC between PAA100 and PSA100

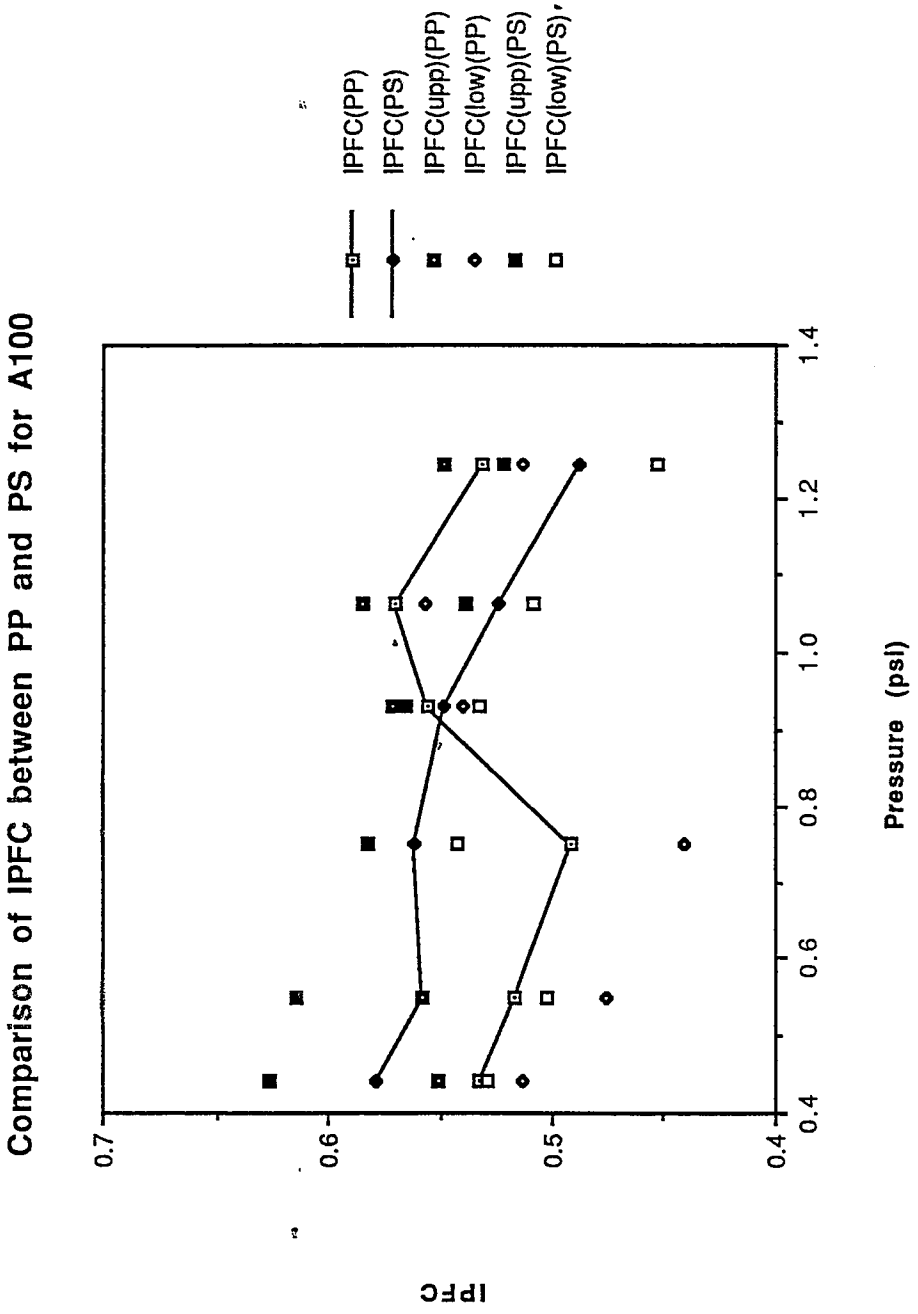

Figure 8.11: Comparison of IPFC between PPA100 and PSA100

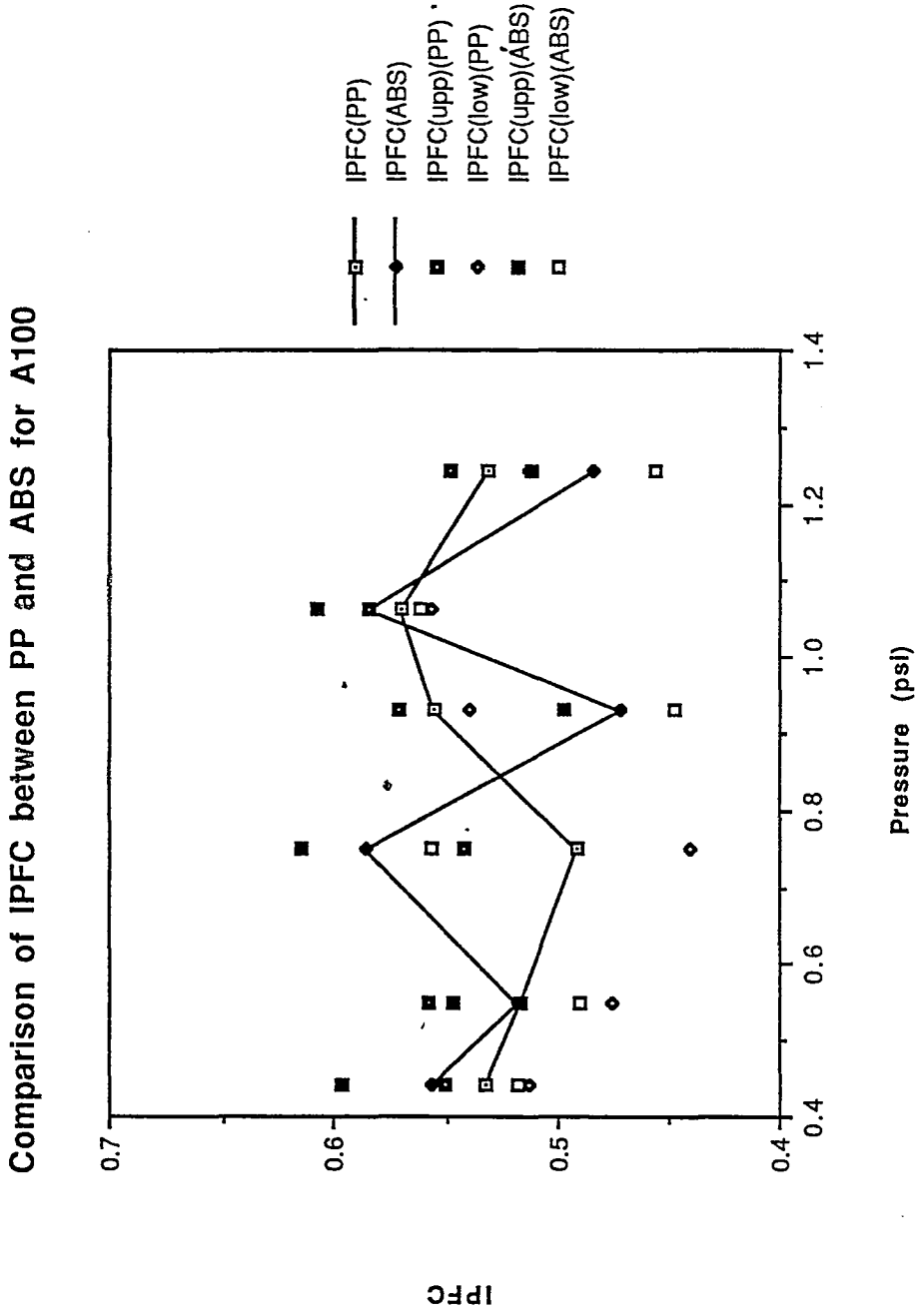

Figure 8.12: Comparison of IPFC between PPA100 and ABSA100

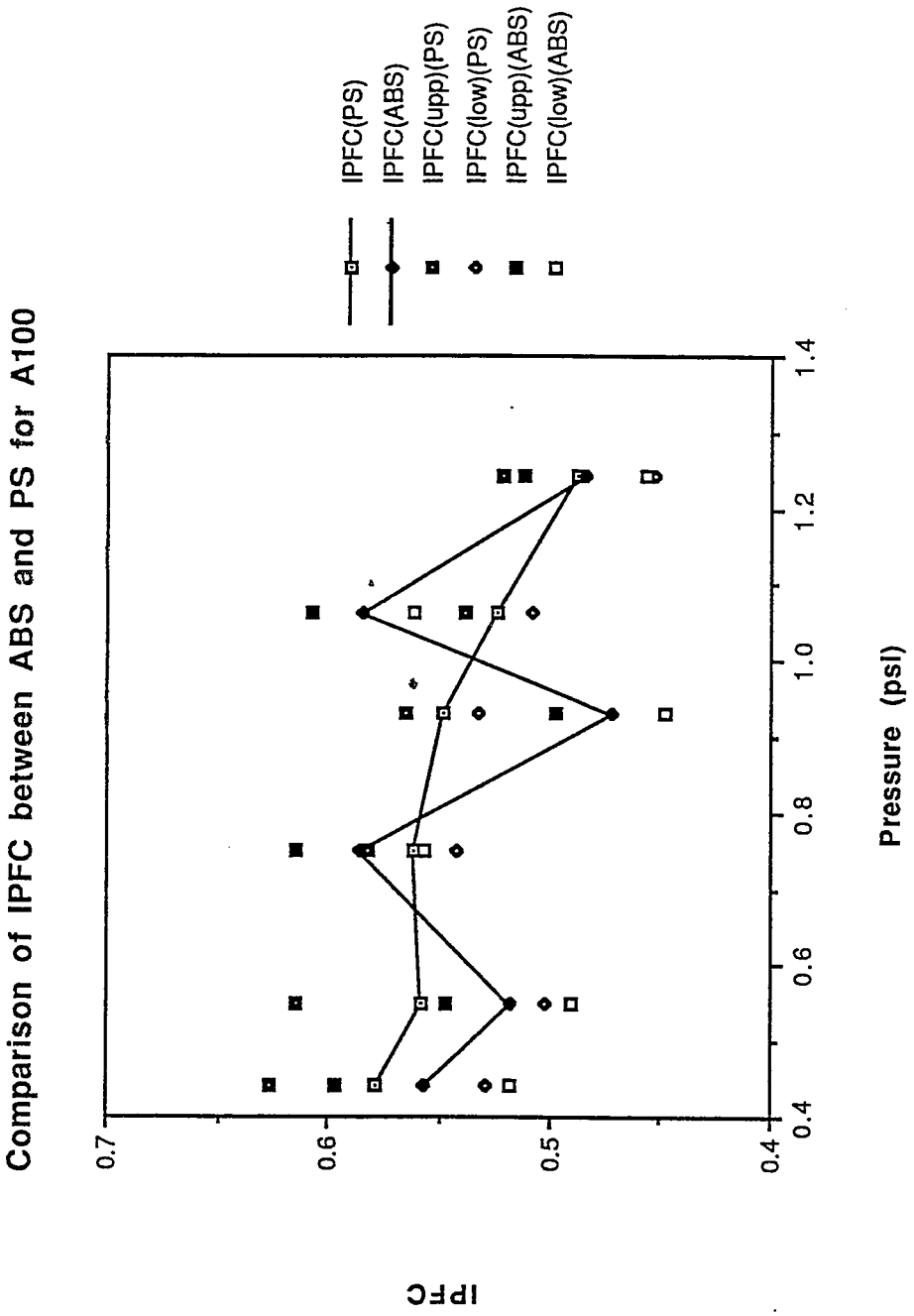

Figure 8.13: Comparison of IPFC between PSA100 and ABSA100

tween PP and PS. The IPFC for PS is higher than for PP when the pressure is more than approximately 0.68(psi). And the modulus of PS is greater than of PP as discussed in Chapter 6.

Figure 8.20 shows the comparison of the IPFC for bilobal cross section between PP and ABS materials. The IPFC for PP is higher than for ABS for each corresponding pressure. However, the modulus of PP is lowest among ABS, PA, PET, and PS.

Figure 8.21 shows the comparison of the IPFC for bilobal cross section between ABS and PS materials. Clearly, the IPFC for PS is higher than for ABS for each corresponding pressure. Further more, the modulus of PS is greater than of ABS.

On the whole, from Figure 8.18 to Figure 8.21, it seems that only when modulus is higher, it follows that higher modulus corresponds higher IPFC. The correlation of IPFC with its corresponding tensile modulus is plotted as shown in Figure 8.22, Figure 8.23, and Figure 8.24, respectively.

Figure 8.22 shows the correlation of IPFC and modulus with normal loads 4.845 (psi). The IPFC greatly decreases when the modulus is less than approximately 2,000 (Mpa) and increases when the modulus is more than 2,000 (Mpa).

Figure 8.23 shows the correlation of IPFC and modulus with normal loads 8.239 (psi). The IPFC greatly increases when pressure is more than approximately 2,000 (Mpa).

Figure 8.24 shows the correlation of IPFC and modulus with normal loads 13.699 (psi). The IPFC also greatly increases when pressure is more than approximately 2,000 (Mpa).

Therefore, when the modulus is higher than approximately 2,000 (Mpa), the IPFC will increase greatly.

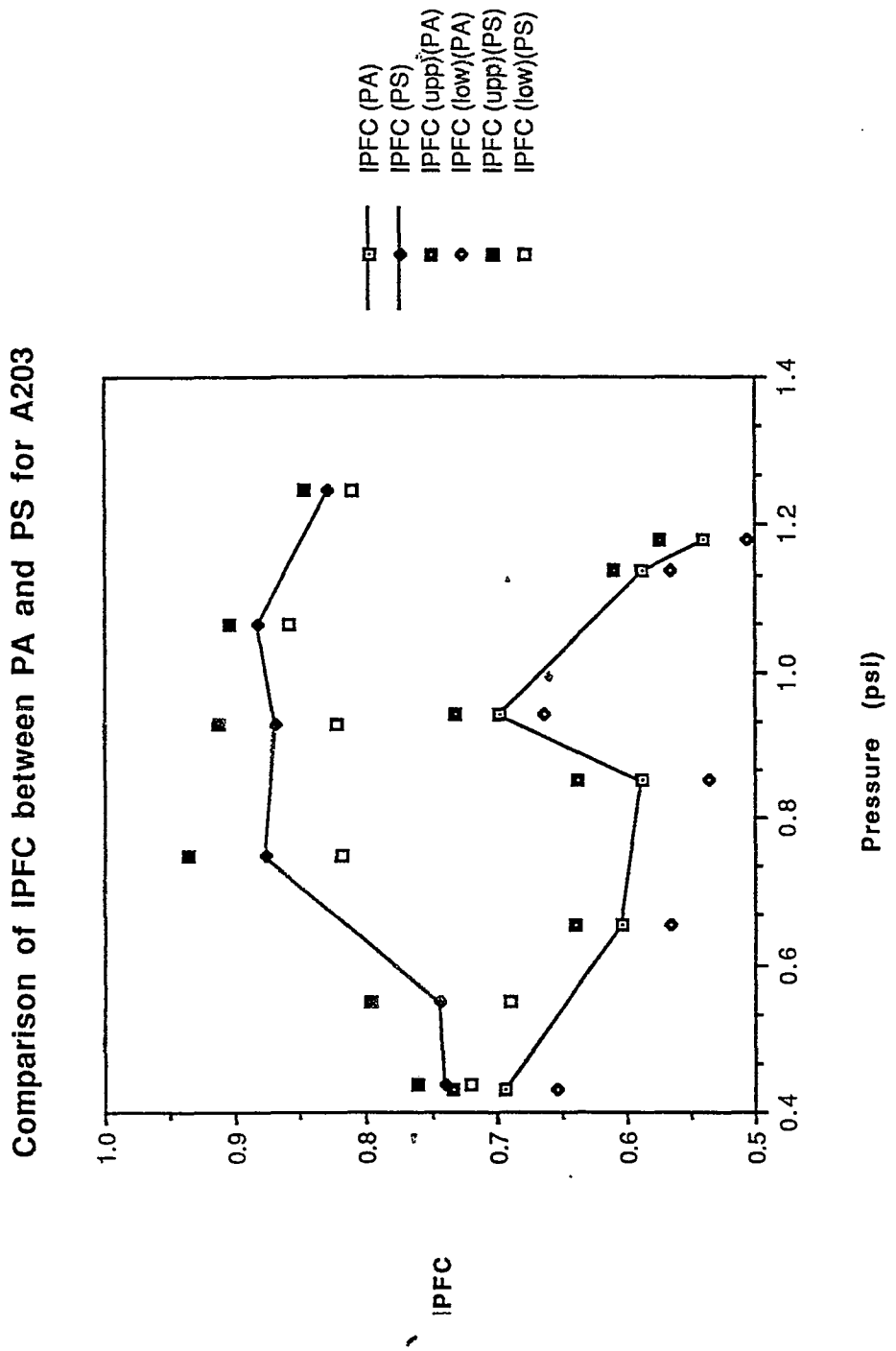

Figure 8.14: Comparison of IPFC between PAA203 and PSA203

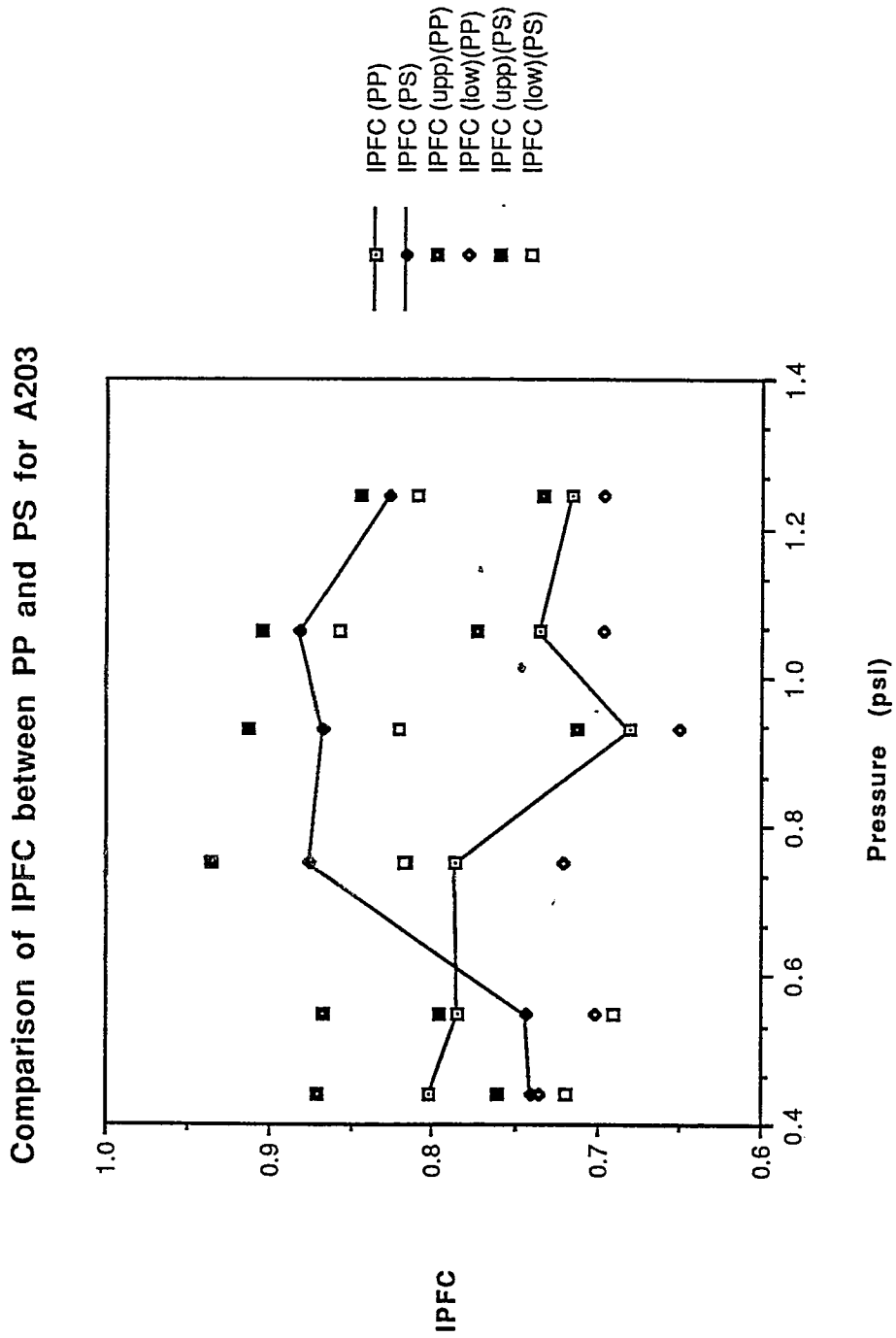

Figure 8.15: Comparison of IPFC between PPA203 and PSA203

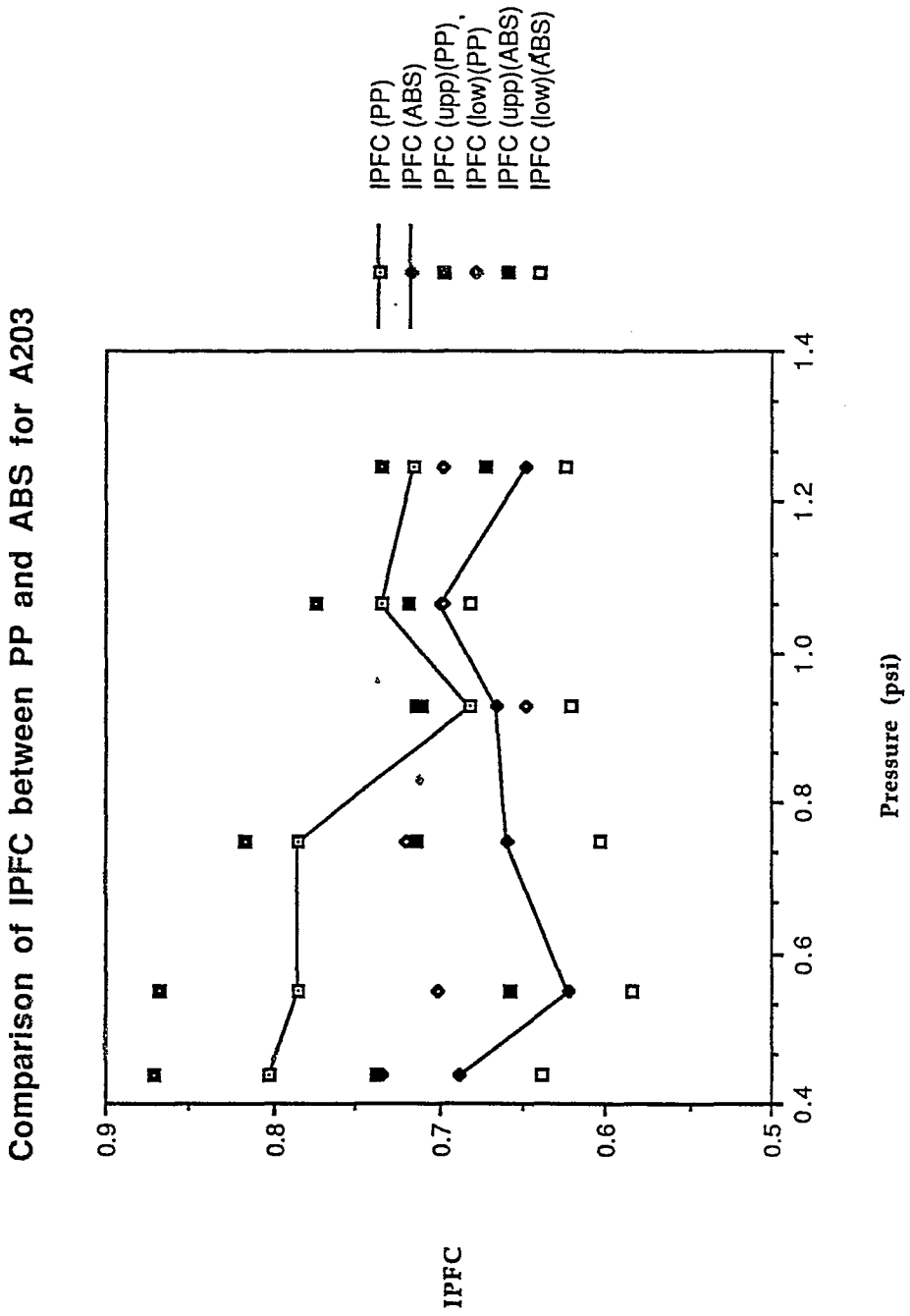

Figure 8.16: Comparison of IPFC between PPA203 and ABSA203

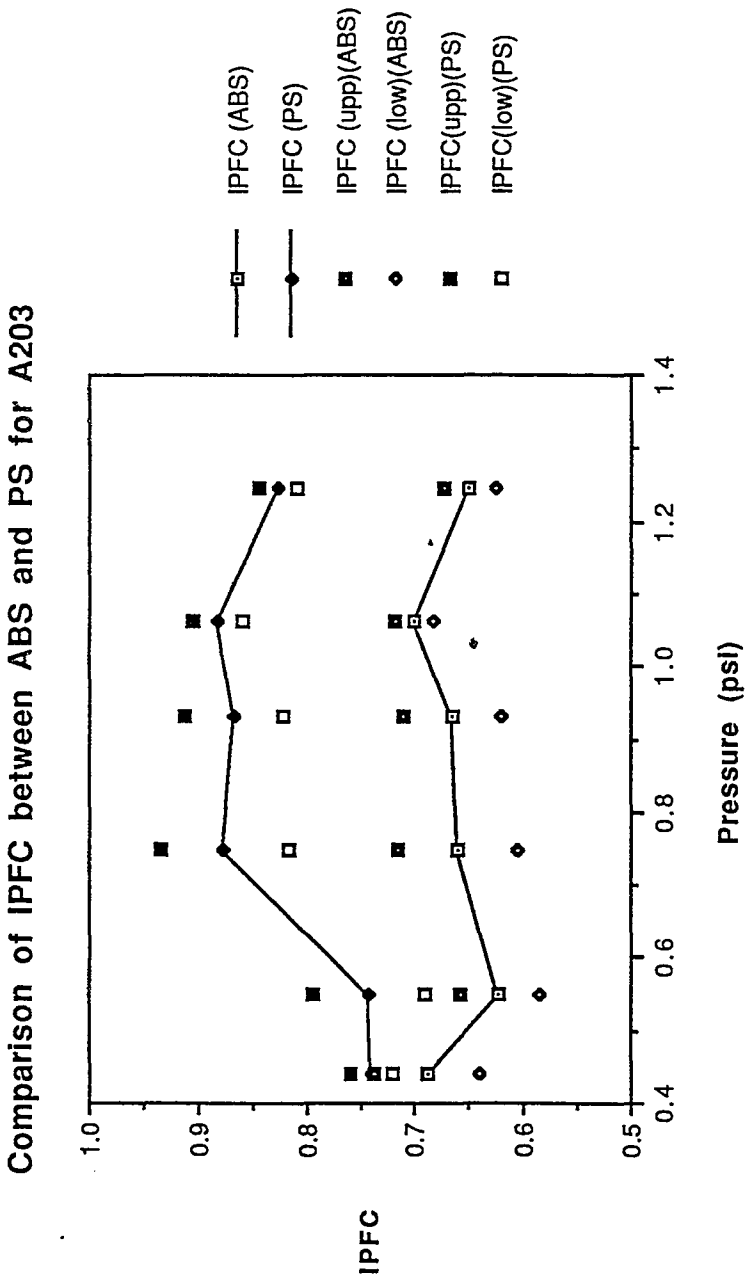

Figure 8.17: Comparison of IPFC between PSA203 and ABSA203

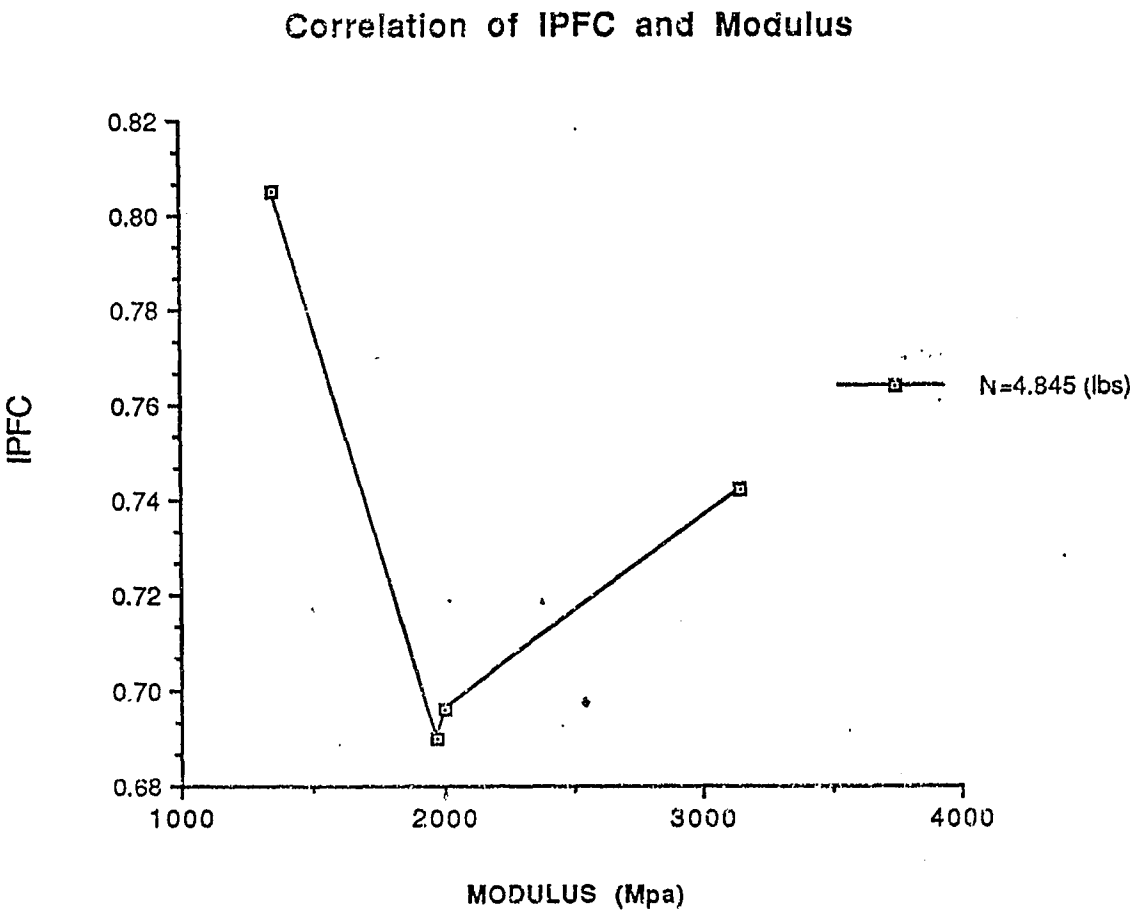

Figure 8.18: Correlation of IPFC and modulus with normal loads 4.845 (lbs)

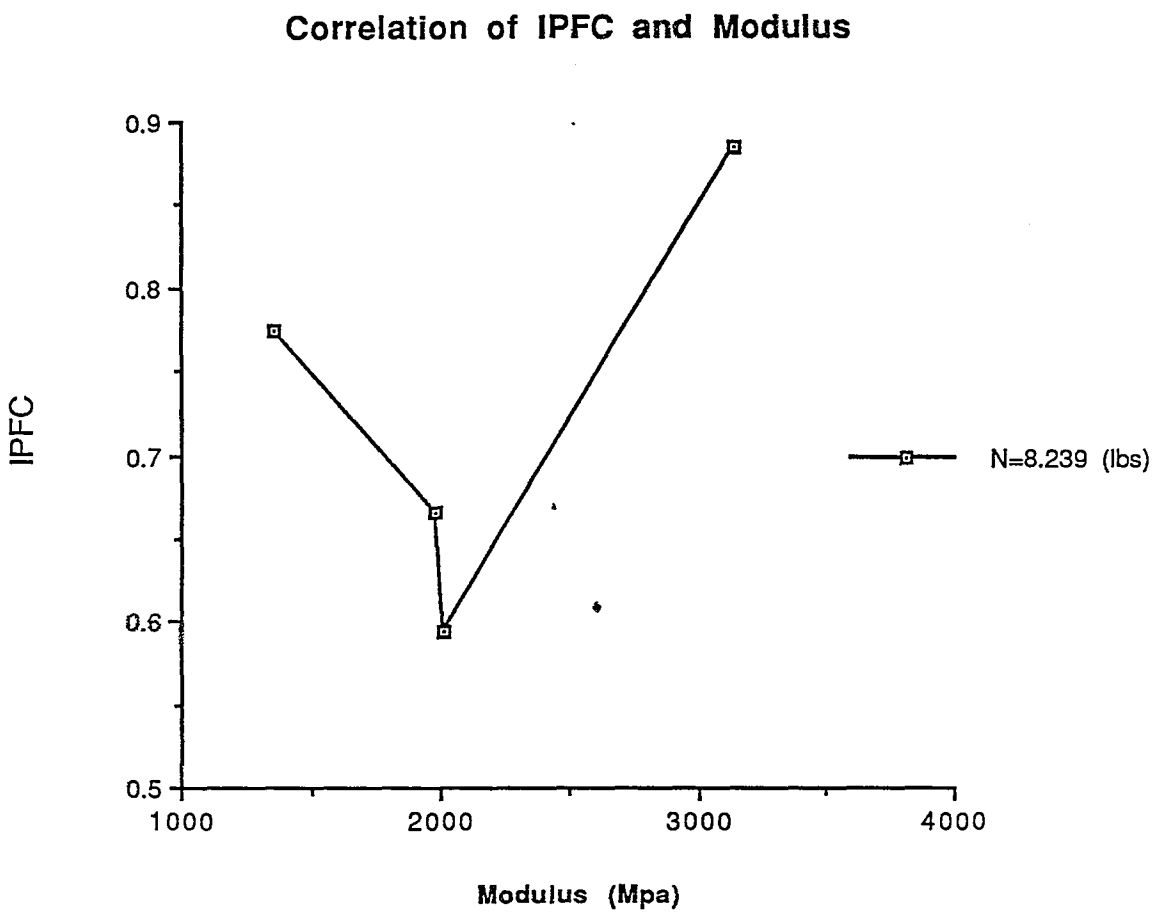

Figure 8.19: Correlation of IPFC and modulus with normal loas 8.239 (lbs)

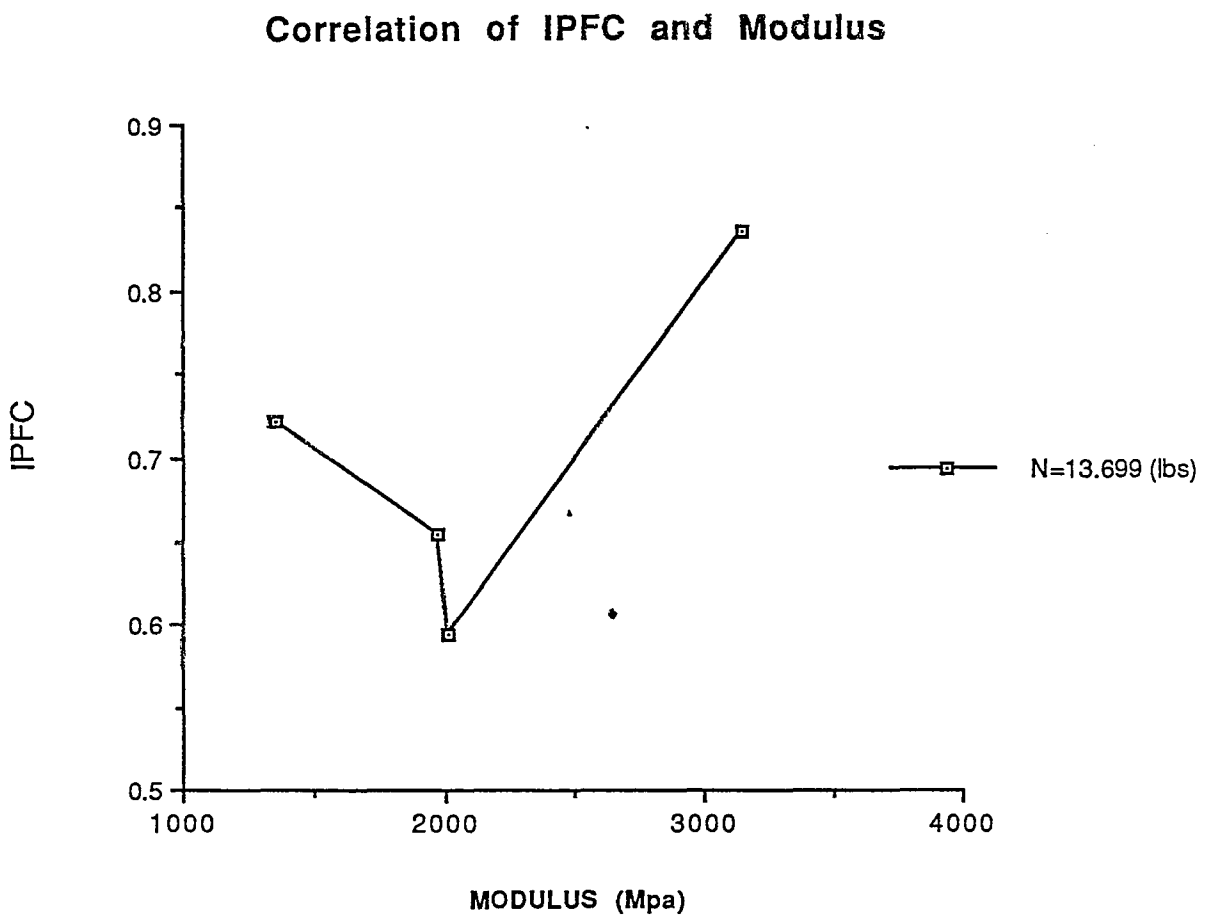

Figure 8.20: Correlation of IPFC and modulus with normal load 13.239 (lbs)

Chapter 9

CONCLUSIONS

9.1 Enhancement of IPFC: Effect of Cross Section Shape

The reason to enhance the IPFC seems to be quite clear now. Based on the melting mechanism theory in a single screw plasticating extruder, the sturdier solid bed generates melt that can be free of air bubbles. And this sturdier solid bed can also reduce surging, or fluctuation of temperature, pressure, and flow rate because strong solid bed requires more for external forces to overcome and to break up. Therefore, the larger the IPFC, the steadier is the extrusion precess.

By making profiled cross–sections pellets, the IPFC is improved from the aspect of both mean value of total contact points, or lines for those randomly arranged pellets and experimental results discussed in previous chapters. The experimental results show that the IPFC for pellets with bilobal cross sections is greater than for pellets with circular cross sections for Acetal Copolymer, PET, PP, PS and ABS.

9.2 Enhancement of IPFC: Effect of Modulus

As discussed in chapter 8, the tensile modulus of the polymer can affect the IPFC. High modulus materials yield less elastic or plastic deformation than low modulus materials. In equation 4.3, α represents a viscoelastic deformation at the contact points. For polymer with high modulus, the α would tend to unity.

Also, by making the profiled cross sections, the modulus seems to be larger than the circular cross sections as shown in the figures of chapter 8.

Chapter 10

FUTURE WORK

10.1 Develop a New Apparatus for More Accurate Determination of the IPFC

The shear cell which is used in this work is a better approximation to the real case of what a solid polymer experiences in the screw extruder. However, the force loading problems do exist as the experiments going on.

- The normal load being applied so far is less twenty pounds. As discussed in chapter III, compaction exists in the test process when the normal load is applied. The larger the normal load, the more it will be for compaction. Since the polymer pellets are not really rigid, they will deform permanently. And since the contact area between pellets becomes larger, the value of IPFC for the larger normal load will be definitely different with one of the smaller normal load.

- Because the moment the movable ring starts moving is observed only by eyes, there is no doubt that a reading error occurs. And also because the weight is added by hands , it requires heavy work.

The new test apparatus needs to be improved on these points.

Figure 10.1 shows a schematic of an advanced test apparatus. The normal load can be applied by pneumatic cylinder, and the shear force by linear actuator.

The magnitude of the normal load can be controlled by an air pressure regulator. And the linear actuator consists of motor, gear box, and screw. If the motor is on, then the screw will be rotated to either pull, or push the movable ring of shear cell. Then the actuator senses and records this tensions, which is the shear force on the particulate bed.

The new device solves the loading problems and decreases the reading error. In addition, the new device can generate continuously either large or small forces.

10.2 New Profile Shapes and Different Pellet Sizes

Produce different sizes and different shapes of profiled cross sections of polymer pellet so as to make a detailed comparison to verify the theory discussed in previous chapters.

The new profiled shapes would be like oval, concave, multilobal, crescent and triangular. Figure 10.2 shows the cross sections of possible profiled cross sections for the pellets. These profile shapes are based on the pellets interlocking ability.

As discussed previously, if two pellets have more real contact points, the surface tends to have more irregularities and asperities. And then those irregularities and asperities tend to hold pellets together tightly and cause the total shear force to be greater.

Clearly, for crescent, concave, and triangular pellets, under certain greater pressure, high compaction will occur. Many true contact points will result with random arrangements. And, for oval and multilobal cross section pellets, they would also have many contact points if under pressure and well compacted. In addition, since they are symmetric, it would be easy to make the dies, and therefore, more practical.

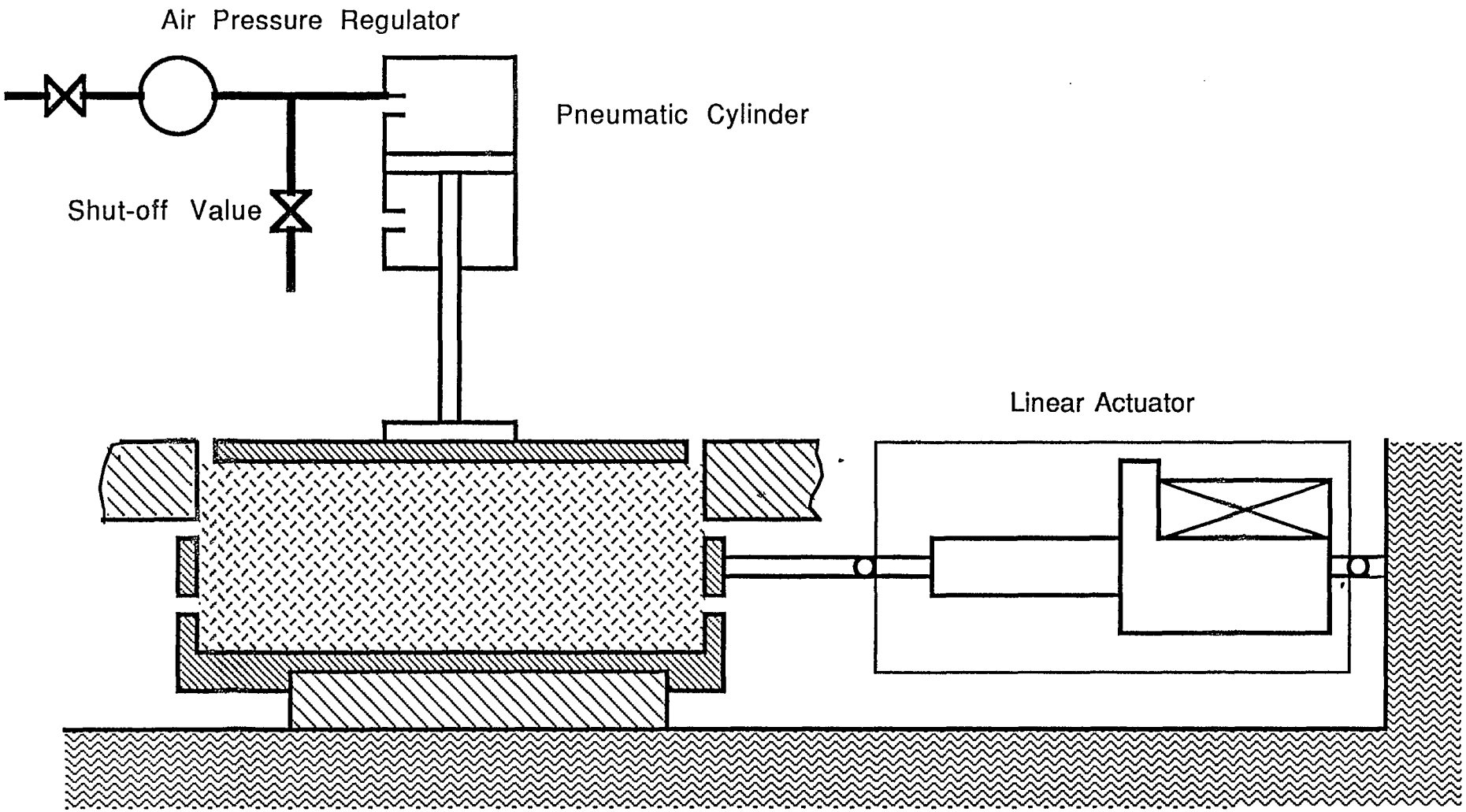

Figure 10.1: Advanced test device

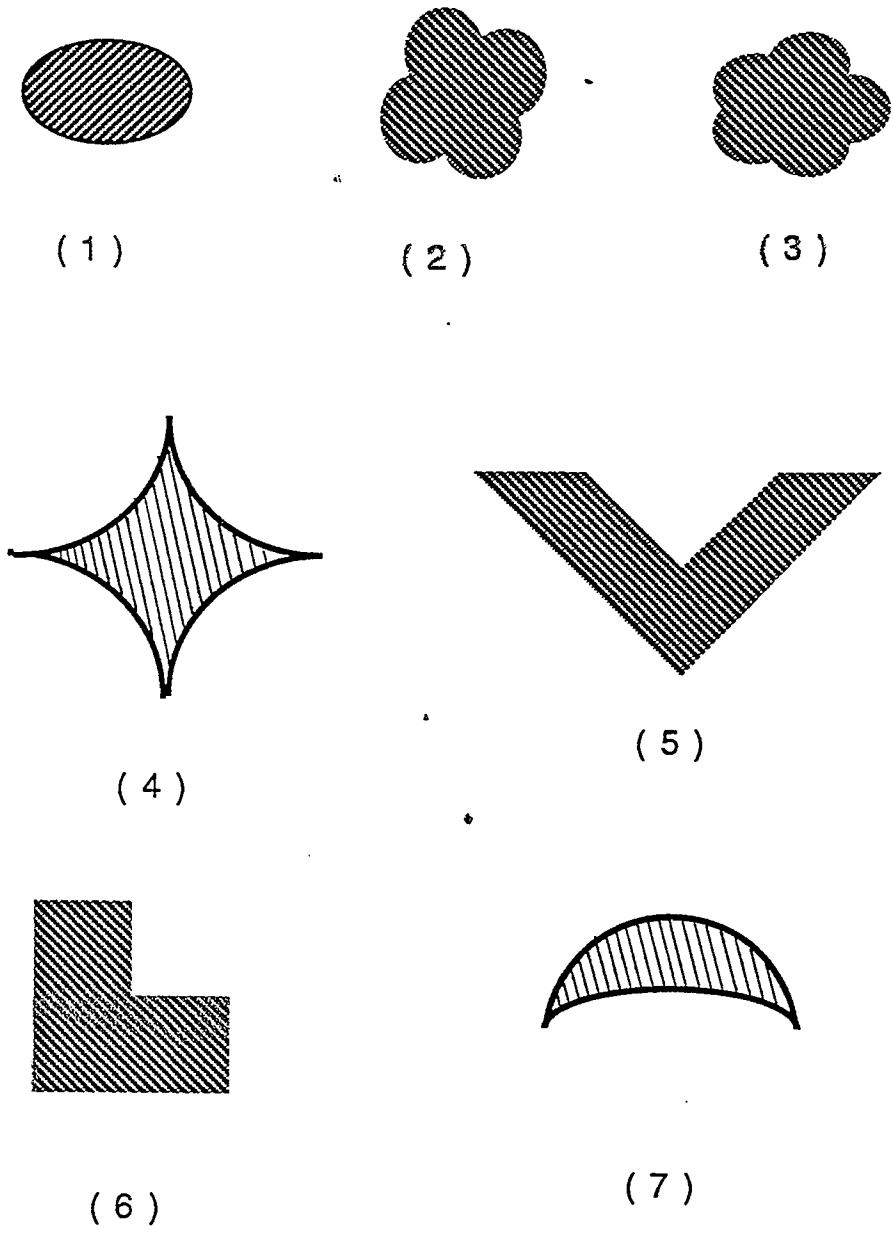

Figure 10.2: New profile pellets

10.3 Field Trials

Field testing on an industrial extruder to determine if improvements of flow rate, quality, and output could be achieved by increasing the IPFC and how profiled pellets could influence the outputs.

The field trials would be the following:

1. Use the circular cross section pellets of all test materials including acetal copolymer, PP, PA, ABS, PET, PS in the single screw extruder with smooth feed throats and run it to determine the throughput rate.

2. Use the bilobal cross section pellets, trilobal cross section pellets, and those new shape pellets like concave, triangular, crescent, and multilobal of all test materials which we have proved that their IPFC is greater than circular cross section in the above extruder and run the extruder to determine the throughput rate. And compare these results to the equivalent results in item 1.

3. As discussed before, since the grooved feed sections increase intial compression and increase material turbulence for conveying, outputs are improved greatly by grooved feed throats with intensively cooled feed sections compared to smooth feed throats. Put the circular cross section pellets of all materials in the helical grooved feed throats extruder to determine the throughput rate. Also put them in the axial grooved feed throat extruder to determine the throughput rate. And compare these results to the equivalent results in item 1.

4. Use the bilobal cross section pellets, trilobal cross section pellets and those new shape pellets of all test materilas in the helical grooved feed throat extruder and run this extruder to determine the throughput rate. Again put these pellets in the axial grooved feed throats and run it to determine the throughput

rate. And compare these results to the equivalent results in item 2.

5. Since the barrier screws are designed to separate the solid bed from the melt pool, it inhibits solid bed to breakup. Use the circular cross section pellets of all test materials in the barrier screw extruders, including the Hartig MC–3 screw, Maxmelt screw, the Barr–2 screw, the "Efficient" screw, and the VPB screw and operate those extruders to determine the throughput rate. And compare these results to the equivalent results in item 1.

6. Use the bilobal cross section pellets, trilobal cross section pellets, and those new shape pellets in the barrier screw extruders, including the Hartig MC–3 screw, Maxmelt screw, the Barr–2 screw, the "Efficient" screw, and the VPB screw and operate those extruders to determine the throughput rate. And compare these results to the equivalent results in item 2.

7. Use the circular cross section pellets of all test materials in extruders with barrier screws plus grooved feed throats and operate these extruders to determine the throughput rate. And compare these results to the equivalent results in item 1 to item 6.

8. Use the bilobal cross section pellets, trilobal cross section pellets, and those new shape pellets in extruders with barrier screws plus grooved feed throats and operate these extruders to determine the throughput rate. And compare these results to the equivalent results in item 1 to item 7.

After all these experiments, a detailed comparison from 1 to 8 can be made with no doubt to determine how the IPFC affects the throughput for all kinds of industrial extruders.

Appendix A

BASE RESIN & CODES

NO.	MATERIAL	ABBRE.	MANUFACTURER	GRADE	CODE
1.	Polypropylene	PP	Soltex	P40	PP1
				0326-61	PP2
				SOFT	PP3
2.	Polystyrene	PS	Hoechst Celanese	CLEAR	PS
3.	Nylon	PA	Plaskon	917	PA1
				XPN	PA2
				CLEAR	PA3
				BLACK	PA4
			Hoechst Celanese	3300D	PA5
				7520-2	PA6
4.	Polyethlene	Portiflex	Solvey		PE1
5.	Thermoplastic Polyester	PET	Hoechst Celanese	CX–2003	PET1
				BLACK 3300D	PET2
6.	Acrylonitrile Butadene Styrene	ABS			ABS
7.	Celcon Acetal Copolymer		Hoechst Celanese	U10-01	PC1
				M25	PC2
				M90	PC3
				M270	PC4
				M450	PC5

Appendix B

PROFILED DIE & CODES

The profile die specification:

- A201 (hole size of 0.0785" in diameter)
- A202 (hole size of 0.0625" in diameter)
- A203 (hole size of 0.0625" in diameter)
- A204 (hole size of 0.094" in diameter)
- A301 (hole size of 0.0625" in diameter)

Five dies have been constructed. These have been designed A201, A202, A203, A204, and A301. The first digit indicates the number of lobes in the die channel. The dimensions of the dies are presented as follow, respectively, while A100 represents base shape, ie. circular cross section which is not made by the single screw extruder in the plastics laboratory.

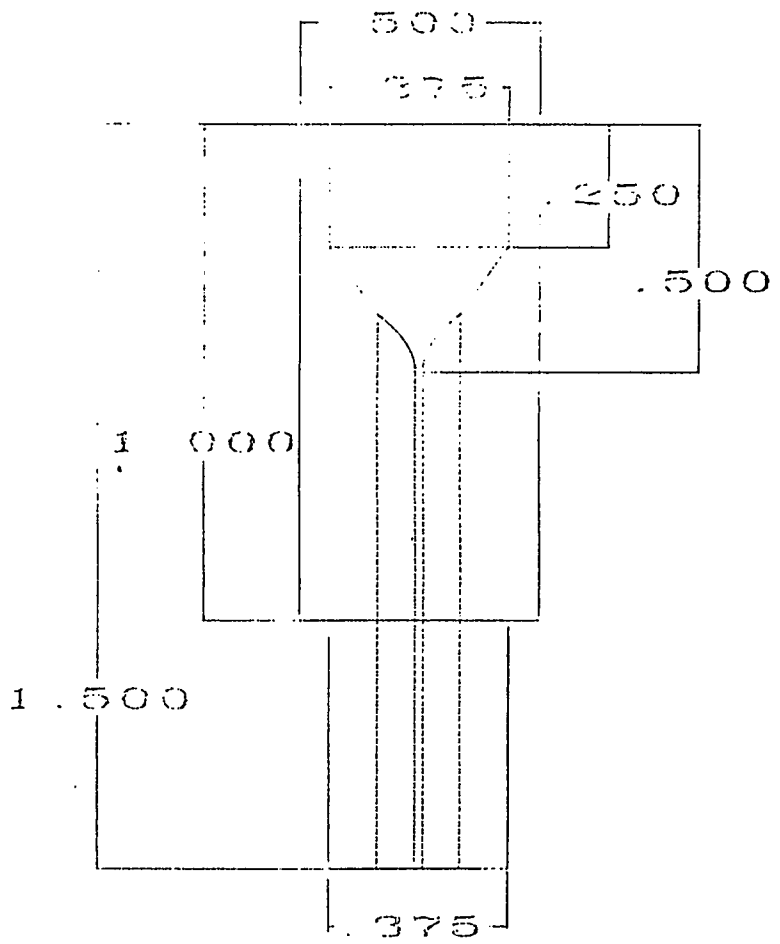

profile die A201

UNITS : INCH
MATERIAL : STAINLESS

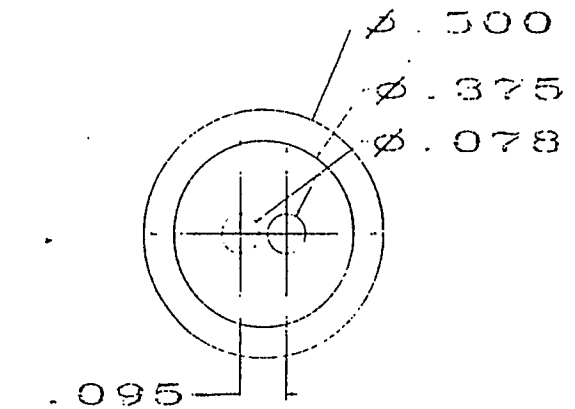

Figure B.1: Profile Die A201

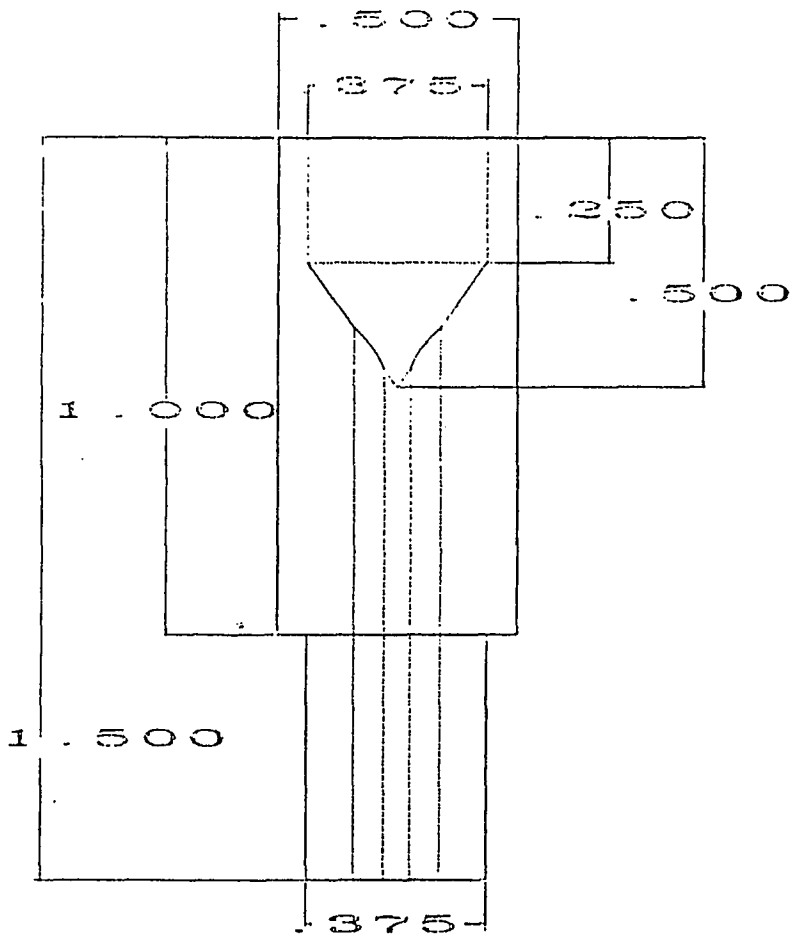

profile die A202

UNITS INCH
MATERIAL STAINLESS

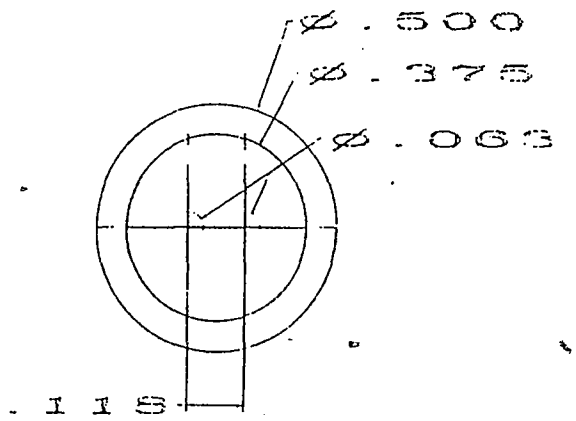

Figure B.2: Profile Die A202

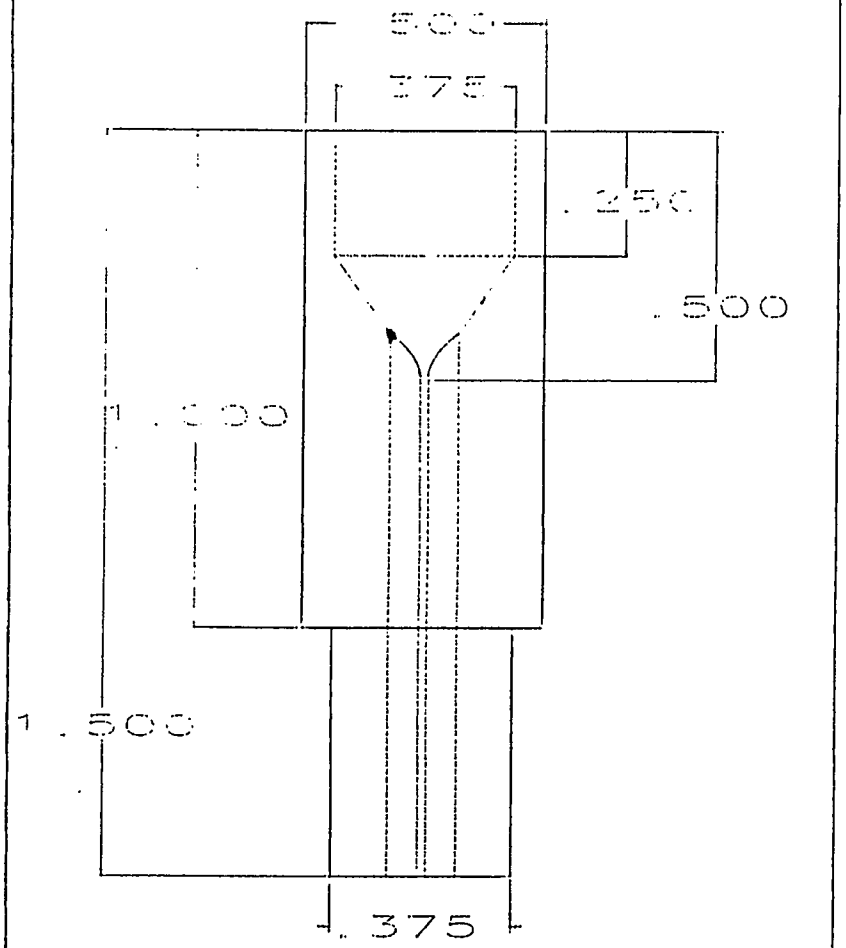

profile die A203

UNITS : INCH
MATERIAL : STAINLESS

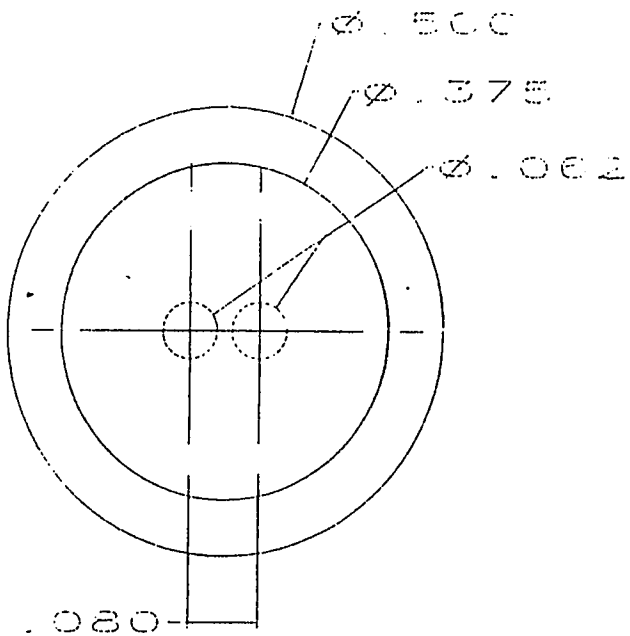

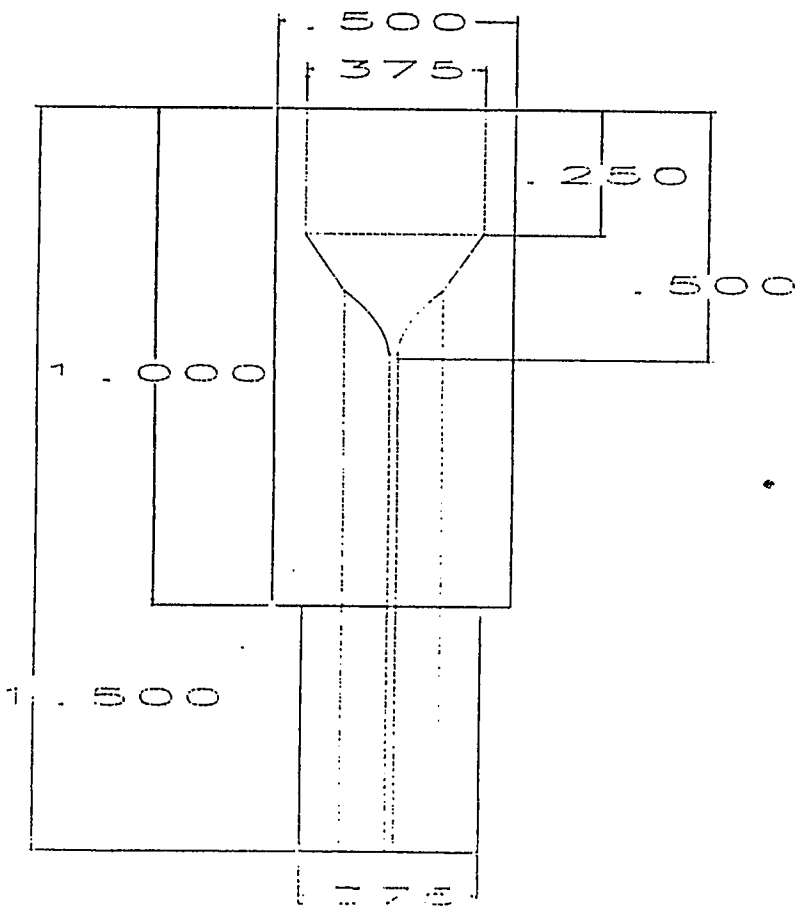

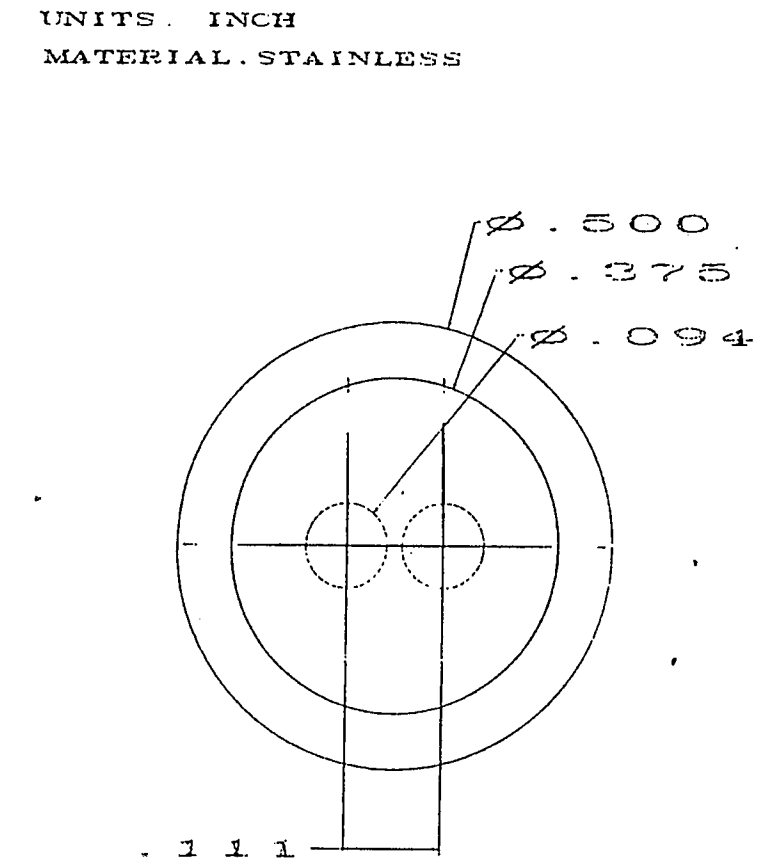

Figure B.4: Profile Die A204

Bibliography

[1] *Plastics World*, 1990

[2] Imrich Klein, Zehev Tadmor,*Engineering Principles of Plasticating Extrusion,* 401 (1978)

[3] Zehev Tadmor, Imrich Klein, *Engineering Principles of Plasticating Extrusion,* 401 (1978)

[4] B. H. Maddock, *A Visual Analysis of Flow and Mixing in Extruder,* Society of Plastics engineers, New york, January 1959; also Soc. Plast. Engs. J. , 15,383 (1959)

[5] L. F. Street, *Plastifying Extrusion,* Int. Plas. Eng., 1, 289 (1961)

[6] Street, L., *Mod. Plastics,* 30, 130 (1953)

[7] Tadmor et al, I.J. Duvdevani, and I.Klein, *Melting in Plasticating Extruders—Theory and Experiments,* Polym.Eng.Sci., 7, 198-217 (1967)

[8] Z. Tadmor, Costas G. Gogos, *Pronciples of Polymer Processing,* 467 (1978)

[9] Z. Tadmor and I. Klein, *Engineering Principles of Plasticating Extrusion,* Van Nostrand Reinhold, New York, 1970

[10] Maddock, B.H., *Technical Papers, Volume V, 15 Annual Technical conference.* Soc. Plastics Eng., New York (January, 1959), also Soc. Plastic Engrs. J., 15, 383 (1959)

[11] J. T. Lindt, *polym. Eng. Sci.*, 16, 284, (Apr, 1976)

[12] C. Maillefer, *Mod. Plast.*, 40, 132 (1963)

[13] R. Barr, *Plastics Engineering*, (Jan. 1981)

[14] Furey, M.J., *Ind.Eng., Chem.*, 61.13 (1969)

[15] Bowden, F.P., and Tabor, D., *The Friction and Lubrication of Solids* Part II, Oxford University Press, London, 1964

[16] G. M. Gale, Friction Measurements on Plastics Powders and Granulates for Extruder Feed Zone Design, Rubber and Plastics Research Association, Shawbury, Shrewsbury, England

[17] R. L. Brown and J. C. Richards, *Principles of Powder Mechanics*, Pergamon Press, Oxfords, 1969

[18] Zehev Tadmor, Costas G. Gogos, *Principles ofPolymer Processing,* 245 (1978)

[19] D. Train, C. J. Lewis, *Agglomeration of Solids by Compaction,* Paper presented at the Third Congress of the European Federation of Chemical Engineerings, London, June 20–29, 1962

[20] Zehev Tadmor, Costas G. Gogos, *Principles of Polymer processing,* 260, (1978)

[21] D. Train and C. J. Lewis, *Agglomerization of Solids by Compaction,* Paper presented at the third congress of the European Federation of Chemical Engineers, London, June 20–29, 1962.

[22] W. H. Wollaston, *Phil. Trans.* , 119, 1 (1829).

[23] K. Schneider, *Druckausbereitung und Druckverteilung in Schuttgutern*, Chem. Ing. Techn., 41, 142 (1969)

[24] E. Goldacker, *Undersuchungen zur Inneren Reibung von Pulvern, insbesondere im Hinblick auf die Forderung in Extrudern,* Dissertation, Institut fur Kunststoffverarbeitung (IKV), Aachen

[25] Laurie Hoover–Siegel, *Grooved feed throats increase extruder outputs,* Plastics World, (may, 1983)

[26] Dr. Ing. Klaus Schneider, Aachen, *Friction Behavior of Plastic Granules,* Kunststoffe, vol. 59 (Feb. 1969)

[27] Hui Chang, R. A. Daane, *Coefficient of Friction for Solid Polymers in Various Forms,* Plastics Research, Beloit Corporation

[28] A. S. Lodge and H.G. Howell, Proc. Phys. Soc. B band, 67 (1954)

[29] Hall, Holowenko, Laughlin, *Machine Design*

[30] Norman S. Matloff *Probability Modeling and Computer Simulation,* An Intergrated Introduction with Applications to Engineering and Computer Science

[31] *Cumulative Normal Distritrubion Function,* Computed by P. J. Hildebrand from Statistical Thinking for Behavioral Scientists by David K. Hildebrand

[32] *Encyclopedia Polymer Science and Engineering,* 2nd edition

[33] F. W. Tortolano, *Workhouse Plastics,* Technology Focus/Engineering Plastics, 5–7–90

[34] F. W. Tortolano, *Workhouse Plastics,* Technology Focus/Engineering Plastics, 5–7–90